UNIVERSIDADE DE LISBOA
FACULDADE DE CIÊNCIAS
DEPARTAMENTO DE ENEGENHARIA GEOGRÁFICA, GEOFÍSICA E ENERGIA.

Validation and Quality Assessment of HF Radar Wave Measurements in the Algarve Shore

Francisco Ferreira da Cunha Barros

Mestrado em Ciências Geofísicas
Meteorologia e Oceanografia

Dissertação orientada por:
Professor Doutor Joaquim Dias
Doutora Luísa Lamas

2019

Resumo Alargado:

A validação e aferição da qualidade das medições de agitação marítima efetuadas por radares HF (alta frequência) têm o intuito de aumentar o conhecimento sobre os processos oceânicos em zonas costeiras através da sua monotorização. Neste estudo, foram considerados os radares HF de Sagres e de Alfanzina situados na costa Algarvia, Portugal sendo que foram utilizadas como referência para as suas medições, as medições efetuadas por diferentes boias ondógrafo colocadas em diferentes regiões da costa e sujeitas a variados estados do mar. Nomeadamente, foram utlizadas a boia costeira de Sines e as boias oceânica (*offshore*) e costeira de Faro.

Os radares HF estudados são da marca CODAR, modelo SeaSonde, funcionam com uma frequência central de 13.5MHz sendo que os parâmetros da ondulação por estes medidos são a altura significativa (SWH), o período médio (MWP) e a direção média (MWD). Todos os sistemas de monotorização de estados do mar utilizados neste estudo são geridos pelo Instituto Hidrográfico.

Uma vez que os dados deste tipo de radares são obtidos para diferentes coroas circular discretizadas em função do seu alcance (*range-cells*) e uma vez que não era previamente conhecida qual a range-cell mais favorável para a comparação com os dados obtidos pelas boias ondógrafos foi considerada uma range-cell média constituída pela média de todas as range-cells colocando assim as medições do radar numa coroa circular a 15 km do local do seu local de instalação sendo posteriormente verificada a validade desta hipótese recorrendo-se a um diagrama de extremos e quartis.

Este estudo está divido em duas secções. Na primeira secção os dados obtidos pelos radares HF foram comparados individualmente com os dados obtidos por cada boia ondógrafo. Nomeadamente, os dados do radar de Sagres foram comparados com os dados da boia costeia de Sines e com os dados das boias *offshore* e costeira de Faro enquanto que os dados do radar de Alfanzina foram comparados individualmente com dados obtidos pelas boias de Faro para o período de 1 a 24 de Abril de 2018. Assim, foi concluído que os radares HF efetuam medições dos estados de mar numa dada coroa circular e como tal conseguem detetar uma maior quantidade de estados de mar em oposição às medições individuais das boias ondógrafo.

Na segunda secção deste trabalho, as medições obtidas pelos radares HF foram validades e aferidas com recurso a um sinal combinado obtido através da junção dos dados de várias boias ondógrafos. Consequentemente, os dados do radar HF de Sagres foram comparados tendo por base um sinal composto pelas medições da boia costeira de Sines e pelas medições das boias *offshore* e costeira de Faro enquanto que, o radar HF de Alfanzina foi comparado com um sinal composto pelas medições das boias de Faro. Este tipo de abordagem foi primariamente considerado para o período de 1 a 24 de Abril de 2018 e foi posteriormente estendido para o período de 1 de Janeiro a 24 de Abril de 2018.

Os dados obtidos entre os sistemas de medição foram validados recorrendo-se a diagramas de dispersão e respetivos ajustes lineares, ao passo que a aferição da sua qualidade foi estudada com base na representação das respetivas séries temporais, da representação das distribuições direcionais de energia medidas por ambos os sistemas de medição, através de diagramas de dispersão para o erro relativo calculado, por representação em histogramas dos parâmetros medidos quer pelos radares HF que pelas boias ondógrafo e através da elaboração de histogramas direcionais (“rosa-das-ondas”), sendo que estes dois últimos métodos foram apenas aplicados para o período temporal mais extenso. Como teste final para a validação das medições de radar HF, um teste de Kolmogorov-Smirnov (K-S) com base na hipótese nula e com um nível de significância de 1% foi aplicado às séries temporais obtidas por ambos os sistemas de medição.

Deste modo foi concluído que as séries temporais obtidas pelo radar HF de Sagres para os parâmetros de SWH e MWD podem ser validadas com recurso a um sinal combinado obtido por medições da boia costeira de Sines e das boias *offshore* e costeira de Faro.

Quando consideradas as medições de MWP obtidas por estes dois sistemas de medição, o facto de os parâmetros dos ajustes lineares de MWP serem semelhantes entre os dois períodos temporais, permite reforçar a precisão e coerência das medições de MWP efetuadas pelo radar HF Sagres. No entanto, devido à não concordância entre as séries temporais obtidas pelos dois sistemas de medição e

devido a que o diagrama de dispersão das medições de MWP não mostrar uma clara relação linear, faz com que as medições deste parâmetro não sejam consideradas válidas para o radar HF de Sagres.

Em relação às medições de SWH obtidas quer pelo radar HF de Alfanzina quer pelo sinal combinado das medições das boias de Faro, foi possível verificar que existe uma boa concordância entre as séries temporais de SWH obtidas por estes sistemas sendo ambos os testes K-S aplicados aceites para o período de 1 a 24 de Abril de 2018. Com base nos resultados obtidos, foi considerado que os valores de SWH medidos pelos radares de HF de Alfanzina são válidos e podem ser validados com base nas medições de um sinal combinado obtido por medições das boias *offshore* e costeira de Faro.

Considerando os dados de MWD obtidos pelo radar HF de Alfanzina, é possível verificar que estes não são corretamente descritos pelos valores de MWD medidos por um sinal combinado das boias *offshore* e costeira de Faro. Nomeadamente através das análises das distribuições direcionais de energia média obtidas para cada um dos sistemas de medição, é possível verificar que parte do sinal de MWD medido pelo radar HF de Alfanzina não é detetado por este sinal combinado, respetivamente para medições de MWD no intervalo de 90º a 150º. Assim, é necessária uma análise mais profunda aos dados de MWD obtidos por este radar HF de modo a validar este tipo de medições.

O facto de que os parâmetros dos respetivos ajustes lineares de MWP entre os dados obtidos pelo radar de Alfanzina e pelo sinal combinado não serem constantes ou pelo menos semelhantes entre as duas séries temporais consideradas assim como uma sobrestimação dos valores medidos pelo radar, faz com as medições de MWP efetuadas por este radar sejam consideradas como não validas.

Relativamente aos limites mínimos e máximos teorizados para as medições de SWH pelos radares HF em função das suas frequências centrais, foi verificado que o radar HF de Sagres não é capaz efetuar medições de SWH de 0.5 m (limite mínimo teorizado) detetadas no entanto por todas as boias ondógrafo utilizadas para a sua validação, sendo o seu valor mínimo de medições de SWH de 1 m. Quanto ao comportamento do radar HF de Alfanzina em relação a este limite, foi verificado que o funcionamento deste radar se encontra de acordo com este valor, sendo o mesmo capaz de efetuar medições de SWH de 0.5 m. Em relação ao limite máximo teorizado (7.07 m), não foram verificadas ocorrências de valor de SWH iguais ou superiores a este valor máximo em nenhuma das séries temporais estudadas, quer dos radares HF quer obtidos pelas boias ondógrafo e como tal, não foi retirada nenhuma conclusão acerca do funcionamento dos radares perante este limite máximo de SWH.

Foi ainda verificada a existência de um limite mínimo para as medições de MWP para o radar HF de Sagres, sendo que a única informação sobre os valores limites de MWP encontrada na bibliografia foi referida por Lipa and Nyden (2005), sem ser referida qual a razão destes limites de MWP.

A partir dos resultados das distribuições direcionais de energia e das rosa-das-ondas obtidos para ambos os sistemas de radar HF estudados, verificou-se a existência de estados de mar bastante energéticos associados a MWD originárias da costa. Uma vez que quando colocada a hipótese de dados da range-cell média se considerar que as medições de radar são efetuadas numa dada coroa circular situada a 15 km da costa, foi concluído que esta distância é demasiado reduzida para a geração de estados de mar tão energéticos através de vaga e como tal este tipo de medições obtidas pelos radares foram consideradas como pouco prováveis.

Por fim, o facto de as rosa-das-ondas elaboradas para os radares HF representarem direções médias de estados de mar semelhantes aos histogramas direcionais climatológicos obtidas por Costa *et al.* (2001) para as regiões de Sines e de Faro, serve de suporte à validade e qualidade das medições de MWD por parte dos radares HF assim como ao seu abrangente angulo de medições de estados de mar.

Palavras-Chave: Oceanografia; Costa Algarvia; Agitação Marítima; Radares HF; Teses-Mestrado 2019.

Abstract:

The aim of this study was to validate and evaluate the quality of the data collected by CODAR SeaSonde HF radar systems (central frequency 13.5 MHz) located on the Algarve shore, with respect to their measurements of significant wave height (SWH), mean wave period (MWP) and mean wave direction (MWD), using, as a reference, several ODAS (Ocean Data Acquisition System), (Meindl (1996)) buoys moored at different locations.

This work is divided into two main sections. First, HF radar measurements were validated individually using single ODAS buoys systems. The Sagres HF radar system was tested with measurements performed by either the Sines coastal, Faro offshore or Faro coastal buoys whereas the Alfanzina HF radar system was assessed with measurements by either the Faro offshore or the Faro coastal buoys. Posteriorly, HF radar measurements were validated with data retrieved by a combined signal composed of measurements performed by each buoy system. Namely, the Sagres HF radar system was tested using a combined signal composed of measurements performed by both the Sines coastal and Faro offshore and coastal buoys, whereas the Alfanzina HF radar system was assessed with a combined signal composed of measurements by both the Faro offshore and coastal buoys. All the measuring systems used for this study as well as their retrieved data are managed by the Portuguese Hydrographic Institute (Instituto Hidrográfico).

The first section of this work was applied to a 24 days period in April 2018, namely from the 1st to the 24th of April and the second section of this work was firstly assessed for the same temporal period in April 2018 and was subsequently extended for a larger time-series ranging from the 1st of January to the 24th of April 2018.

It has concluded that as HF radar performs measurements of the sea-surface within a given range-cell around the radar site, for sea-regions of sea-bimodality, its measurements should not be validated using a single buoy but instead, a system composed of ODAS buoys subject to the same sea-states as captured by the HF radar should be considered.

The SWH and MWD time-series obtained by Sagres HF Radar showed a significant agreement with the combined signal composed by both Sines coastal and Faro offshore and coastal buoys. However, the MWP time-series did not show a good agreement with the combined signal and further work should be performed to understand how the MWP is retrieved from the HF radar measurements.

As for the Alfanzina HF radar system, the retrieved SWH time-series was similar to the combined signal from the Faro offshore and coastal buoys. However, for the MWP and MWD time-series the same could not be observed. The Alfanzina HF radar MWP showed good agreement with the combined signal for the first temporal period but not for the extended period. The MWD retrieved by the Alfanzina HF radar was not significantly similar to the combined signal for both the time periods. It is hypothesized that the combined signal fails to describe the North-Westward sea-states, which might be detected by the HF radar.

The theoretical limits for the SWH retrieved by the HF radar systems were also investigated. It was concluded that, for both the HF radar systems considered, neither of the retrieved values were equal or superior to the higher theoretical limit presented by Lipa and Nyden (2005). As for the lower SWH limit it was found that the Sagres HF radar limit was not able to retrieve SWH values lower than 1 m, whereas the Alfanzina HF radar system was capable of accurately measuring SWHs of 0.5 m, in agreement with the lower SWH limit described in the literature (Saviano *et al.* (2019)).

It was verified that the Sagres HF radar system was not capable of retrieving MWP values lower than 6 s. This limit values of MWP measurements should be further investigate particularly by verifying the method of MWP retrievals.

Furthermore, it was verified that both the HF radar systems showed very energetic signals associated with MWD from shore, which was considered suspicious, although similar behaviour was described in Liu et al. (2011), although these authors do not comment the occurrence such wave measurements.

The directional histogram plot (*waverose*) showed that the MWD from Sagres and Alfanzina agree with the climatological sea-states obtained for Sines and Faro (Costa *et al.* (2001)). The *waverose* for the Sagres HF radar showed a combination of the climatological sea-states obtained for Sines and Faro while the *waverose* for the Alfanzian HF radar is similar to the climatological results for Faro, with both of these results being valid for the more extended time-series, thus further supporting HF radar MWD measurements.

As a final statement, the author would like to acknowledge the internship at Instituto Hidrografico from which this dissertation bloomed as a result.

Key-Words: Oceanography, Algarve Coast; Surface-Waves Monitoring; HF Radar; Master-Thesis 2019.

Table of Contents:

List of Figures and Tables:

1 Introduction:

1.1 Overview and Motivation:

Present relations between society, economics, and the environment have exposed the thin link between a sustainable future and the possible alteration of the planet Earth's dynamical systems (Ocean and Atmosphere) as we have known them (Peixoto and Oort, 1992). Regarding that the world oceans cover about 72% of the Earth's surface representing a fundamental ecosystem for marine and land beings and that 10% of the world population lives in coastal areas that are less than 10 meters above sea level (Small and Nicholls, (2002), Gordon *et al.*, (2007)) and also when considering that the oceans serve as massive heat (Trenberth and Solomon, 1993) and anthropogenic CO_2 sinks (Raven and Falkowski, 1999) a better understanding of these systems becomes crucial for the planet future and species conservation.

Also, concerning the current state of art of the renewable energies systems (Narula, 2018), one can recognise that the characterization of local oceanic coastal processes such as surface currents and wave properties will have a significant impact for tidal current energies systems and offshore wind farms to reduce risk associated with these business sectors and to increase their energetic efficiency. Prior to that, it is also important to ensure the safety of the coastal population from possible hazards and extreme events and once again, the characterization of coastal waters is of major concern.

Regarding the exposition above, there is the need for near real-time monitoring systems capable of measuring not only sea-surface currents but also capable of performing wave characterization measurements to achieve local maps of the sea-surface at a given time and location. Several oceanic remote sensors can be used to achieve this task, but a few can be considered as multivalent as HF radar systems which in turn can be used to perform measurements of several physical parameters as sea-surface currents, wave properties, and wind direction and also have the benefits of being an either onshore or offshore system.

Hence, the validation of the Algarve HF radar systems network was chosen as a MSc degree thesis in geophysical sciences field of physical oceanography and meteorology in order to support future sea surface studies for oceanic renewable energies application, for a more precise monitoring of the sea-surface aiming for the safety and well-being of people habiting coastal regions, a more secure and planned nautical navigation and fisheries and also due to a deeper curiosity to understand offshore and coastal oceanic processes.

1.2 State of the Art HF Radar Systems:

High Frequency (HF) radar systems typically exploit the interactions between the sea-surface and high frequency electromagnetic waves (typically between 5-20 MHz) to obtain in near real-time measurements of the sea-surface currents (top 2 m of the water column and as far as 200 km offshore depending on the working frequency) and several wave properties such as significant wave height (SWH), mean wave period (MWP) and mean wave direction (MWD) up to 35 km offshore with resolutions ranging from 0.5 km up to 3 km leading to the characterization of the fundamental sea conditions at any given time and location.

Interactions between sea waves and HF electromagnetic waves have been known and studied for more than sixty years now (Crombie 1955 and Wait 1966). Sea surface currents methods were theorized by Teague (1971), developed by Barrick (1976) and have already been validated by several teams and authors (Essen *et al.* 1984, Teague 1991) for different locations and radar sites around the world. As for wave characterization methods, although reeling on a robust mathematical theory (Barrick 1977) they are still under development (Lipa and Nyden 2005) with several validating efforts being carried by a variety of research groups (Liu *et al.* (2010), Lorente *et al.* (2015)) and will constitute the principal focus of this work.

HF radar systems measurements depend on numerous external factors, such as atmospheric and oceanic conditions, antenna location, electromagnetic noise around the radar site and the type of the radar antenna (either direction-finding antennas or beam-forming antennas) (Huang and Gill, 2019) which hinders the task of validating its measurements for a long time series of data and for several radar sites at once.

The wave measurement retrievals are based on the principle that sea surface waves act as a Bragg scattering grating for the electromagnetic radar waves (Crombie 1955; Lipa and Nyden 2005). This means that interaction between electromagnetic waves and sea waves that are moving in a radial path either away or towards the radar site with wavelengths that are exactly half of the wavelengths of the electromagnetic waves result in scattered electromagnetic waves with the same wavelengths as the sea wave traveling in the same radial direction as the initial electromagnetic wave. Since these electromagnetic waves have the same temporal and spatial coherence, they interact constructively and as a result, a peak of energy is detected in the HF radar system spectra.

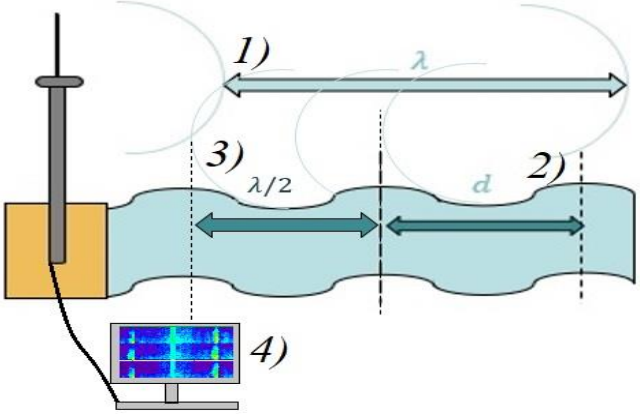

Figure 1.01: HF radar working principle schematics: 1) A pulse frequency modulated electromagnetic wave with a given central frequency is generated by the HF radar system. 2) The electromagnetic wave interacts with the ocean waves that have a wavelength that is half of the wavelength of the electromagnetic wave traveling in the radar radial direction and Bragg scattering occurs. 3) As a result of Bragg scattering, an electromagnetic wave with the same wavelength as the ocean waves are scattered. 4) Due to constructive interference of scattered electromagnetic waves, an energy peak is detected in the HF radar spectra and hence the ocean variance density spectrum can be rebuilt from the 1st and 2nd order spectrum maxima. Here λ is the electromagnetic wave wavelength and d is the sea-wave wavelength.

As definition of a radar measurement (the reason between the energy of the emitted electromagnetic wave and the received wave), it is thus possible to retrieve sea-surface current properties from the 1st order maxima (Barrick, 1972), (Stewart and Joy, 1973) and thus reconstructing the ocean variance density spectrum due to the Doppler frequency shift of this maxima, representing a positive shift in the frequency if the sea current is moving towards the HF radar antenna or in a negative Doppler shift if it is moving away from the HF radar antenna.

As for wave properties, they are retrieved from the 2nd order maxima of the radar spectra (Barrick, 1977) through the same reconstruction of the ocean variance density spectrum, using either an integral inversion method or a least-square fitting method (Lipa and Nyden, 2005), being these maxima due to the Bragg scattering associated with a Doppler frequency shift and once again increasing the maxima frequency if the wave is moving towards the radar antenna and reducing the maxima frequency if the wave is moving away from the radar antenna.

Posterior to the retrieving of sea surface currents parameters and SWH, MWP and MWD regarding a given wave-set characterization, methods for the correction of possible direction angles errors (MWD parameters) due to deviations in the antenna pattern from an ideal pattern can be considered and implemented via a software correction (Lipa and Barrick, 1977), (Wyatt and Liakhovetski, 2003) and (Paduan *et al*., 2006).

1.2.1 Physical Limitation of the Sea-States Measured by the HF Radar Systems:

Since that, a significant part of the energy measured in the HF radar spectrum is due to the interactions between the radar electromagnetic waves and the sea-surface waves it is possible to define a limiting value for the SWH parameter since this parameter is related to the square of the total mechanical energy of a given sea-state (Calisal (1983)). Lipa and Nyden (2005) showed that a saturation value for SWH (H_{sat}) can be related to the electromagnetic wave number, k_0, meaning that for sea waves with an SWH value higher than H_{sat}, the HF radar spectrum is saturated and thus the retrieving of wave properties is impossible. H_{sat} can be computed from the following relation (Lipa and Nyden (2005)):

$$H_{sat} = \frac{2}{k_0} \quad (1.01);$$

It is also present by Saviano *et al.* (2019) that there is a minimum SWH value of 0.5 m from which lack of energy in the radar spectrum occurs resulting in a low signal-to-noise[1]ratio for the retrieving of wave properties from the second-order maxima in the HF radar spectrum and thus making it impossible to retrieve SWH values lower this value.

1.2.2 Water Depth Assumption:

When accounting for the minimum necessary water-depth for the good retrieving of HF radar measurements, Lipa and Nyden (2006) presented the following relation.

$$\frac{2\pi d}{L} > 0.8 \quad (1.02);$$

Where d is the water depth at a given location and L is the wavelength of the dominant oceanic wave.

Using the following relation valid for a monochromatic wave, it is possible to determine the central wavelength λ of a given electromagnetic wave pulsed by a given HF radar system:

$$\lambda = \frac{c}{f} \quad (1.03);$$

Where c is the propagation speed of the electromagnetic wave in vacuum and f the HF radar central frequency.

Thus, recalling the Bragg principle, from which it is expected for the HF radar generated electromagnetic waves to interact with the oceanic waves that have a wavelength that is half of the wavelength of the initial electromagnetic wave (see section 1.2), a value for the dominant oceanic wave wavelength can be exploited from the next relation:

$$L = \frac{\lambda}{2} \quad (1.04);$$

Substituting equation 1.04 into equation 1.02 one arrives to the water depth limit for HF radar wave measurements given by the following relation:

$$d > \frac{0.2\lambda}{\pi} \quad (1.05)$$

[1] By signal-to-noise ratio it is meant the power of a given signal divided by the power of the noise imposed on the respective retrieved signal. In this study, the considered signal and its respective noise are of electromagnetic nature.

1.3 HF Radar Systems in Continental Portugal:

In Continental Portugal, there are five HF radar systems constituting two HF radar networks: The Lisbon district network and the Algarve network. These networks are managed by the Portuguese Hydrographic institute (Instituto Hidrográfico) where their data is used to produce hourly sea-surface current maps for the two network regions.

Figure 1.02: HF radar network in Continental Portugal: Lisbon district and Algarve shore network. Image from hidrografico.pt @ 18/06/2019

The location of the radar systems comprise a variety of topographic condition ranging from an open sea site (Forte S.Julião) to promontory (Cabo Espichel, Cabo de Sagres and Farol de Alfanzina) to a beach site with a vast sand area (Monte Gordo) which in turn, results in a specific tuning of the radar system for each specific location and sea-state.

Figure 1.03: HF radar systems sites in Continental Portugal: top left, Forte S.Julião; top right, Cabo Espichel; Bottom left, Cabo de Sagres and bottom right Farol de Alfanzina. Images from Google Images.

Figure 1.04: HF radar system site in Monte Gordo, Portugal. Image from Google Images.

The data retrieved by these HF Radar Systems is used for several projects such as the *MyCoast Project* where in association with several onshore and offshore systems contributes to build a coordinated Atlantic Coastal Operational Observatory in the Atlantic area.

1.4 ODAS Buoys as Comparison Systems:

For the validation of the HF radar systems measurements, it was used as comparison parameters the data retrieved from three differently located ODAS buoys (see figure 2.01 for the location of the buoys) subjected to different sea-states.

This network of ODAS buoys is composed of two coastal buoys (*Faro Costeira* and *Sines Costeira*) and one offshore buoy (*Faro Oceânica)* and their data are managed by the Portuguese Hydrographic Institute. The data from these buoys is outputted in 30 minutes or 60 minutes sets. All the data acquired by the buoys were obtained using the spectral method, where an FFT (Taft, 2004) was applied to the accelerometers data onboard the buoys to reconstitute the wave spectrum (variance density spectrum).

1.5 Expected Sea-States in the West and South Coast of Continental Portugal:

According to Costa *et al.* (2001), who characterized the Portuguese sea-states using historical data (May 1988 – December 2000 for the Sines region and September 1986 – December 2000 for the Faro region) retrieved from different ODAS buoys systems, it is possible to identify at least three main oceanic regions for Continental Portugal namely, Figueira da Foz, Sines and Faro. For the current study the Figueira da Foz region will not be considered due to distance from the HF radar network in Algarve. Nevertheless, this location should be considered in future radar network studies.

Costa *et al.* (2001) described a mean value of SWH of 1.7 m for Sines and of 1 m for Faro with standard deviation values of 0.9 m and 0.6 m respectively. The percentage of SWH values bigger than 3 m meters was 22 % for Sines and 2 % for the Faro.

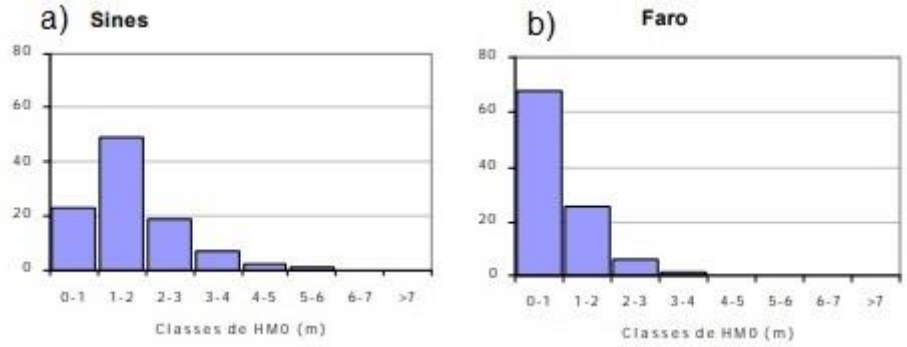

Figure 1.05: SWH (m) histograms for two different sea-states in Portugal: a) For the Sines region, representing South-Eastward, Eastward and North-Eastward sea-states and b) For the Faro region, representing North-Eastward, Northward, North-Westward and Westward sea-states. From Costa *et al.* (2001).

As for the MWP parameter, it was observed a mean value of 6.6 s for the Sines region and a mean value of 4.7 s for the Faro region with standard deviation values of 1.8s and 1.1s respectively. Values of MWP superior than 9 s represent less than 20% of the MWP distribution for the Sines region and for the Faro region MWP values superior than 7 s represent less than 4% of its distribution.

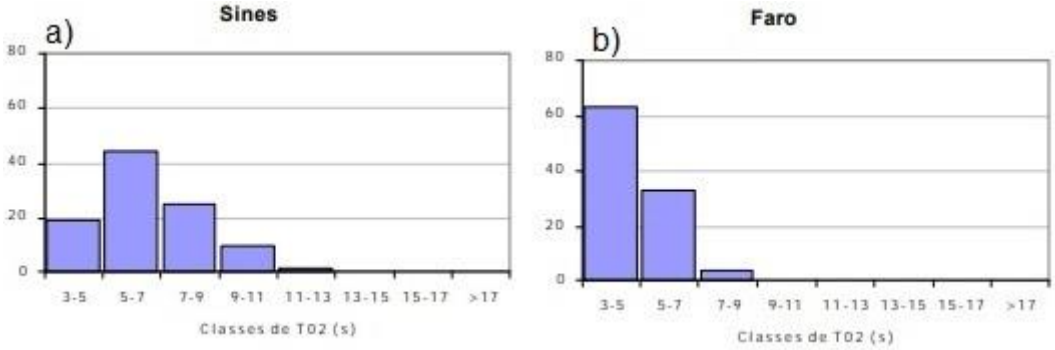

Figure 1.06: T_m (s) histograms for two different sea-states in Portugal: a) For the Sines region, representing North-West, West and South-West sea-states and b) For the Faro region. From Costa *et al* (2001).

For the θ_{Tp}[2] (direction at peak) parameter, Costa *et al.* (2001) showed that in Sines 97 % of the observations are composed from sea-states with South-Eastward and Eastward main directions and that events from South-West represent less than 3 % of the occurrences.

As for the Faro region, Costa *et al.* (2001) identified two dominant sea-states, one composed from the North-Westward and Westward direction corresponding to 26.7 % of the observations, and the other from the East, South-East and South directions, corresponding to 72.6 % of the observations (Figure 1.07.b).

[2] Different than the mean wave direction (MWD) → The mean wave direction, θ_m, is defined as the mean of all the individual wave directions in a time-series representing a certain sea state whereas θ_{Tp} (Costa *et al.* used the TH_{Tp} notation) represents the direction associated with the waves with a maximum energy peak.

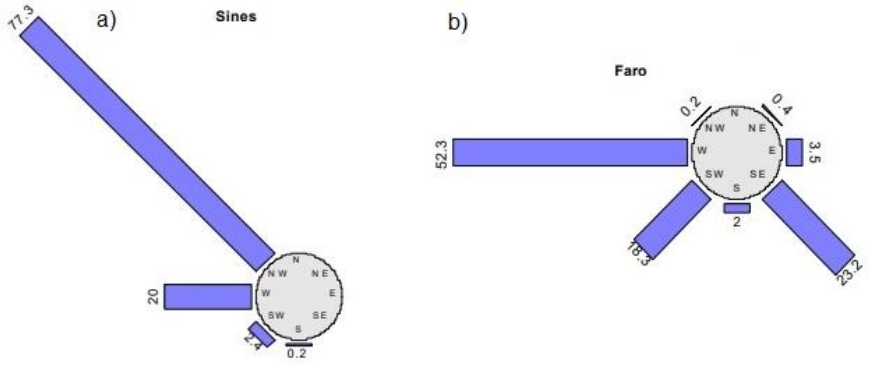

Figure 1.07: θ_{Tp} parameter directional histogram for two different sea-states in Portugal: a) For the Sines region, representing North-West, West and South-West sea-states and b) For the Faro region. From Costa *et al*. (2001).

This differences in θ_{Tp} between Sines in the West coast and Faro in the South coast are due to the morphology of the Portuguese coast. The latter is unaffected by the North-Western sea-states while Sines is unlikely to capture the East and South-Eastern sea-states forced by easterly wind events (*"Ventos de Levante")* that can be observed in the South Coast. The North-Eastward and North components may be observed in both regions and might be due to swell propagating from the Equatorial Atlantic Ocean (Costa *et al.*, 2001)).

Also, due to the two-dominant sea-states identified for the South coast, Costa *et al*. (2001). identified that the peak period (T_p) parameter depends on the wave-set direction and that this relation is due to the fact that the two-dominant sea-states have different genesis zones (Costa *et al*. (2001)), being the higher values of T_p associated with West and South-West sea-states. Wave-sets from the South-East direction represent T_p values that are most of the time inferior to 11 s. According to the authors, more frequent observations for the South coast are associated to H_s values inferior to 1m and T_p values inferior to 11 s. $H_s$values higher than 3 m results most often from the South-West direction.

1.6 Main Objectives and Thesis Structure:

The main goal of this thesis was firstly to create a methodology suitable for validating the Algarve HF radar systems wave measurements and to assess the quality of their measurements. It was also set as a goal to identify the most suitable oceanic conditions for the good functioning of HF radar system to perform high quality and reliable wave measurements as well as to identify the physical limitation of these systems and to verify them with the actual HF radar theory.

In terms of its structure, this thesis was composed by a general introduction where the state of the art concerning the basic theoretical knowledge about HF radar measurements was presented. It was also showed in this section the location of the two principal HF radar networks in Continental Portugal. Furthermore, the ODAS buoys systems were used to validate and to assess the HF radar wave measurements are presented. It was lastly shown in the introductory section, the main expected sea states in Continental Portugal studied from climatological data.

Subsequently, in the Data and Methods sections the range of measurements and minimum necessary water depth for HF radar wave measurements were computed and shown. It is also presented in this section the wave parameters retrieved by both the HF radar and the ODAS buoys systems. The mean range-cell hypothesis is present and described in this section and there is also a section referencing to the difference of sampling frequencies between the two considered systems. As final remark of the data and methods section, it is presented the two comparison methods considered in this study as well as the validation and assessment tests performed and also, a description of the two considered time-series.

In the Results section, the results obtained when considering the two comparison methods are presented for each of the two considered HF radar sites. The first comparison method was only subjected to the shorter temporal period whereas the second comparison method was firstly validated considering the shorter temporal period and was posteriorly applied to the more extensive temporal period.

In the Discussion section the results presented in the Results section are discussed and assessed to decide if a given retrieved wave parameter by the HF radar systems could be validated or not and to understand the physical limits of the HF radar systems.

Lastly, in the Summary and Conclusion section, a brief summary of the discussed results is presented to further support the conclusions that were made. It can also be read in this section suggestion for future work concerning the HF radar wave measurements in order for deeper understanding of their working principle and measuring capabilities.

2 Data and Methods:

2.1 Description of the Algarve HF Radar Network:

The HF radar systems used in this study are CODAR SeaSonde (CODAR 2016) surface wave HF radar systems with main functioning characteristics described in table 2.01. Each HF radar systems works within a given angular aperture specifically defined for each radar location and can perform wave characterization (i.e. SWH, MWP and MWD measurements) within this defined angular aperture from a minimum radar range till the maximum radar range defined by its frequency. Furthermore, HF radar measurements are discretized into several radial steps creating a given set of range-cells. According to Huang and Gill (2019), the radial steps are defined by the HF radar central working frequency.

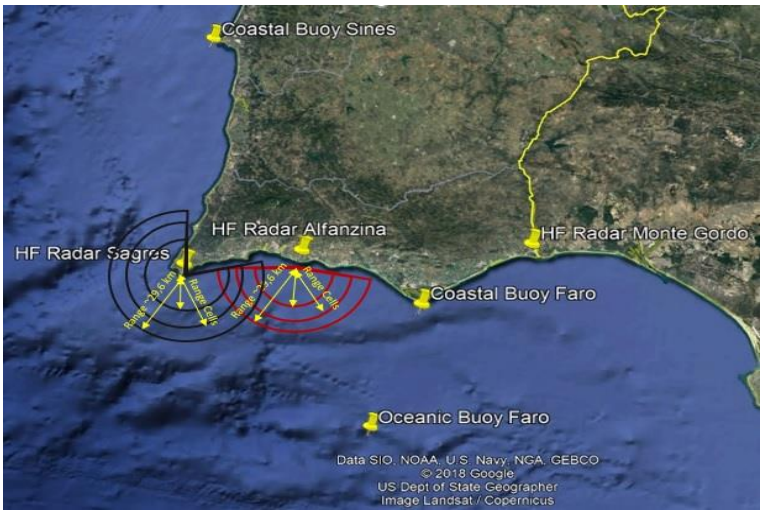

Figure 2.01: Algarve shore HF radar network and ODAS buoys systems used in this study. A descriptive HF radar range and range cell discretization are also represented for the Sagres and Alfanzina radar sites.

HF radar data is averaged and then made available in 10 minutes intervals for the wave-characterization data. The following table represents the fundamental working characteristics of the HF radar systems for the Algarve network.

Table 2.01: Description of the functioning characteristics of the HF radar composing the Algarve network.

	HF Radar Sagres	HF Radar Alfanzina	HF Radar Monte Gordo
Central Frequency (MHz)	13.5	13.5	12.5
Bandwidth Frequency (KHz)	80.9	80.9	99.3
Minimum Radar Range (Km)	3.71	3.71	1.51
Maximum Radar Range (Km)	29.67	29.67	22.67
Range-cell Resolution (Km)	1.85	1.85	1.51

From table 2.01, it is possible to verify that the Sagres and Alfanzina HF radars have a central frequency of 13.5 MHz and hence results from substituting these central frequency value into equation 1.01 a H_{sat} value of 7.07 m, indicating that SWH values around this limit should be interpreted with care.

Also, it was showed by Saviano *et al.* (2019) that SWH values lower than 0.5 m result in lack of energy in the radar spectrum occurs resulting in a low signal-to-noise ratio for the retrieving of wave properties from the second-order maxima in the HF radar systems spectrum and thus making it impossible to retrieve wave parameters from the radar spectrum.

Again, using this central frequency value concerning the Sagres and Alfanzina HF radar systems and substituting into equation 1.03 it is possible to compute the value of the central electromagnetic pulsed-wave wavelength λ and hence from equation 1.05 one arrives at a minimum necessary depth for HF radar wave measurements of $d > 1.465\ m$.

According to figure D.02 in Appendix D, where the Portuguese bathymetry is represented and regarding that the radar range cell resolution is of 1.85 km for each of the studied HF radar systems, it is possible to conclude that although the Portuguese bathymetry varies considerably within shorth spatial distance, the assumption of deep water for the Algarve HF radar network is met when taking into consideration the containment equation 1.05 for the minimum water depth required for HF radar wave-measurements. This means that there is no restrainment due to the water depth to discard the measurements performed by the closer to shore range-cells.

2.1.1 Note on HF radar systems studied:

From all the HF radar systems on the Algarve network, only data from the Sagres and Alfanzina radar sites was considered. This was due to the fact that vast sand area, as the one near Monte Gordo HF radar system (Figure 1.04), may act as an attenuator for the radar signal resulting in a low signal-to-noise ratio and thus causing erroneous and suspicious data.

The HF radar sea state data have a temporal resolution of 10 minutes while ODAS buoys data have a temporal resolution of either 30 or 60 minutes. Therefore, HF radar and the ODAS buoys data were rearranged to match their temporal resolution. To this end, the data were averaged into 4-hour time intervals for the first time period (1st to the 24th of April 2018) and were posteriorly averaged into 6-hour time intervals for the second period (1st of January 2018 until 24th of April 2018).

2.2 Wave Parameters Used for HF Radar Systems Validation:

To validate the measurements performed by HF radar systems the SWH, MWP and MWD values retrieved by these systems were compared with the values obtained by the ODAS Buoys systems[3] for the same temporal period.

2.2.1 Significant Wave Height:

The significant wave height is defined as the mean of the highest one-third of waves in the wave record and can be obtained based on the observation of i^{th} wave height from a N set of waves.

$$SWH = \frac{1}{N/3}\sum_{i=1}^{N/3} H_i \quad (2.01);$$

[3] Obtained by the ODAS buoys spectral method (see section 1.4).

Recalling Holthuijsen (2007), it is also possible to obtain the SWH parameter from the variance density spectrum regarding the relation for sea-states with a narrow wave spectrum and for a deep-water location:

$$SWH \approx 4\sqrt{m_0} \quad (2.02);$$

Where m_0 represents the 0th order moment of the variance density spectrum.

Since the potential energy of a surface wave is proportional to the square of its amplitude, the SWH assumes a crucial importance since it provides insight about the potential energy of a given wave set.

2.2.2 Mean Wave Period:

Th wave period is defined as the time interval between one zero-down crossing and the next. Statistically it is possible to define the mean wave period parameter (MWP) for a given wave-set with N waves, where $T_{0,i}$ is the wave period of the i^{th} wave-set as:

$$MWP = \frac{1}{N}\sum_{i=1}^{N} T_{0,i} \quad (2.03);$$

Again, recalling Holthuijsen (2007), the MWP can also be obtained from the variance density spectrum from the following relation:

$$MWP = \sqrt{\frac{m_0}{m_2}} \quad (2.04);$$

Where m_2 represents the 2nd order moment of the variance density spectrum.

According to Holthuijsen (2007) the value of m_2 is sensitive to small errors or variations in the measurement or analysis technique due to physical limitations of the sampling system when integrating the variance density spectrum and due to noise resulting from measurements that might be present in the variance density spectrum. Therefore, equation 2.04 should be used carefully considering the limit frequency of the sampling system and the noise in the measurements, particularly in the higher-frequency range of the spectrum.

2.2.3 Mean Wave Direction:

Mean Wave Direction, MWD, is defined as the mean of all individual wave directions in time-series representing a certain sea-state.

According to Kuik *et al.* (1988), there are several methods for retrieving the MWD parameter from the wave variance density spectrum reconstructed by several different sensing systems, namely the directional distribution method, the line moments method and the circular moments method.

Following the work Kuik *et al.* (1988), MWD information can be retrieved from the lowest order Fourier coefficients using the following relation (circular moments method):

$$MWD = \arctan\left(\frac{b_1}{a_1}\right) \quad (2.05);$$

Where a_1 and b_1 are the first Fourier coefficients for the even and odd Fourier series and can be deduced by the method derived by Lipa and Barrick (1983).

As for the ODAS buoys systems, MWD information is obtained by a FFT to the data retrieved by the pitch and roll sensors as described by Taft (2004).

2.3 Mean Range-Cell Hypothesis:

As mentioned before, HF radar measurements are discretized within range-cell intervals resulting in a radial resolution equal to the radar range-cell dimension. Following Huang and Gill (2019) the HF radar range cell resolution, ΔR, can be estimated for a pulsed HF radar system by the following relation:

$$\Delta R = \frac{c.\tau}{2} \quad (2.06);$$

Where c is the speed of propagation of an electromagnetic wave in vacuum and τ is the width of the radar pulse. A scheme of the HF radar range cell discretization can be seen in figure 2.01.

Since it was initially unknown which range cell was more suitable for the comparison with the ODAS buoys measurements a box plot of radar range-cells measurements grouped into 5 km distance intervals till the maximum radar range was made to compare the HF radar measured parameters with the ones retrieved by the ODAS buoys systems (as example see figure 3.04).

It was then hypothesized, that to reduce the high variability within each range-cell and to have achieve a compromise between the quality of the comparison within each measured parameter these range-cell sets should then be averaged to create a mean range-cell set for all the derived parameters.

Following Regan *et al. (2011)* this hypothesis assumes that the wave spectrum is homogeneous over a given radar range-cell and thus a cluster of range-cells can also be used as a parameter to quantify the wave refraction and diffraction phenomena at a given region, which for the present study was applied to the HF radar system in Sagres to assess the types of sea present at that location.

2.4 Equivalence of Sampling Rates:

HF radar systems have a temporal resolution output of 10 minutes while ODAS buoys systems have a temporal resolution output of either 30 or 60 minutes. This means that HF radar systems data had to be rearranged to match the temporal resolution of the ODAS buoys systems. To this end, the mean range cell data (see section 1.7 and section 2.1) from the HF radar systems and ODAS buoys measurements were averaged into 4 hours time-interval sets for the first temporal studied period ranging from the 1st to the 24th of April 2018 and were subsequently averaged into 6 hours time-intervals for the second temporal studied period covering from the 1st of January 2018 to the 24th of April 2018.

2.5 Single Buoy Method:

In this section of the current study, HF radar systems were individually tested against single ODAS buoys measurements for the SWH, MWP and MWD parameters. The Sagres HF Radar systems was individually compared with measurements performed by both the coastal buoy in Sines and with the offshore and coastal buoys from Faro whereas the Alfanzina HF radar system was individually tested only with the Faro offshore and coastal buoys.

2.5.1 Assessment Methods:

To test the similarity between HF radar and the ODAS buoys systems the SWH, MWP and MWD time-series retrieved by each system were plotted for the 1st of April to the 24th of April period. HF radar measurements were also compared against ODAS buoys measurements for the SWH, MWP and MWD parameters using a scatter plot while performing a linear fit to these data sets to assess the Pearson linear coefficient to exploit the linear relation that may exist between these measuring systems. It was also plotted for each measuring system a directional mean wave energy (MWE, see appendix C) distribution polar plot. Relative error scatter plots for each measured parameter were also created. RMSE, mean and standard deviation values were computed for each parameter retrieved by each of the studied measuring systems. Also, box-plots constituting of the measurements retrieved for each of the range-cells sets as well as for the mean range-cell set and their respective ODAS buoys system measurements were created regarding each of the retrieved wave-parameters (SWH, MWP and, MWD).

2.6 Combined Signal Method:

After the analysis of the single buoy method, it was considered as a hypothesis that the SWH, MWP and MWD signals retrieved by the HF radar systems are representative of several sea-states that occur around the HF radar site. Thus, a combined signal composed of measurements retrieved by several ODAS buoys subjected to the same sea-states as the HF radar was created. This hypothesis was mainly supported by the principle that HF radar systems perform measurements within a given angular sector and from the directional energy distribution plot for each of the measuring systems. To test this hypothesis, HF radar systems measurements were tested with the measurements attained by the combined signal. For the Sagres HF radar system, the combined signal was composed of measurements performed by the Sines coastal buoy and by the Faro offshore and coastal buoys. As for the Alfanzina HF radar system, the composed signal was constituted by measurements performed by both the Faro offshore and coastal buoys.

To build the combined signal a parameter, δ, was defined in a way that the buoy measurement that would be used for the building of the combined signal at a given instant would be the buoy that would minimize this δ value for a given retrieved parameter by the HF radar as described by the relation below:

$$\delta = \min(HF_{radar} - buoy) \quad (2.07);$$

With this method, it is hypothesized that the signal retrieved by a single HF radar is representative of several sea-states. This is due to the measurements performed by a given HF radar system being within a given circular sea area as described in section 2.1. Thus, it is expected for the signals retrieved by the Sagres and Alfanzina HF radar systems to be composed of the measurements performed by the ODAS buoys subjected to the same sea-states as these HF radar systems as shown by the following formulas.

$$HF_{Sagres} = A(t) * Sines_{coastal} + B(t) * Faro_{offshore} + C(t) * Faro_{coastal} \quad (2.08);$$

And;

$$HF_{Alfanzina} = D(t) * Faro_{offshore} + E(t) * Faro_{coastal} \quad (2.09);$$

Where A, B, C, D and E are some unknown coefficients that are function of time and of the retrieved parameter and, HF_{Sagres} and $HF_{Alfanzina}$ represent the value retrieved by each of the HF radar systems again for each of the retrieved parameters. When concerning with the mean values of A, B, C, D and E ($\langle A \rangle$, $\langle B \rangle$, $\langle C \rangle$, $\langle D \rangle$ and $\langle E \rangle$), one achieves to the relative occurrence coefficients.

The relative occurrence coefficients represent the number of times a given ODAS buoys system (i.e., the Sines coastal buoy or the Faro buoys) was used for the creation of the combined signal. It is

expected since the HF radar system measures within a given circular crown (see figure 2.01), that these relative occurrence coefficients translate into the relative frequency of occurrence of a given sea-state at the radar site. In particular, it is expected that the relative occurrence coefficients related to the Sines buoy represent the South-Eastward sea-states, the relative occurrence coefficients related to Faro offshore buoy represent North-Eastward/Westward sea-states and the relative occurrence coefficients related to the Faro coastal buoy represent the Westward sea-states.

Hence, the relative occurrence coefficients were defined according to the following formula:

$$Relative\ Occurence\ Coefficients = \frac{number\ of\ measurents\ given\ buoy}{total\ number\ of\ measurements} \quad (2.10);$$

Finally, it was considered as a hypothesis that as the studied time-series expands in time, the relative occurrences coefficients for the MWD parameter, should meet the climatological sea-states frequency present in Section 1.5, figure 1.07, due to the fact that these coefficients were hypothesized to be representative of the relative frequency of occurrence of its respective sea-states at the radar sites.

The combined signal comparison method was first applied for the first time period (from the 1st to the 24th of April 2018) and then extended to the longer period (from the 1st of January to the 24th of April 2018).

2.6.1 Assessment Methods:

Data sets were tested by plotting the time series of the HF radar measurements and its respective composed signal for the SWH, MWP and MWD parameters. Furthermore, a scatter plot for each of the measured parameter was elaborated from the combined signal versus the HF radar measurements, where a linear fit was performed to the datasets to assess the Pearson linear coefficient and to undercover a possible linear relation between these two-measuring systems.

MWE directional distribution plots were elaborated for the HF radar system and for the combined signal measurements regarding each studied of the considered temporal period. Relative errors scatter plots between the composed signal and the HF radar measurements were also computed for each of the retrieved parameters. Also, scatter plots were created to assess the contributions of each buoy to the composed signal and to determine which sea-condition drove the HF radar system for a given retrieved parameter.

Histograms of the measured values for each parameter were created to assess which buoy contributed more often to the composed signal and to assess the quality and range of the HF radar measurements. RMSE values for each retrieved physical property were computed for each radar location considering the composed signal as a reference, as well as the mean and standard deviation values. For the more extensive time-series analysis, the range-cell box plots were also elaborated and lastly, HF radar system measurements were compared with the climatological sea-states using SWH (*waveroses)* and MWP polar histograms.

A final Kolmogorov-Smirnov (K-S) test for goodness of fit (Massey, 1951), based on the null hypothesis with a significant level of 1% was applied to the HF radar data and the signal composed from several buoys for all the wave parameters described before. The goal of this test was to assess if the data from each signal was indeed due to the same physical phenomena (a given sea-state) or if the data sets were originated from different physical processes.

Lastly, a brief description of the computed parameters such as the relative error, standard deviation and mean values, RMSE, Pearson linear coefficient and MWE can be checked from appendix C.

3 Results:

3.1 Sagres HF Radar System:

3.1.1 Sagres HF Radar System Against Single ODAS Buoys Measurements:

In the following figures, it is presented the time-series of the SWH, MWP and MWD parameters retrieved by both the Sagres HF radar system, the Sines coastal buoy and the Faro offshore and coastal buoys for the temporal period ranging from the 1st to the 24th of April 2018 where the missing data for the Faro coastal buoys occurred for the 5th of April.

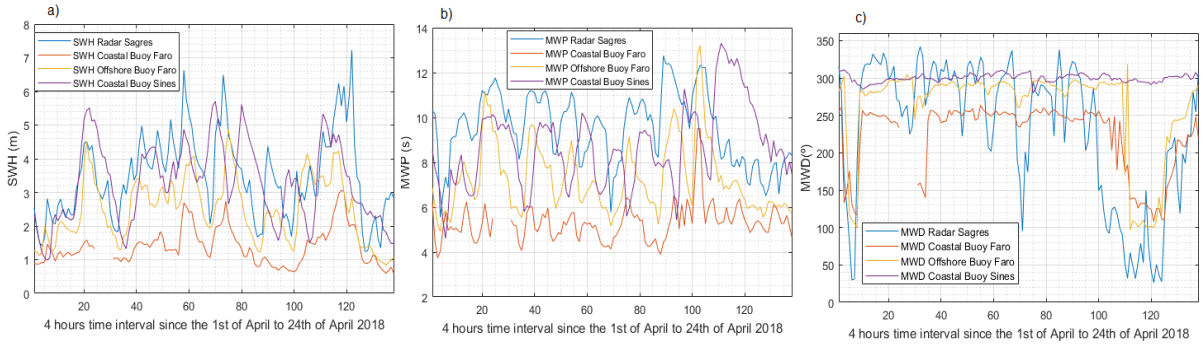

Figure 3.01: Time-series representation regarding the a) SWH, b) MWP and c) MWD parameters retrieved by the Sines coastal buoy (purple), the Sagres HF radar system (blue), the Faro offshore buoy (orange) and the Faro coastal buoy (red) for the 1st to the 24th of April 2018 period.

It is presented in the table 3.01 the mean, standard deviation, RMSE and Pearson linear coefficient values (presented in Appendix C), obtained by each of the measuring systems throughout the whole analysed period. The scatter plots computed when regarding the Sagres HF radar measurements versus the ODAS buoy measurements as well as its respective linear fit can be seen in Appendix A, figure A.01 to figure A.03 and table A.01 to table A.03.

Table 3.01: Statistical parameters computed for the SWH, MWP and MWD time-series retrieved by the Sines coastal buoy, Sagres HF radar system, the Faro offshore buoy and the Faro coastal buoy for the 1st to the 24th of April 2018 period.

	Sagres HF Radar	Sines Coastal Buoy	Faro Offshore Buoy	Faro Coastal Buoy
$\langle SWH \rangle$ (m)	3.46	3.28	2.49	1.38
$\langle MWP \rangle$ (s)	9.51	8.68	7.29	5.31
$\langle MWD \rangle$ (º)	230.54	299.76	260.5	221.63
σ_{SWH} (m)	1.25	1.19	0.97	0.55
σ_{MWP} (s)	1.56	1.77	1.57	0.83
σ_{MWD} (º)	94.03	5.57	61.25	46.85
$RMSE_{SWH}$ (m)	--	1.22	0.86	0.88
$RMSE_{MWP}$ (s)	--	2.45	1.04	1.49
$RMSE_{MWD}$ (º)	--	93.34	66.02	71.25
$Pearson\ Coefficient_{SWH}$	--	0.49	0.73	0.81
$Pearson\ Coefficient_{MWP}$	--	-0.11	0.78	0.35
$Pearson\ Coefficient_{MWD}$	--	0.09	0.71	0.70

The following set of figures represent the obtained results for the 1st to the 24th of April temporal period mean directional energy distribution retrieved for each of the measuring systems for the first analysed period during the month of April 2018 computed by the association of a given MWE value to its respective MWD and MWP values.

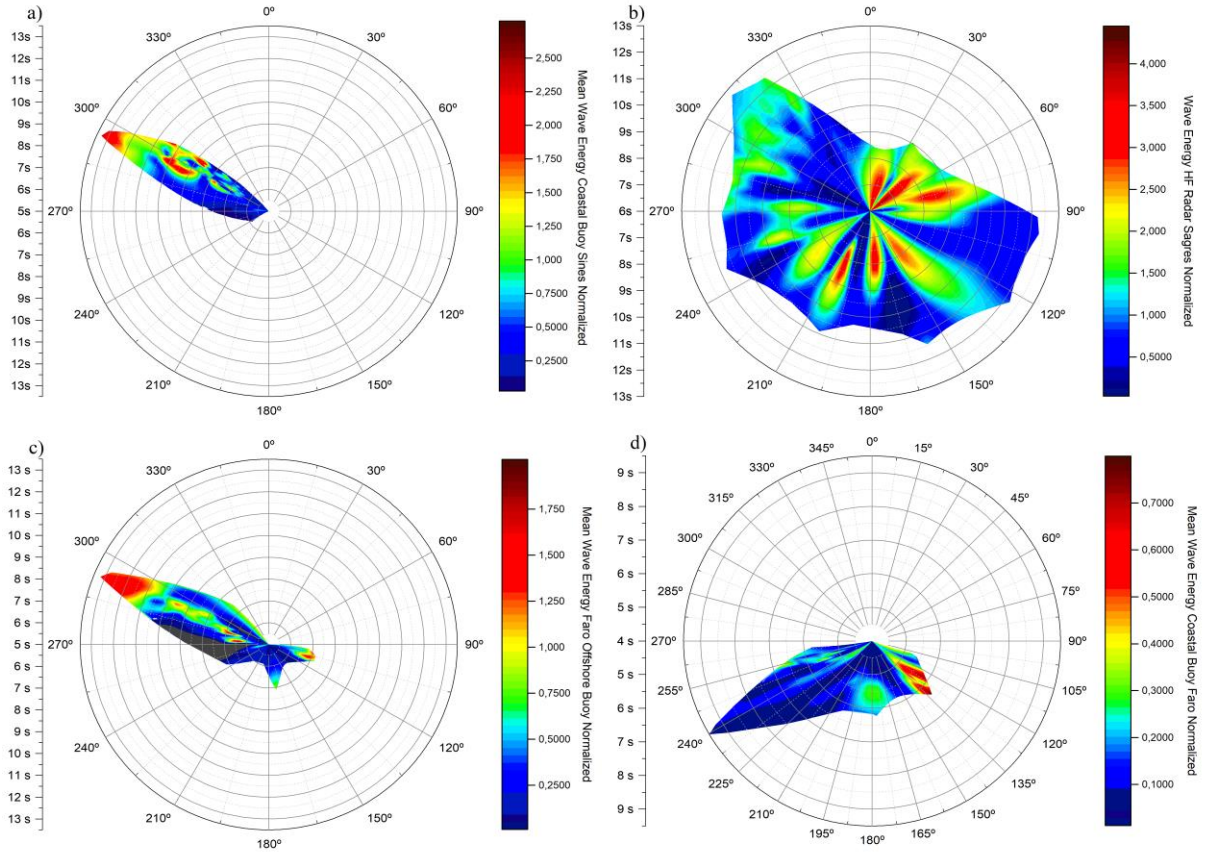

Figure 3.02: MWE directional distribution for the a) Sines coastal buoy, b) Sagres HF radar system, c) Faro offshore buoy and d) Faro coastal buoy concerning the 1st to the 24th of April 2018 period. The MWE polar plots are normalized by the mean MWE computed for the Sagres HF radar system.

It is presented below as the following scatter plots, the results obtained for the computation of the relative error values (explained in Appendix C) relative to the differences within the Sagres HF radar system and the Sines and Faro buoys in the sequence of this study.

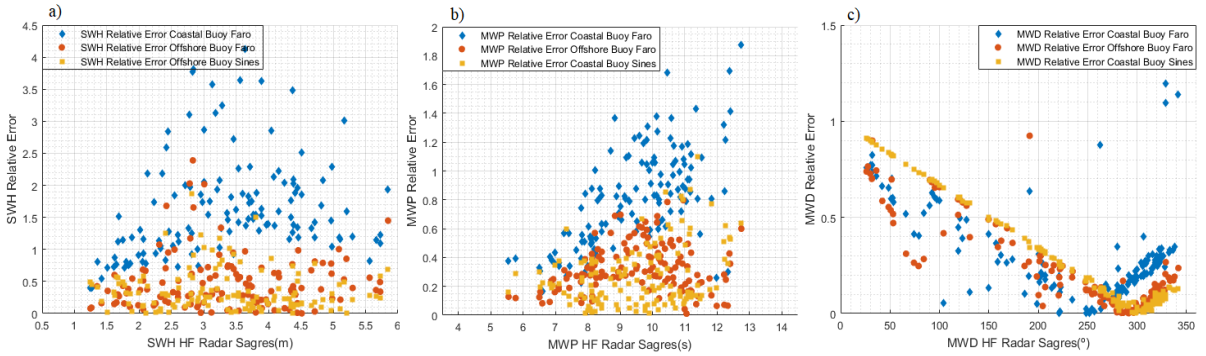

Figure 3.03: Relative error scatter plot for the a) SWH, b) MWP and d) MWD parameters computed for the measurements obtained within the Sagres HF radar and the Sines coastal buoy (orange), the Faro offshore buoy (red) and the Faro coastal buoy (blue) *versus* the measurements retrieved by the Sagres HF radar.

It is presented in figure 3.04 the results obtained for the HF radar range cell grouped values considering the mean range cell hypothesis discussed in section 2.3 for the SWH, MWP and MWD parameters. The range-cells sets were grouped into 5 km intervals from shore as 5-10 km, 10-15 km, 20-25 km and 25-30 km and assessed with the mean range-cell and the buoys measured values.

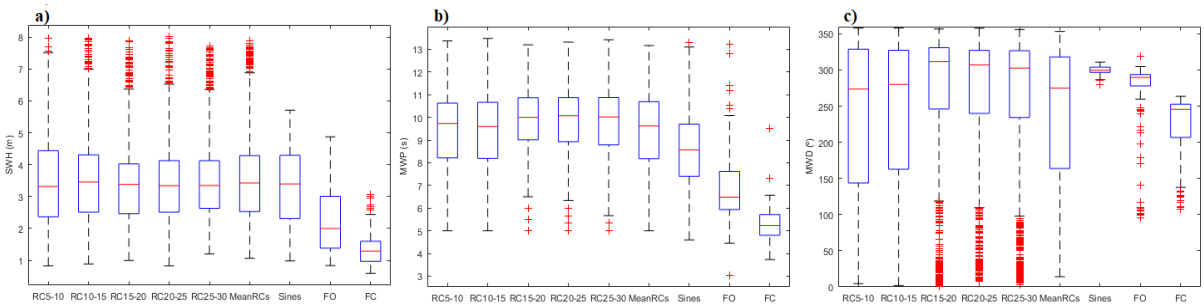

Figure 3.04: Box-plot diagram representing the measurements retrieved by each range-cells sets grouped into 5 km intervals, i.e. 5-10 km, 10-15 km, 15-20 km, 20-25 km and 25-30 km by the Sagres HF radar system concerning the a) SWH parameter, b) MWP parameter and c) the MWD parameter as well as the measurements attained by the mean range-cell hypothesis and the Sines coastal, Faro offshore and Faro coastal buoys for the 1st to the 24th of April 2018 temporal period.

3.1.2 Sagres HF Radar System Against Combined Signal Method Measurements From the 1st to the 24th of April 2018:

The following set of figures represent the results obtained for the comparison of measurements performed between the Sagres HF radar system and the combined signal resulting from measurements performed by the Sines and Faro buoys as described in section 2.6.

Figure 3.05 represents the obtained time-series for each retrieved parameter by either the HF radar system and the combined signal from several ODAS buoys measurements.

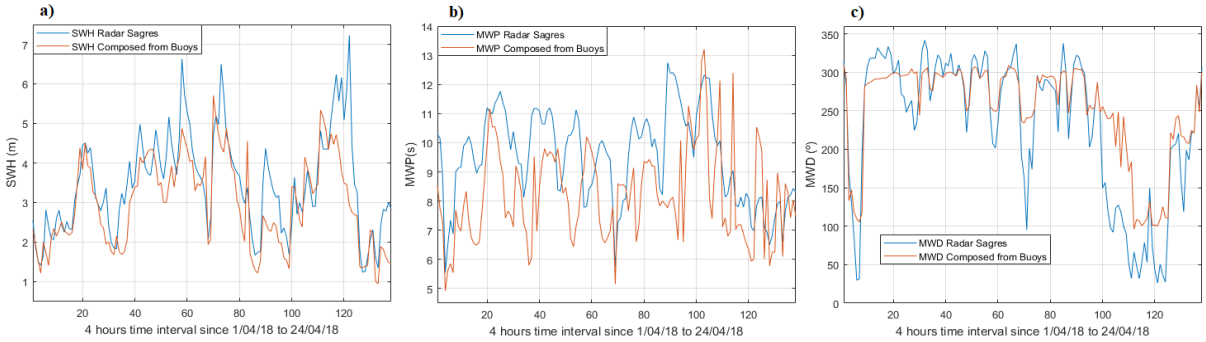

Figure 3.05: Time-series representation regarding the a) SWH, b) MWP and c) MWD parameters retrieved by the Sagres HF radar system (blue) and by the combined signal composed from measurements performed by both the Sines coastal and Faro offshore and coastal ODAS buoys.

Figure 3.06 represents the data scattering of values retrieved by the measuring systems where a linear fit was performed to each of these data sets as an attempt to assess a possible linear relation between the HF radar and the combined signal.

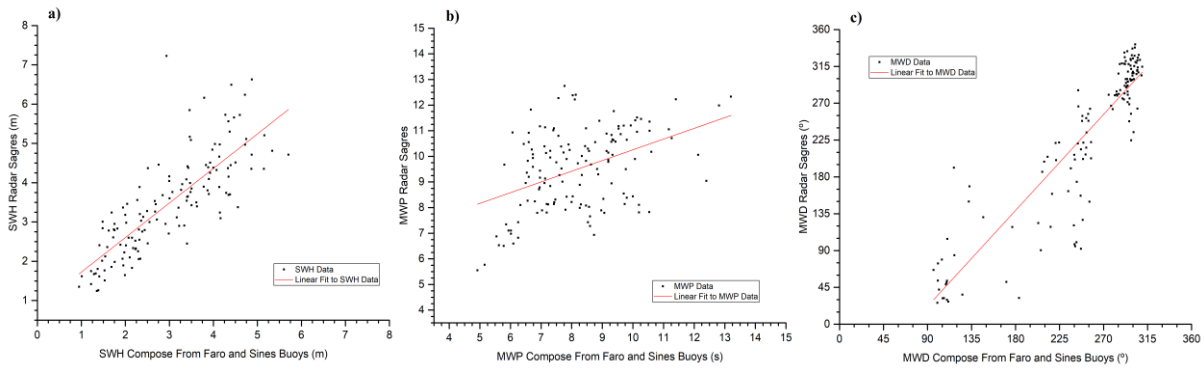

Figure 3.06: Scatter plot of the values obtained by the combined signal for the a) SWH, b) MWP and d) MWD parameters versus the values retrieved by the Sagres HF radar system from the 1st to the 24 of April 2018 temporal period.

Table 3.02 represents the linear fit parameters obtained when considering a possible linear relation between the Sagres HF radar system and the combined system for all the retrieved parameters.

Table 3.02: Linear fit parameters obtained when considering the SWH, MWP and MWD data retrieved by both the Sagres HF radar system and a combined signal composed of measurements performed by the Sines coastal and Faro offshore and coastal buoys, where m, b and r^2 represent respectively the slope the bias and the square of the Pearson linear correlation coefficient.

	SWH	MWP	MWD
m	0.88	0.42	1.30
Δm	0.06	0.08	0.05
b	0.85 (m)	6.07 (s)	-95.45 (º)
Δb	0.18 (m)	0.63 (s)	14.17 (º)
r^2	0.64	0.18	0.80

Table 3.03 summarizes the statistical properties of the retrieved data sets, namely the mean and standard deviation values, the accuracy of the HF radar system when testing its results against the results derived by the combined signal through the RMSE value and the *strength* of a linear relation within measuring systems using the Pearson linear correlation coefficient.

Table 3.03: Statistical parameters computed for the SWH, MWP and MWD time-series obtained by the Sagres HF radar system and by the combined signal from the 1st to the 24th of April 2018 temporal period.

	Sagres HF radar	Combined Signal
$\langle SWH \rangle$ (m)	3.46	2.98
$\langle MWP \rangle$ (s)	9.51	8.22
$\langle MWD \rangle$ (º)	230.54	250.25
σ_{SWH} (m)	1.25	1.14
σ_{MWP} (s)	1.56	1,60
σ_{MWD} (º)	94.03	67.80
$RMSE_{SWH}$ (m)	--	0.76
$RMSE_{MWP}$ (s)	--	1.68
$RMSE_{MWD}$ (º)	--	45.67
$Pearson\ Coefficient_{SWH}$	--	0.80
$Pearson\ Coefficient_{MWP}$	--	0.43
$Pearson\ Coefficient_{MWD}$	--	0.90

It is presented in table 3.04 results for the Kolmogorov-Smirnov test (see Appendix C) applied to the two measuring systems for each of the retrieved parameters assuming the standard null hypothesis.

Table 3.04: Results of the applied Kolmogorov-Smirnov test to the SWH, MWP and MWD data-sets attained by both the Sagres HF radar system and by the combined signal composed of measurements performed by the Sines coastal and Faro offshore and coastal buoys for the 1st to the 24th of April 2018 temporal period considering the standard null hypothesis with a significance level of 1%.

K-S test: HF Radar Sagres – Composed signal from Sines and Faro Buoys;	Result Null Hypothesis	P-value
SWH	Accepted	0.013
MWP	Rejected	$6.54 * 10^{-8}$
MWD	Rejected	$5.80 * 10^{-4}$

Figure 3.07 represents the MWE directional distribution results obtained for the Sagres HF radar system[4] and by the combined signal for the temporal period ranging from the 1st to the 24th of April 2018. MWE directional distribution plots were normalized respectively by the mean MWE computed for the Sagres HF radar system and by the mean MWE computed for the combined signal regarding the same temporal period to further investigate the MWD associated to a MWE maximum.

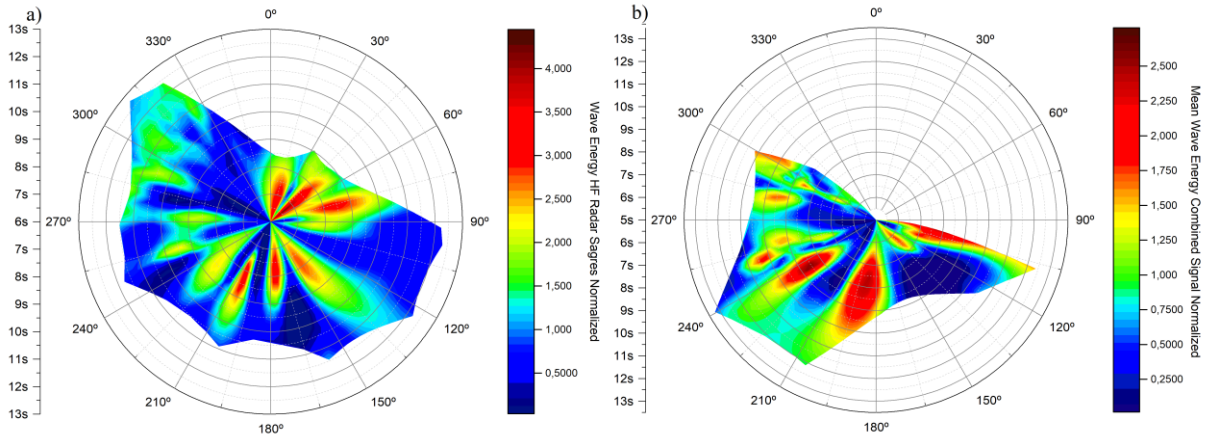

Figure 3.07: MWE directional distribution for the a) Sagres HF radar system and b) the combined signal composed of measurements performed by both the Sines coastal and the Faro offshore and coastal buoys concerning the 1st to the 24th of April 2018 period. The MWE polar plots are normalized by the mean MWE computed for the Sagres HF radar system.

The following figure represents the relative error values attained for each of the retrieved parameters retrieved by both the Sagres HF radar system and the combined signal.

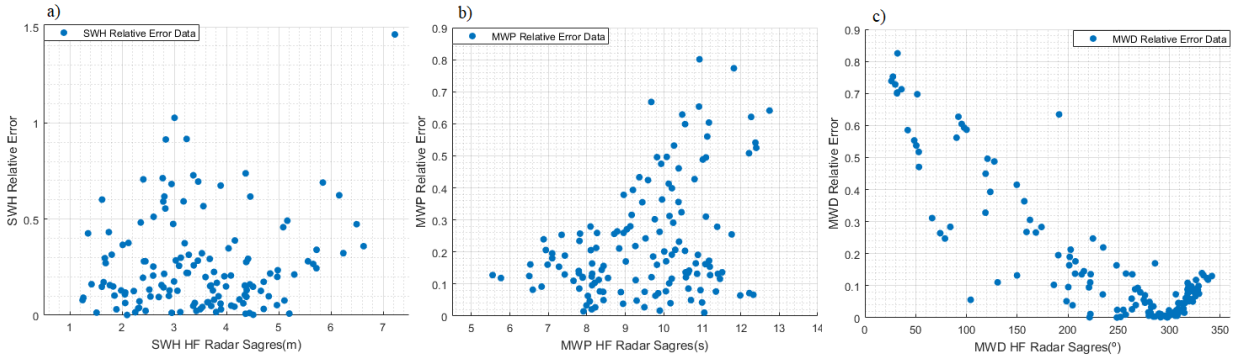

[4] The MWE directional distribution computed for the Sagres HF radar system concerning the temporal period from the 1st to the 24th of April 2018 is here presented again just for the sake of comparison with the MWE directional distribution computed for the combined signal regarding the same temporal period.

Figure 3.08: Relative error scatter plot for the a) SWH, b) MWP and d) MWD parameters *versus* the Sagres HF radar measurements. Relative error values were computed for the measurements obtained between the Sagres HF radar and the combined signal composed of measurements performed by the Sines coastal and the Faro offshore and coastal buoys concerning the 1st to the 24th of April 2018 temporal period.

Figure 3.09 shows the HF radar system time-series for each retrieved parameter and a scatter plot representing which buoy was used for the combined signal at a given point of measurements.

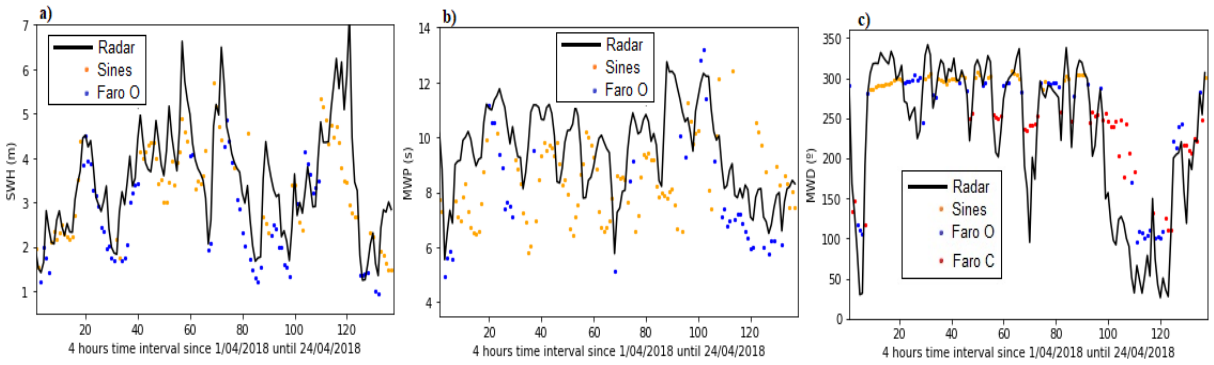

Figure 3.09: Representation of the attained times-series for the a) SWH, b) MWP and d) MWD parameters concerning the measurements retrieved by the Sagres HF radar system (black) and the buoy measurement used for a given measurement point for the composition of the combined signal, i.e. Sines coastal buoy (orange), Faro offshore buoy (blue) and Faro coastal buoy (red) regarding the temporal period from the 1s to the 24th of April 2018.

It is presented in the following table the relative occurrence coefficients for the contribution of each ODAS buoy for the combined signal for each retrieved physical parameter.

Table 3.05: Relative occurrence coefficients computed due to the relative contribution of each of the ODAS buoys for the composition of the combined signal regarding the SWH, MWP and MWD parameters.

Relative Occurrence Coefficients	Sines Coastal Buoy	Faro Offshore Buoy	Faro Coastal Buoy
SWH	0.56	0.44	0
MWP	0.72	0.29	0
MWD	0.33	0.35	0.32

3.1.3 Sagres HF Radar System Against Combined Signal Method Measurements From the 1st of January to the 24th of April 2018:

The following set of figures represent the results obtain by the Sagres HF radar system and by the combination of the Sines coastal and Faro offshore and coastal buoys for the period ranging from the 1st of January 2018 to 24th of April 2018.

Figure 3.10 represents the SWH, MWP and MWD time-series obtained by the Sagres HF radar system and by the combined signal.

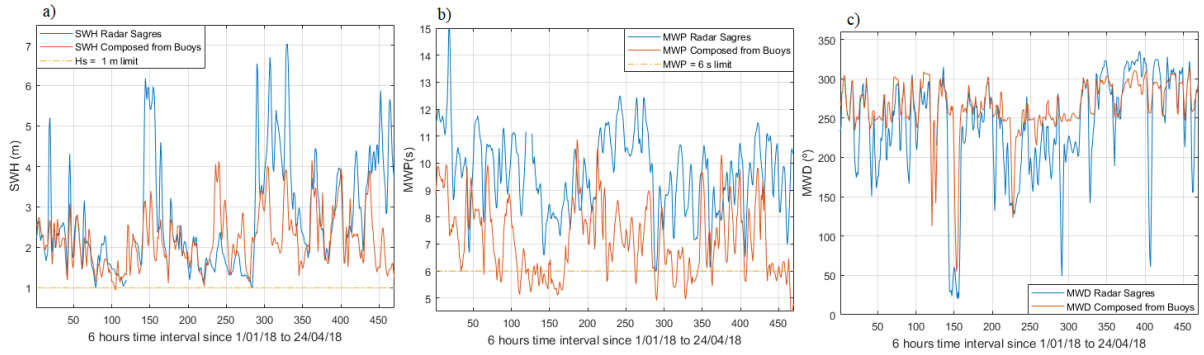

Figure 3.10: Time-series representation regarding the a) SWH, b) MWP and c) MWD parameters retrieved the Sagres HF radar system (blue) and by the combined signal composed from measurements performed by both the Sines coastal and Faro offshore and coastal ODAS buoys from the 1st of January to the 24th of April 2018 temporal period. In figure a) the dashed line represents the minimum SWH values of 1 m retrieved by the Sagres HF radar system and in b) the dashed line represents the minimum MWP values of 6 s retrieved by the Sagres HF radar system.

Figure 3.11, shows a scatter plot representation of each of the retrieved parameters by the combined signal versus the respective parameter retrieved by the HF radar system, also a linear fit was performed to these datasets to determine a possible linear relationship between the two signals.

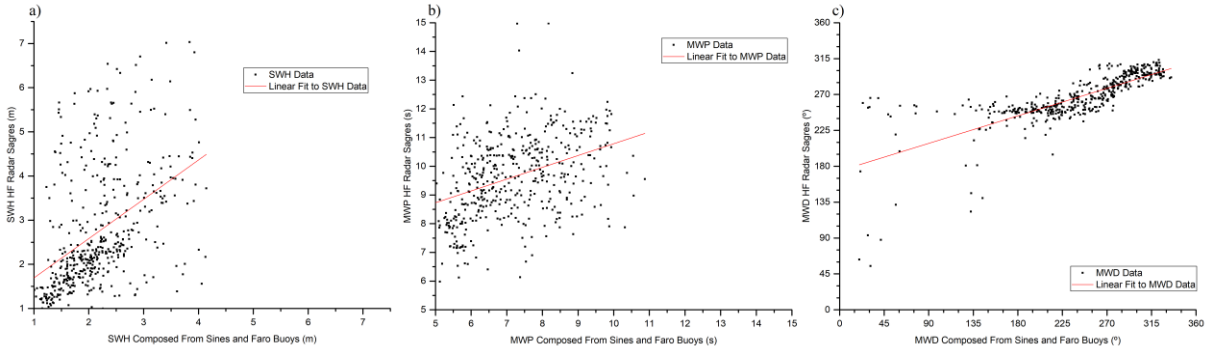

Figure 3.11: Scatter plot of the values obtained by the combined signal for the a) SWH, b) MWP and d) MWD parameters versus the values retrieved by the Sagres HF radar system from the 1st of January to the 24th of April 2018 temporal period.

It is presented in table 3.06 the coefficients of the linear fit performed to the retrieved parameters considering the measurements performed by the Sagres HF radar system and the combined signal regarding the second temporal period.

Table 3.06: Linear fit parameters obtained when considering the SWH, MWP and MWD data retrieved by both the Sagres HF radar system and a combined signal composed of measurements performed by the Sines coastal and Faro offshore and coastal buoys regarding the second temporal period where m, b and r^2 represent respectively the slope the bias and the square of the Pearson linear correlation coefficient.

	SWH	MWP	MWD
m	0.89	0.41	0.38
Δm	0.08	0.05	0.02
b	0.80 (m)	6.67 (s)	174.22 (º)
Δb	0.19 (m)	0.34 (s)	3.70 (º)
r^2	0.20	0.14	0.59

Table 3.07 represents the mean, standard deviation, RMSE and Pearson linear coefficient values computed between the Sagres HF radar and combined signal time-series considering all the retrieved parameters from the 1st of January to the 24th of April 2018 temporal period.

Table 3.07: Statistical parameters computed for the SWH, MWP and MWD time-series obtained by both the Sagres HF radar system and the combined signal from the 1st of January to the 24th of April 2018 temporal period.

	Sagres HF radar	Combined Signal
$\langle SWH \rangle$ (m)	2.74	2.18
$\langle MWP \rangle$ (s)	9.63	7.18
$\langle MWD \rangle$ (º)	240.62	266.48
σ_{SWH} (m)	1.34	0.68
σ_{MWP} (s)	1.43	1.33
σ_{MWD} (º)	64.12	31.99
$RMSE_{SWH}$ (m)	--	1.19
$RMSE_{MWP}$ (s)	--	1.53
$RMSE_{MWD}$ (º)	--	44.52
$Pearson\ Coefficient_{SWH}$	--	0.45
$Pearson\ Coefficient_{MWP}$	--	0.38
$Pearson\ Coefficient_{MWD}$	--	0.77

The next table shows the results of the applied Kolmogorov-Smirnov test considering the null hypothesis method applied between the two retrieved data-sets for the SWH, MWP and MWD parameters.

Table 3.08: Results of the applied Kolmogorov-Smirnov test to the SWH, MWP and MWD data-sets attained by both the Sagres HF radar system and by the combined signal composed of measurements performed by the Sines coastal and Faro offshore and coastal buoys from the 1st of January to the 24th of April 2018 temporal period considering the standard null hypothesis with a significance level of 1%.

K-S test: HF Radar Sagres – Composed signal from Sines and Faro Buoys;	Result Null Hypothesis	P-value
SWH	Rejected	$2.55 * 10^{-10}$
MWP	Rejected	$2.64 * 10^{-75}$
MWD	Rejected	$7.51 * 10^{-26}$

The following figure represents the mean energy directional distribution concerning the temporal period from the 1st of January to the 24th of April 2018 obtained for both the Sagres HF radar system and the combined signal.

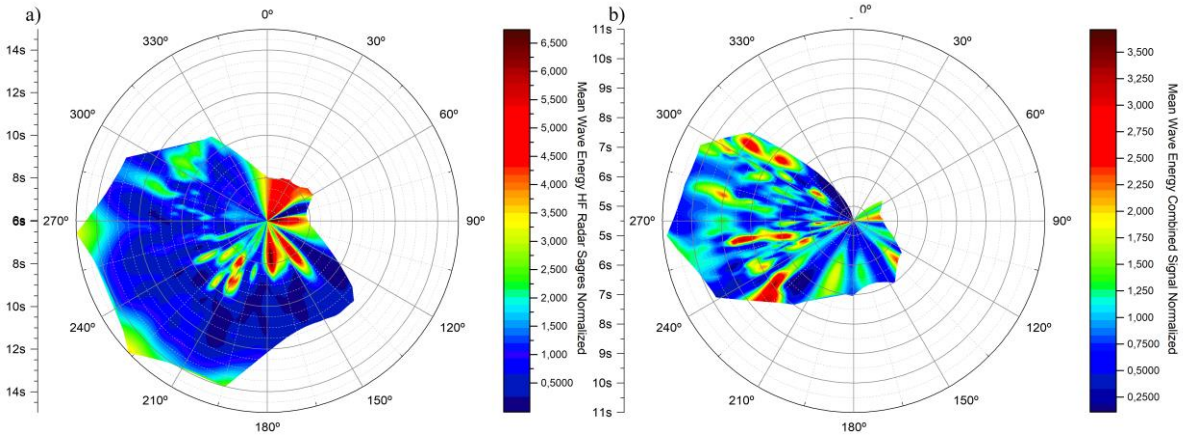

Figure 3.12: MWE directional distribution for the a) Sagres HF radar system and b) the combined signal composed of measurements performed by both the Sines coastal buoy and the Faro offshore and coastal buoys concerning the 1st of January to the 24th of April 2018 temporal period. The MWE polar plots are normalized by the mean MWE computed for the Sagres HF radar system.

Figure 3.13 shows a scatter plot representing the relative error values between the values retrieved by the Sagres HF radar system and by the combined signal computed for each of the retrieved parameters is presented versus the full time-series of its respective parameter retrieved by the combined signal.

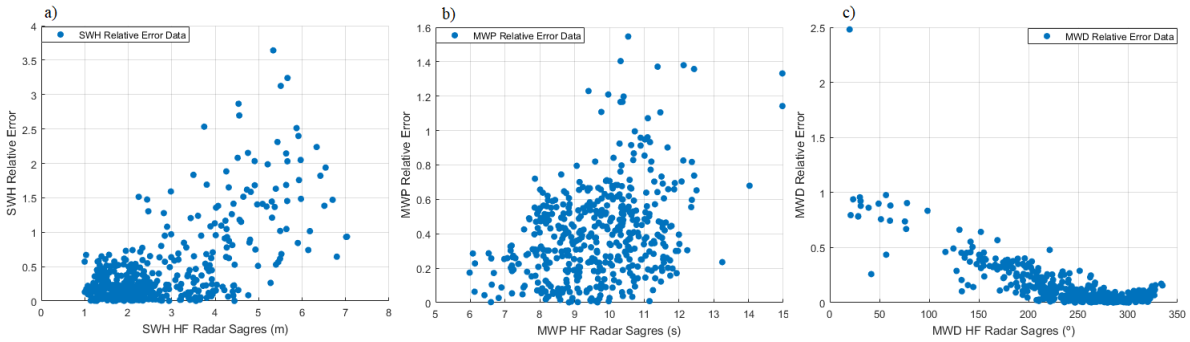

Figure 3.13: Relative error scatter plot for the a) SWH, b) MWP and d) MWD *versus* the values retrieved by the Sagres HF radar. The relative error values were computed for the measurements obtained between the Sagres HF radar and the combined signal composed of measurements performed by both the Sines coastal and the Faro offshore and coastal buoys concerning the 1st of January to the 24th of April 2018 temporal period.

Figure 3.14 shows the signal retrieved by the Sagres HF radar system for each of the retrieved parameters and a scatter plot representing which of the ODAS buoys systems was used for a given point of measurement for the elaboration of the combined signal.

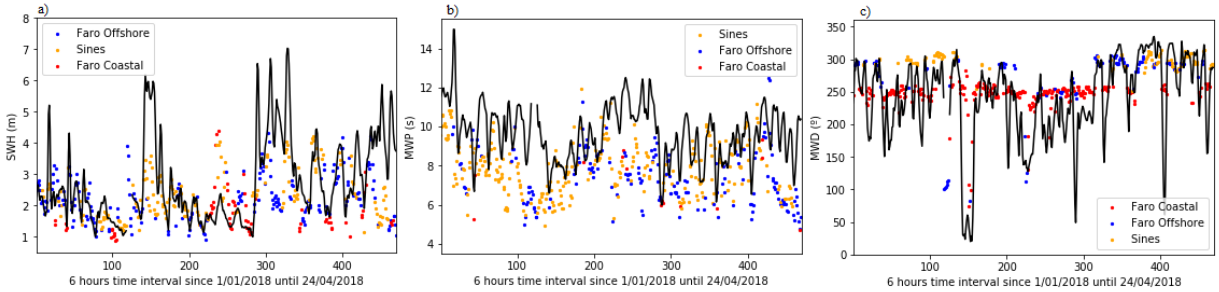

Figure 3.14: Representation of the attained times-series for the a) SWH, b) MWP and d) MWD parameters concerning the measurements retrieved by the Sagres HF radar system (black) and the respective buoy measurement used for a given measurement point to compose the combined signal, i.e. Sines coastal buoy (orange), Faro offshore buoy (blue) and Faro coastal buoy (red) regarding the 1st of January to the 24th of April 2018 temporal period.

It is presented in table 3.08 the relative occurrence coefficients for the contribution of each ODAS buoys system for the combined signal regarding each of the retrieved parameters.

Table 3.09: Relative occurrence coefficients computed due to the relative contribution of each of the ODAS buoys for the composition of the combined signal regarding the SWH, MWP and MWD parameters.

Relative Occurrence Coefficients	Sines Coastal Buoy	Faro Offshore Buoy	Faro Coastal Buoy

SWH	0.40	0.44	0.16
MWP	0.60	0.37	0.03
MWD	0.27	0.21	0.52

Figure 3.15 is a histogram representation of the values retrieved by all the studied measuring systems, namely the Sagres HF radar system, the Sines coastal and the Faro offshore and coastal buoys for the SWH, MWP and MWD parameters, representing the measurements range of each parameter by each of the measuring systems concerning the temporal period from the 1st of January to the 24th of April 2018.

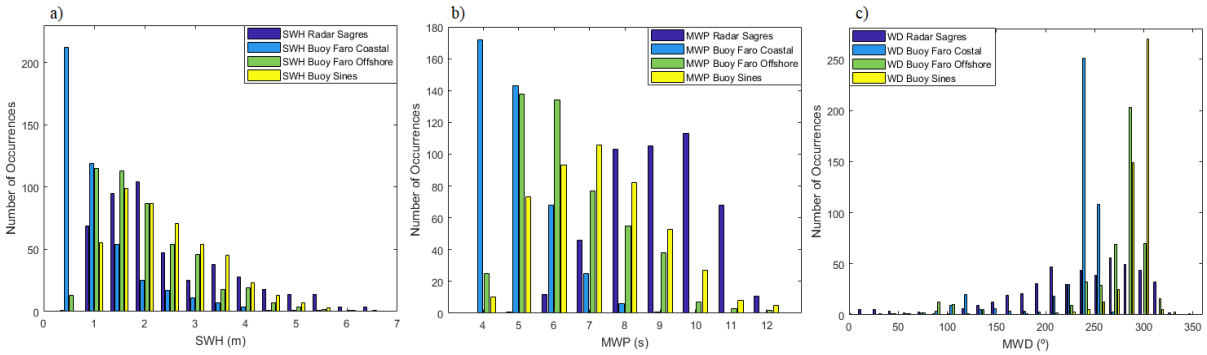

Figure 3.15: Histogram representation of all the retrieved parameters i.e. a) SWH, b) MWP and d) MWD concerning the measurements performed by each measuring system: Sines coastal buoy (yellow), Sagres HF radar system (dark blue), Faro offshore buoy (green) and Faro coastal buoy (blue).

Regarding figure 3.16, a directional histogram plot (*waverose*) was created to assess the wave directions associated with its respective absolute frequency of SWH and MWP values and concerning with the Sagres HF radar measurements.

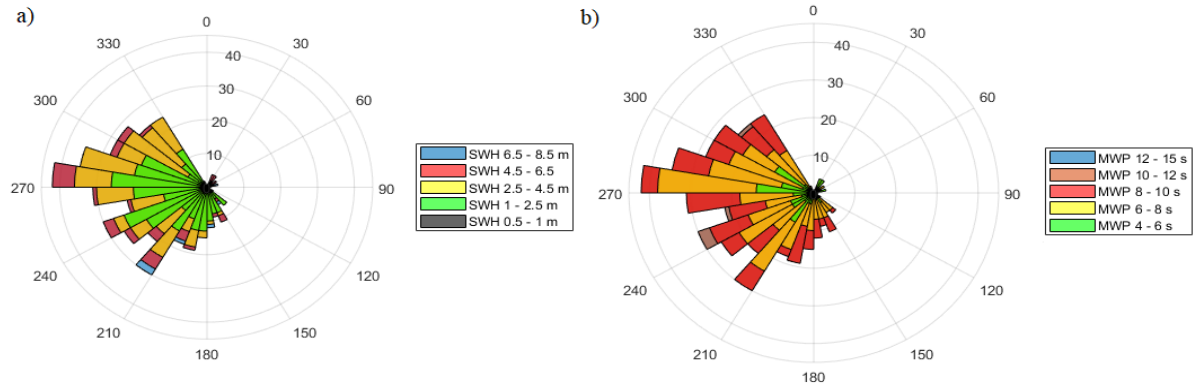

Figure 3.16: Directional histogram concerning the a) SWH and b) MWP parameters retrieved by the Sagres HF radar system concerning the 1st of January to the 24th of April 2018 temporal period.

It can be seen in figure 3.17, the grouped range-cell results according to the mean-range cell hypothesis are presented representative of the HF radar measurements discretized into 5 km intervals, from the 5 km distance from shore till the maximum HF radar range as well as the time-series retrieved for SWH, MWP and MWD parameters concerning the measurements performed by the Sines and Faro buoys.

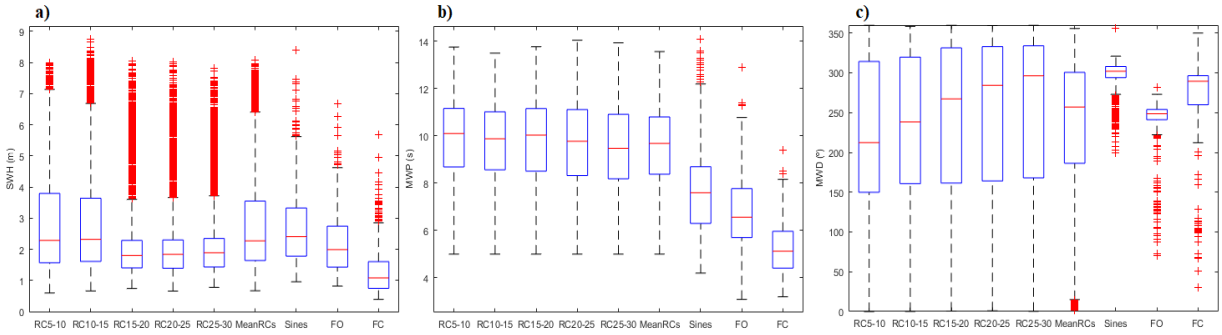

Figure 3.17: Box-plot diagram representation of the measurements retrieved by each range-cells sets grouped into 5 km intervals, i.e. 5-10 km, 10-15 km, 15-20km, 20-25 km and 25-30 km by the Sagres HF radar system concerning the a) SWH, b) MWP and c) the MWD parameters as well as the measurements attained by the mean range-cell hypothesis and the Sines coastal, Faro offshore and Faro coastal buoys concerning the 1st of January to the 24th of April 2018 temporal period.

3.2 Alfanzina HF Radar System:

3.2.1 Alfanzina HF Radar System Against Single ODAS Buoys Measurements:

In this section, the obtained results the measurements of SWH, MWP and MWD parameters retrieved by the Alfanzina HF radar system and the Faro ODAS buoys systems, namely the Faro offshore and the Faro coastal buoys for the 1st of April to the 24th of April period are presented.

Figure 3.18 represents the SWH, MWP and MWD time-series retrieved by the Alfanzina HF radar system and both the Faro buoys for the period ranging from the 1st of April 2018 to the 24th of April 2018.

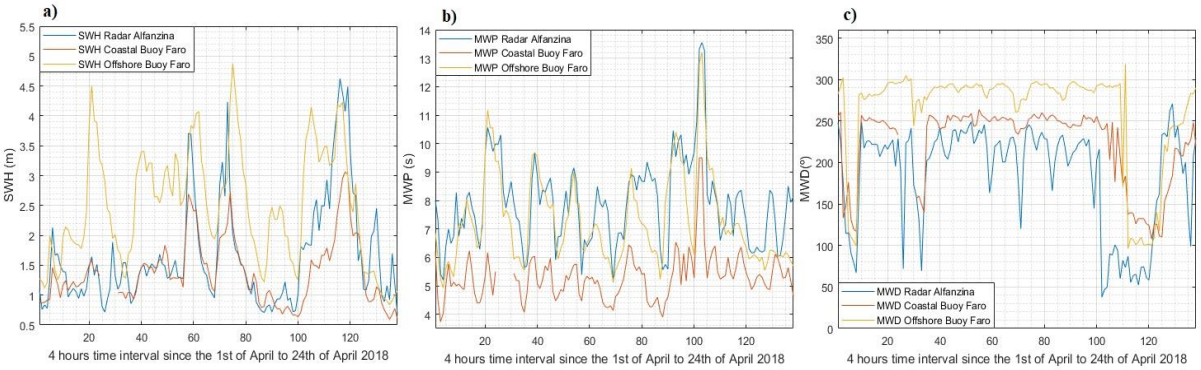

Figure 3.18: Time-series representation regarding the a) SWH, b) MWP and c) MWD parameters retrieved by the Faro offshore buoy (orange), the Alfanzina HF radar system (blue) and the Faro coastal buoy (red) for the 1st to the 24th of April 2018 period.

It is shown in table 3.09 the mean and standard deviation values for SWH, MWP and MWD time-series retrieved by the Alfanzina HF radar system and the Faro ODAS buoys systems as well as the RMSE and Pearson linear coefficient attained when comparing the data-sets obtained by the buoys and the HF radar for the period ranging from the 1st of April to the 24th of April 2018.

Table 3.09: Statistical parameters computed for the SWH, MWP and MWD time-series retrieved by the Faro offshore buoy, the Alfanzina HF radar system and the Faro coastal buoy for the 1st to the 24th of April 2018 temporal period.

	Alfanzina HF radar	Faro Offshore Buoy	Faro Coastal Buoy
$\langle SWH \rangle$ (m)	1.65	2.49	1.38
$\langle MWP \rangle$ (s)	7.88	7.29	5.31
$\langle MWD \rangle$ (º)	185.46	260.5	221.63

σ_{SWH} (m)	0.89	0.97	0.55
σ_{MWP} (s)	1.52	1.57	0.83
σ_{MWD} (º)	62.04	61.25	46.85
$RMSE_{SWH}$ (m)	--	0.90	0.53
$RMSE_{MWP}$ (s)	--	1.01	1.15
$RMSE_{MWD}$ (º)	--	56.55	48.55
$Pearson\ Coefficient_{SWH}$	--	0.52	0.83
$Pearson\ Coefficient_{MWP}$	--	0.78	0.66
$Pearson\ Coefficient_{MWD}$	--	0.58	0.63

Figure 3.19 represents the MWE directional distribution for the Alfanzina HF radar system for the first temporal period studied during April 2018.

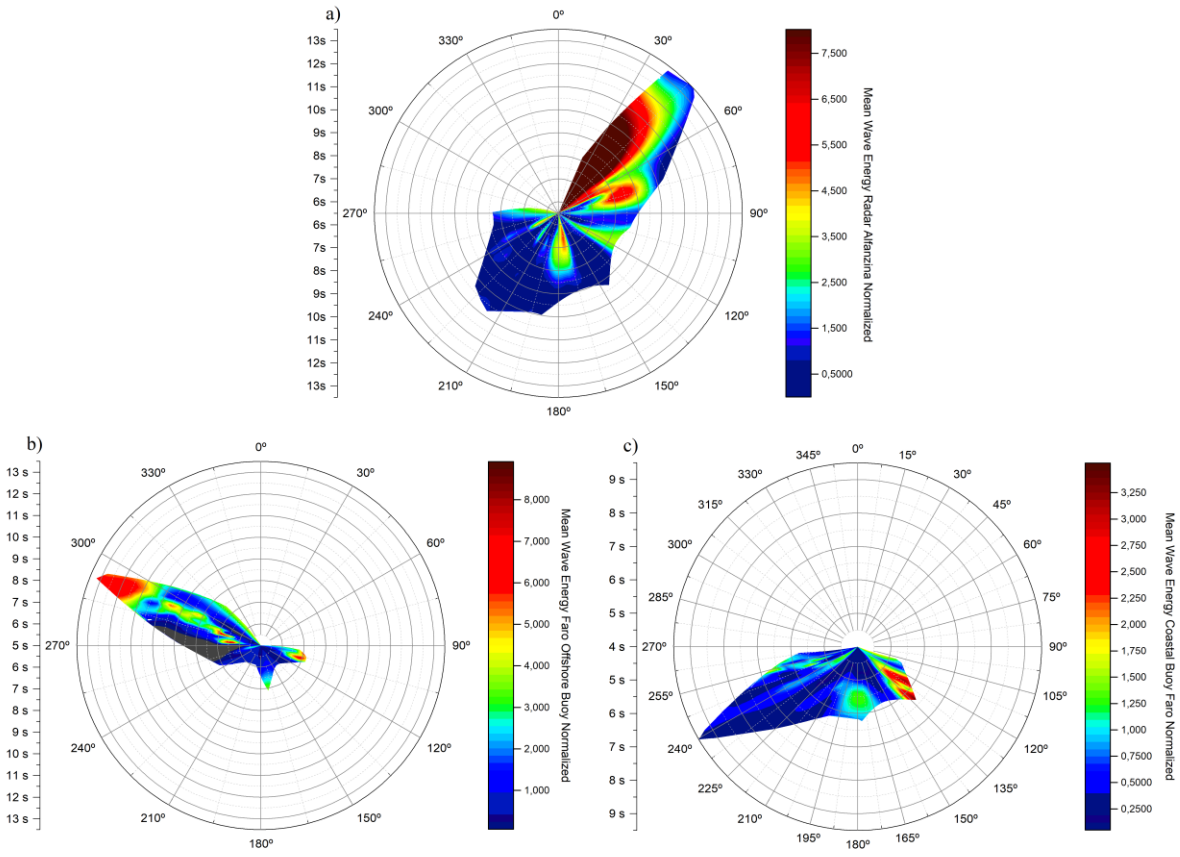

Figure 3.19: MWE directional distribution for the a) Alfanzina HF radar, b) Faro offshore buoy and d) Faro coastal buoy concerning the 1st to the 24th of April 2018 time period. The MWE polar plots are normalized by the mean MWE computed for the Alfanzina HF radar system.

Figure 3.20 represents the relative error values computed for each of the retrieved parameters between the Alfanzina HF radar system and the Faro ODAS buoys measurements.

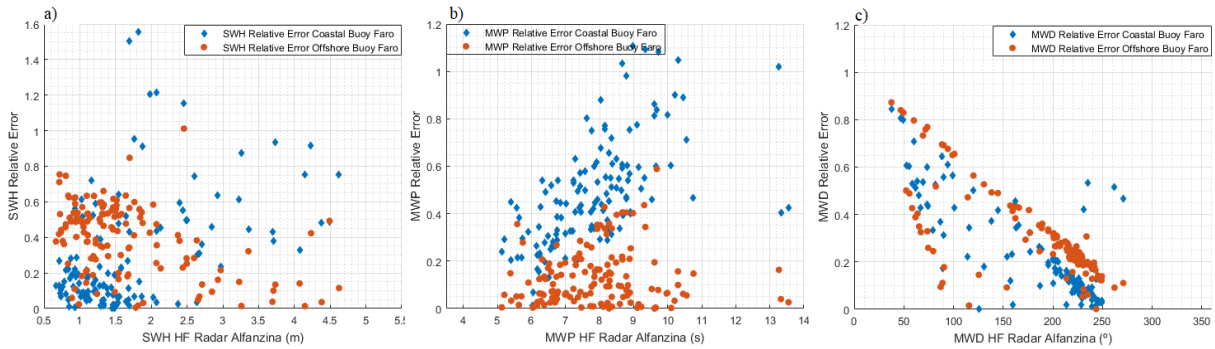

Figure 3.20: Relative error scatter plot for the a) SWH, b) MWP and d) MWD parameters computed for the measurements obtained between the Alfanzina HF radar, the Faro offshore buoy (red) and the Faro coastal buoy (blue) *versus* the measurements retrieved by the Alfanzina HF radar.

Figure 3.21 represents the results obtained for the mean range-cell hypothesis considering the HF radar measurements for the first studied period.

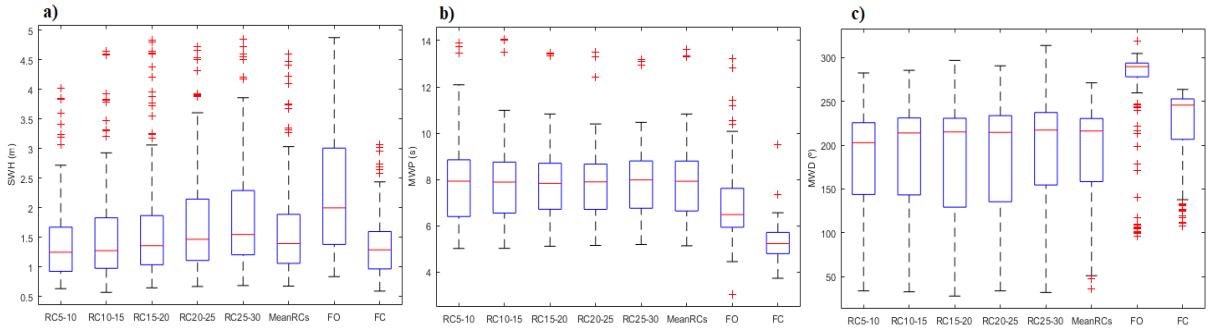

Figure 3.21: Box-plot diagram representing the retrieved values by each range-cells sets grouped into 5 km intervals, i.e. 5-10 km, 10-15 km, 15-20 km, 20-25 km and 25-30 km by the Alfanzina HF radar system concerning the a) SWH parameter, b) MWP parameter and c) the MWD parameter as well as the measurements attained by the mean range-cell hypothesis and the Faro offshore and coastal buoys for the 1st to the 24th of April 2018 temporal period.

3.2.2 Alfanzina HF Radar System Against Combined Signal Method Measurements From the 1st to the 24th of April 2018:

In this section of the study, the signals measured by the Alfanzina HF radar system (i.e., each of the SWH, MWP and MWD time-series) were validated against signals composed from measurements performed by the Faro offshore and coastal buoys. The obtained results were the following:

Figure 3.22 represents the SWH, MWP and MWD time-series retrieved both by the Alfanzina HF radar system and the combined signal composed from the ODAS buoys systems measurements.

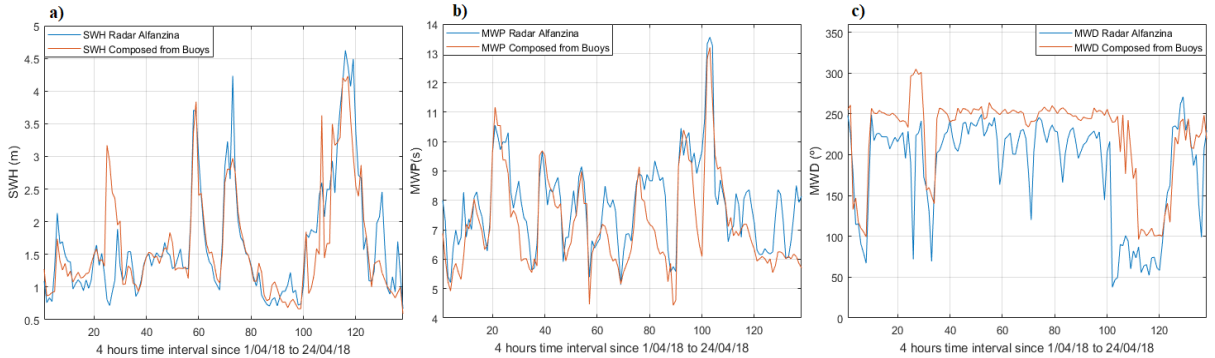

Figure 3.22: Time-series representation regarding the a) SWH, b) MWP and c) MWD parameters retrieved by the Alfanzina HF radar system (blue) and the combined signal composed from measurements performed by both the Faro offshore and coastal ODAS buoys (red) for the temporal period ranging from the 1st to the 24th of April 2018.

Below is a scatter plot representation of each parameter retrieved by the combined signal versus the same respective parameter retrieved by the HF radar system where a linear fit was performed to the data-sets to assess a possible linear relation within measuring systems.

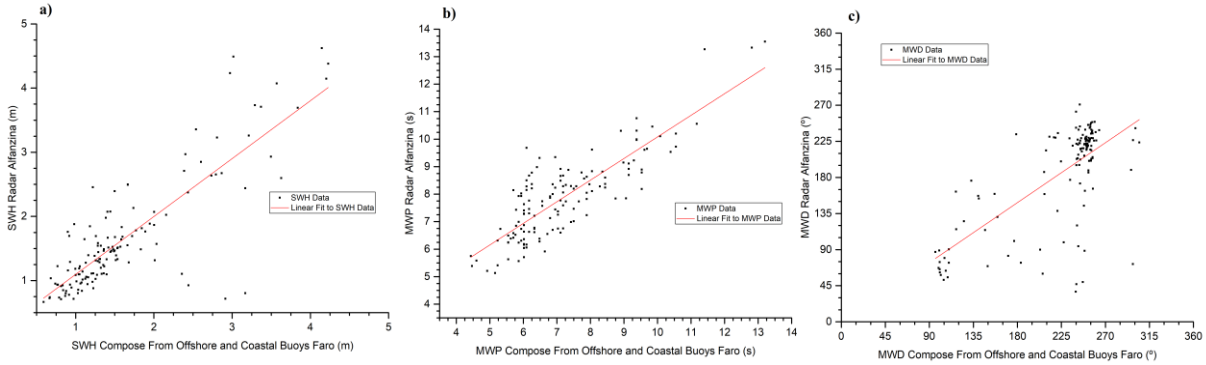

Figure 3.23: Scatter plot of the values obtained by the combined signal for the a) SWH, b) MWP and d) MWD parameters versus the values retrieved by the Alfanzina HF radar system for the 1st to the 24 of April 2018 temporal period.

It is presented in table 3.10 the linear fit parameters attained when considering a possible linear relationship between the data retrieved by the Alfanzina HF radar system and a combined signal composed of measurements performed by both the Faro offshore and coastal buoys.

Table 3.10: Linear fit parameters obtained when considering the SWH, MWP and MWD data retrieved by both the Alfanzina HF radar system and a combined signal composed of measurements performed by Faro offshore and coastal buoys where m, b and r^2 represent respectively the slope the bias and the square of the Pearson linear correlation coefficient.

	SWH	MWP	MWD
m	0.90	0.79	0.83
Δm	0.05	0.04	0.07
b	0.19 (m)	2.22 (s)	-0.95 (º)
Δb	0.09 (m)	0.33 (s)	17.01 (º)
r^2	0.69	0.70	0.49

Table 3.11 shows the mean and standard deviation values as well as RMSE and Pearson linear coefficient values attained for each of the retrieved parameters due to the comparison of the signals retrieved by both the Alfanzina HF radar and by the combined signal composed from the Faro buoys measurements.

Table 3.11: Statistical parameters computed for the SWH, MWP and MWD time-series obtained by the Alfanzina HF radar system and by the combined signal for the 1st to the 24th of April 2018 temporal period.

	Alfanzina HF radar	Combined Signal
$\langle SWH \rangle$ (m)	1.65	1.61
$\langle MWP \rangle$ (s)	7.88	7.20
$\langle MWD \rangle$ (º)	185.46	224.48
σ_{SWH} (m)	0.89	0.82
σ_{MWP} (s)	1.52	1.62
σ_{MWD} (º)	62.04	51.86

$RMSE_{SWH}$ (m)	--	0.49
$RMSE_{MWP}$ (s)	--	0.90
$RMSE_{MWD}$ (º)	--	45.35
$Pearson\ Coefficient_{SWH}$	--	0.83
$Pearson\ Coefficient_{MWP}$	--	0.84
$Pearson\ Coefficient_{MWD}$	--	0.69

It is shown in table 3.12 the results of the Kolmogorov-Smirnov test applied to the two data-sets for each of the retrieved parameters using the null hypothesis method.

Table 3.12: Results of the applied Kolmogorov-Smirnov test to the SWH, MWP and MWD data-sets attained by both the Alfanzina HF radar system and by the combined signal composed of measurements performed by the Faro offshore and coastal buoys for the 1st to the 24th of April 2018 temporal period considering the standard null hypothesis with a significance level of 1%.

K-S test: HF Radar Alfanzina – Composed signal from Faro Buoys;	Result Null Hypothesis	P-value
SWH	Accepted	0.019
MWP	Rejected	$1.87 * 10^{-37}$
MWD	Rejected	$3.79 * 10^{-85}$

Figure 3.24 represents the mean energy directional distribution regarding the time period from the 1st to the 24th of April 2018 obtained for the Alfanzina HF radar system[5] and for the combined signal composed from the Faro ODAS buoys measurements.

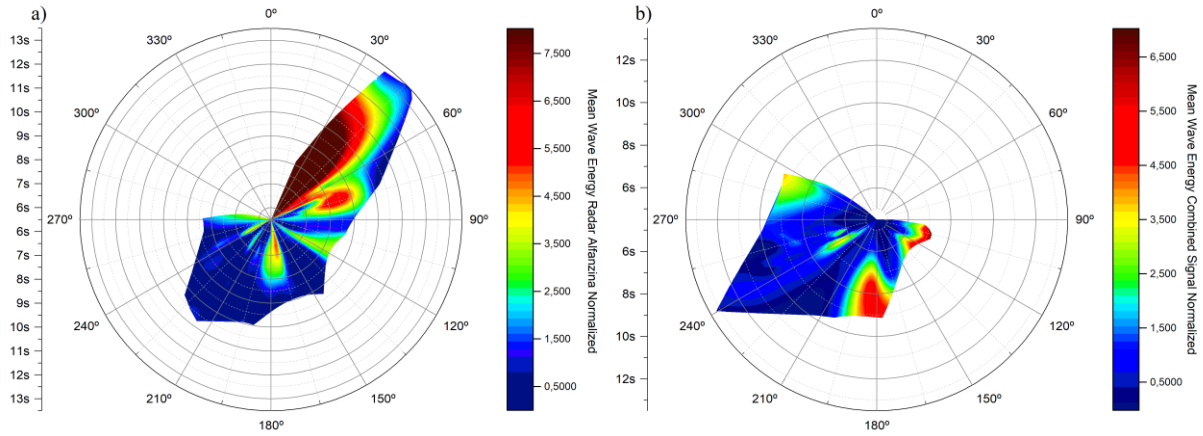

Figure 3.24: MWE directional distribution for the a) Alfanzina HF radar system and b) the combined signal composed of measurements performed by the Faro offshore and coastal buoys concerning the 1st to the 24th of April 2018 temporal period. The MWE polar plots are normalized by the mean MWE computed for the Alfanzina HF radar system.

It is presented in figure 3.25 a scatter plot representation of the SWH, MWP and MWD retrieved parameters by the combined signal versus the relative error values computed between the two measuring signals as in resemblance of what was done in the previous sections.

[5] Again, the MWE directional distribution computed for the Alfanzina HF radar system concerning the temporal period from the 1st to the 24th of April 2018 is presented here again just for the sake of comparison with the MWE directional distribution computed for the combined signal regarding the same temporal period.

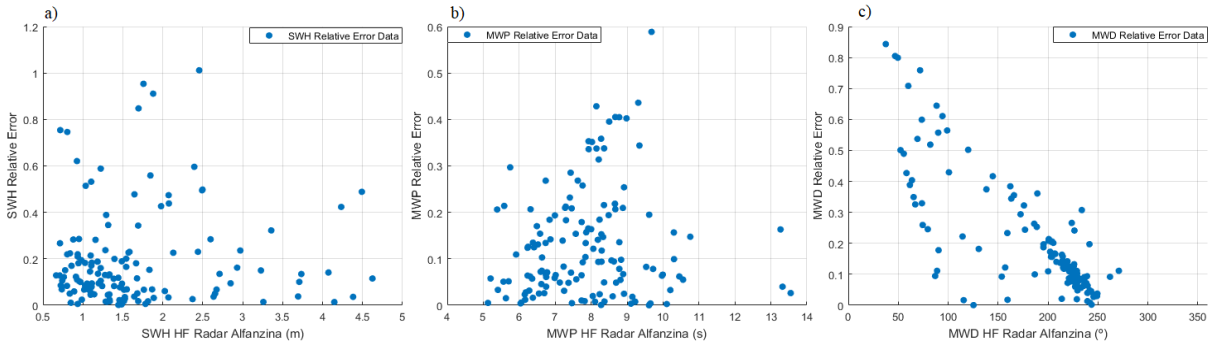

Figure 3.25: Relative error scatter plot for the a) SWH, b) MWP and d) MWD parameters *versus* the Alfanzina HF radar measurements. Relative error values were computed for the measurements between the Alfanzina HF radar and the combined signal composed of measurements performed by both the Faro offshore and coastal buoys concerning the 1st to the 24th of April 2018 temporal period.

In figure 3.26 it is represented the HF radar time-series for each of the retrieved parameters as well as a scatter plot indicating which of the ODAS buoys systems was used for the combined signal at a given point of measurements.

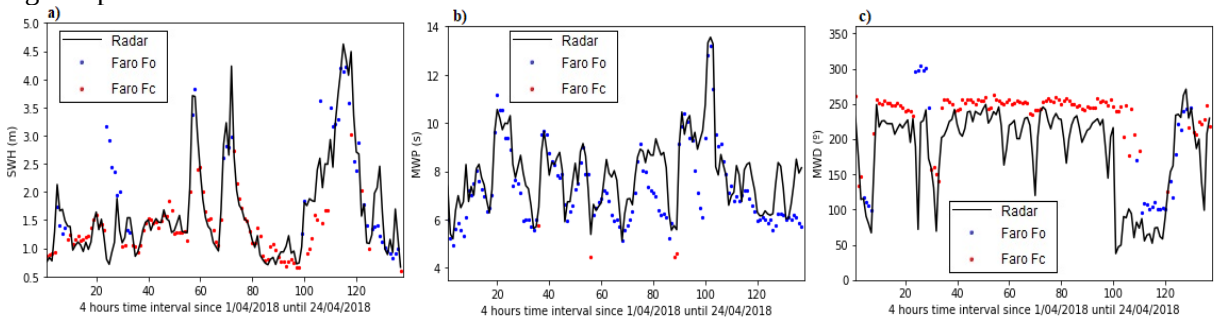

Figure 3.26: Representation of the attained times-series for the a) SWH, b) MWP and d) MWD parameters concerning the measurements retrieved by the Alfanzina HF radar system (black) and the buoy measurement used for a given measurement point to compose the combined signal, i.e. Faro offshore buoy (blue) and Faro coastal buoy (red) from the 1st to the 24th of April 2018 temporal period.

It is present in table 3.13, the relative occurrence frequency coefficients for the contribution of each ODAS buoys systems for the combined signal for each of the retrieved physical parameters regarding the measurements performed by the Alfanzina HF radar system.

Table 3.13: Relative occurrence coefficients computed due to the relative contribution of each of the ODAS buoys for the composition of the combined signal regarding the SWH, MWP and MWD parameters.

Relative Occurrence Coefficients	Faro Offshore Buoy	Faro Coastal Buoy
SWH	0.33	0.67
MWP	0.97	0.03
MWD	0.21	0.79

3.2.3 Alfanzina HF Radar System Against Combined Signal Method Measurements From the 1st of January to the 24th of April 2018:

The following sets of figures have the propose to present the results obtained for the SWH, MWP and MWD parameters retrieved by both the Alfanzina HF radar and the combined signal for the

period ranging from the 1st of January to the 24th of April 2018 with the purpose of validating HF radar wave measurements using the combined signal as a reference system.

Figure 3.27 represents the retrieved time-series for the SWH, MWP and MWD parameters obtained by both the measuring systems.

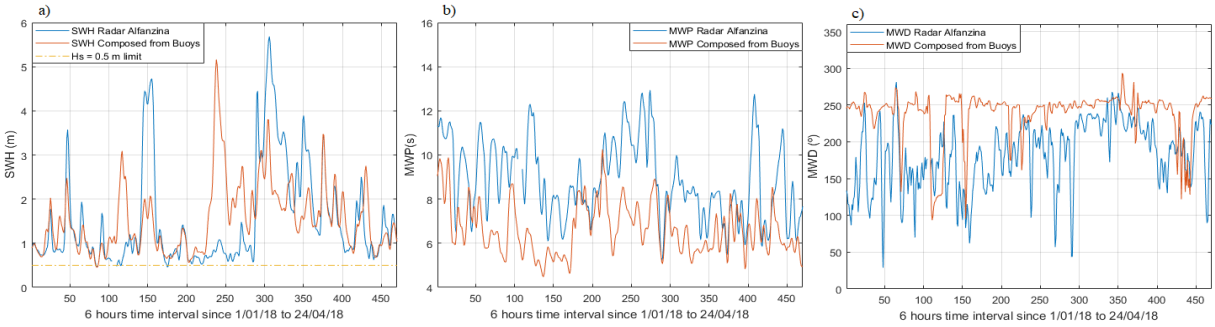

Figure 3.27: Time-series representation regarding the a) SWH, b) MWP and c) MWD parameters retrieved by both the Alfanzina HF radar system (blue) and the combined signal composed from measurements performed by the Faro offshore and coastal ODAS buoys from the 1st of January to the 24th of April 2018 temporal period. In figure a) the dashed line represents the minimum SWH values of 0.5 m retrieved by the Alfanzina HF radar system and in b) the dashed line represents the minimum MWP values of 5.5s retrieved by the Alfanzina HF radar system.

Figure 3.28 represents a scatter plot constituting of measurements resulting from the combined signal versus the HF radar measurements created to exploit a possible linear relationship between the retrieved parameters considering the measurements performed by both systems.

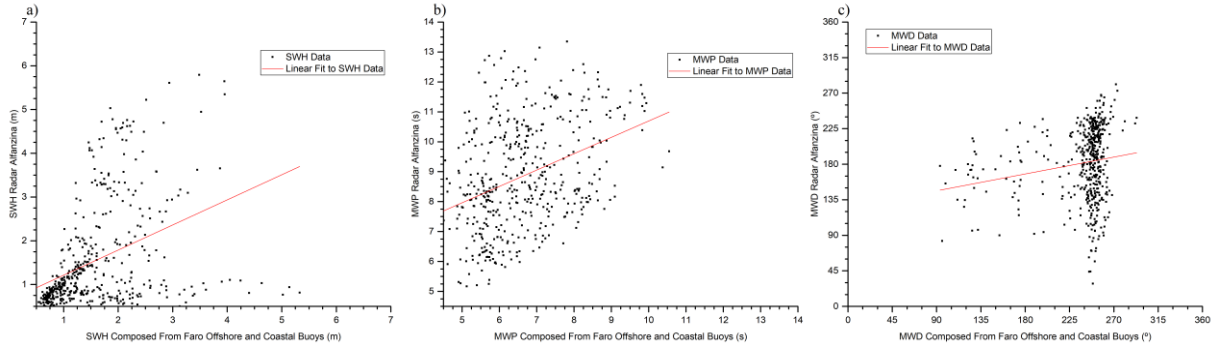

Figure 3.28: Scatter plot of the values obtained by the combined signal for the a) SWH, b) MWP and d) MWD parameters versus the values retrieved by the Alfanzina HF radar system from the 1st of January to the 24th of April 2018 temporal period.

Table 3.14 represents the linear fits parameters obtained when considering a linear relationship between the data retrieved by the Alfanzina HF radar system and the combined signal regarding the second temporal period analyses.

Table 3.14: Linear fit parameters obtained when considering the SWH, MWP and MWD data retrieved by both the Alfanzina HF radar system and a combined signal composed of measurements performed by the Faro offshore and coastal buoys from the 1st of January to the 24th of April 2018 temporal period where m, b and r^2 represent respectively the slope the bias and the square of the Pearson linear correlation coefficient.

	SWH	MWP	MWD
m	0.57	0.55	0.24
Δm	0.06	0.06	0.06
b	0.64 (m)	5.23 (s)	124.94 (º)

Δb	0.11 (m)	0.43 (s)	15.10 (º)
r^2	0.16	0.14	0.03

Table 3.15 represents the mean, standard deviation, RMSE and Pearson linear coefficient values retrieved for each of the measured wave-sets parameters, considering the measurements obtained by both the Alfanzina HF radar system and the combined signal for the temporal period ranging from the 1st of January to the 24th of April 2018.

Table 3.15: Statistical parameters computed for the SWH, MWP and MWD time-series obtained by the Alfanzina HF radar system and by the combined signal from the 1st of January to the 24th of April 2018 temporal period.

	Alfanzina HF radar	Combined Signal
$\langle SWH \rangle$ (m)	1.53	1.56
$\langle MWP \rangle$ (s)	8.86	6.64
$\langle MWD \rangle$ (º)	181.42	238.10
σ_{SWH} (m)	1.16	0.82
σ_{MWP} (s)	1.80	1.21
σ_{MWD} (º)	46.11	33.53
$RMSE_{SWH}$ (m)	--	1.12
$RMSE_{MWP}$ (s)	--	1.76
$RMSE_{MWD}$ (º)	--	52.12
$Pearson\ Coefficient_{SWH}$	--	0.40
$Pearson\ Coefficient_{MWP}$	--	0.37
$Pearson\ Coefficient_{MWD}$	--	0.17

In table 3.16 it is presented the results of the applied Kolmogorov-Smirnov test to the SWH, MWP and MWD signals retrieved by both systems test considering the standard null hypothesis.

Table 3.16: Results of the applied Kolmogorov-Smirnov test to the SWH, MWP and MWD data-sets attained by both the Alfanzina HF radar system and by the combined signal composed of measurements performed by the Faro offshore and coastal buoys from the 1st of January to the 24th of April 2018 temporal period considering the standard null hypothesis with a significance level of 1%.

K-S test: HF Radar Alfanzina – Composed Signal from Faro Buoys;	Result Null Hypothesis	P-value
SWH	Rejected	$1.13 * 10^{-9}$
MWP	Rejected	$5.38 * 10^{-61}$
MWD	Rejected	$1.97 * 10^{-110}$

The following figure represents the obtained results for the mean directional energy distribution for the temporal period ranging from the 1st of January 2018 to the 24th of April 2018 regarding the measurements performed by both the Alfanzina HF radar system and by the combined signal.

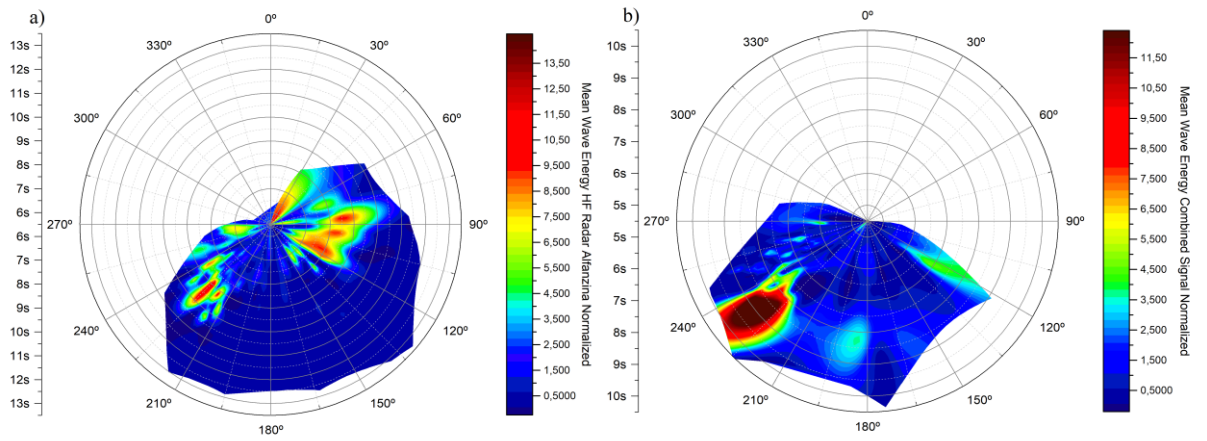

Figure 3.29: MWE directional distribution for the a) Alfanzina HF radar system and b) the combined signal composed of measurements performed by the Faro offshore and coastal buoys concerning the 1st of January to the 24th of April 2018 temporal period. The MWE polar plots are normalized by the mean MWE computed for the Alfanzina HF radar system.

In Figure 3.30 it is shown a scatter plot representing the relative error values associated with measurements performed by both the measuring systems considering the SWH, MWP and MWD parameters.

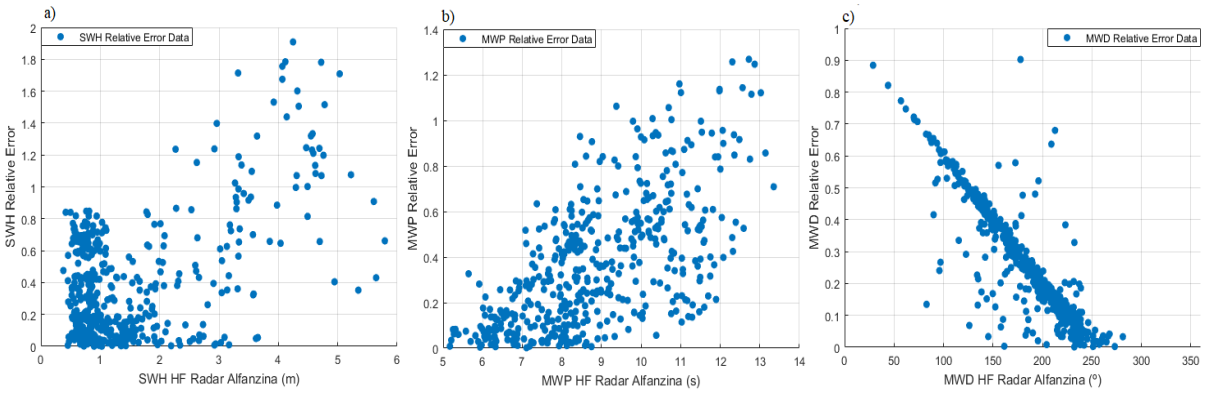

Figure 3.30: Relative error scatter plot for the a) SWH, b) MWP and d) MWD parameters *versus* the values retrieved by the Alfanzina HF radar. Relative error values were computed for the measurements obtained between the Alfanzina HF radar system and the combined signal composed of measurements performed by the Faro offshore and coastal buoys concerning the 1st of January to the 24th of April 2018 temporal period.

It is possible to visualize from figure 3.31 the HF radar time-series as well as a scatter plot composed of measurements performed by both the Faro offshore and Faro coastal buoy. This figure shows which ODAS buoy was used to build the combined signal at a given point of measurements and to assess which sea-state drove the HF radar for a given measurement.

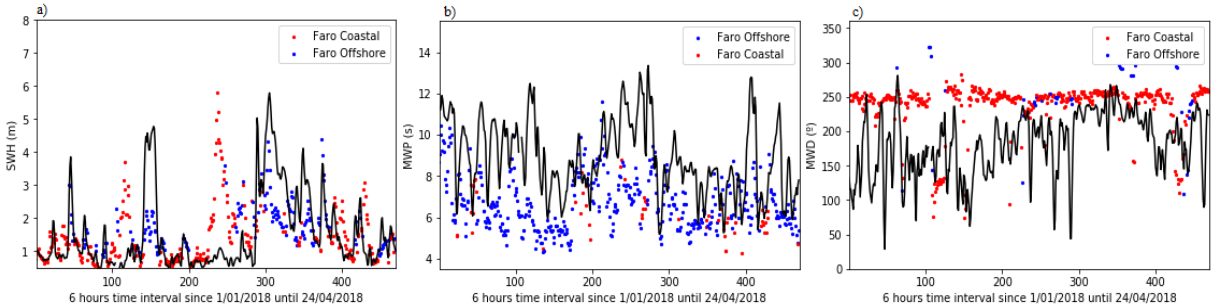

Figure 3.31: Representation of the attained times-series for the a) SWH, b) MWP and d) MWD parameters concerning the measurements retrieved by the Alfanzina HF radar system (black) and the buoy measurement used for a given measurement

point to compose the combined signal, i.e. Faro offshore buoy (blue) and Faro coastal buoy (red) regarding the 1st of January to the 24th of April 2018 temporal period.

It is presented in table 3.17, the relative occurrence coefficients regarding the relative usage of each buoy measurements for the elaboration of the combined signal.

Table 3.17: Relative occurrence coefficients computed representing the relative contribution of each of the ODAS buoys for the composition of the combined signal regarding the SWH, MWP and MWD parameters.

Relative Occurrence Coefficients	Faro Offshore Buoy	Faro Coastal Buoy
SWH	0.37	0.63
MWP	0.88	0.12
MWD	0.09	0.91

Figure 3.32 shows a histogram representation of the values retrieved by the HF radar and the ones retrieved by the Faro buoys. This histogram was created to assess the measuring range of each system and to compare the relative occurrence of a given value for each retrieved parameter.

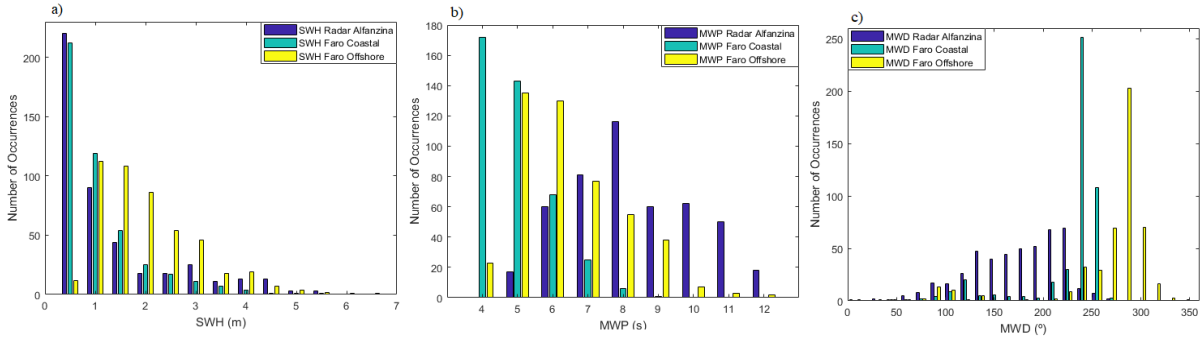

Figure 3.32: Histogram representation of all the retrieved parameters i.e. a) SWH, b) MWP and d) MWD concerning the measurements performed by each measuring system: Alfanzina HF radar system (dark blue), Faro offshore buoy (yellow) and Faro coastal buoy (marine blue) regarding the temporal period from the 1st of January to the 24th of April 2018.

Figure 3.33 represents two *waverose* histograms considering both the SWH and MWP parameters retrieved by the Alfanzina HF radar system. Its main goal is to link these retrieved values of SWH and MWP with its associated MWD parameter.

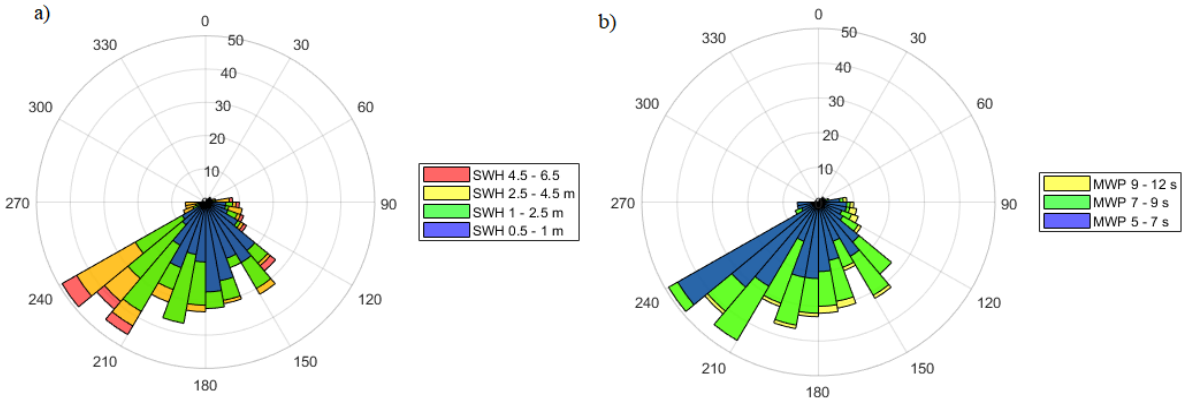

Figure 3.33: Directional histogram concerning the a) SWH and b) MWP parameters retrieved by the Alfanzina HF radar system concerning the 1st of January to the 24th of April temporal period.

Figure 3.34 represents the mean-range cell hypothesis (described in section 2.3) results regarding the Alfanzina HF radar range-cell groups and the Faro ODAS buoys measurements for each of the retrieved parameters.

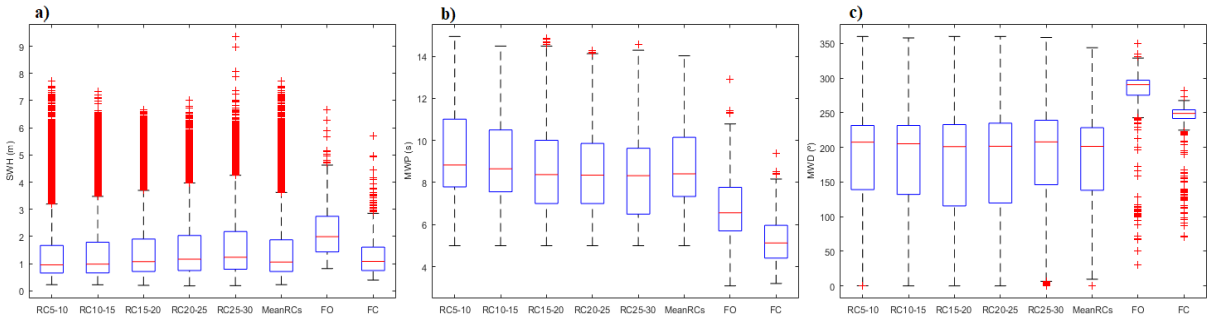

Figure 3.34: Box-plot diagram representation of the measurements retrieved by each range-cells sets grouped into 5 km intervals, i.e. 5-10 km, 10-15 km, 15-20 km, 20-25 km and 25-30 km by the Alfanzina HF radar system concerning the a) SWH, b) MWP and c) the MWD parameters as well as the measurements attained by the mean range-cell hypothesis and the Faro offshore and Faro coastal buoys concerning the 1st of January to the 24th of April 2018 temporal period.

4 Discussion:

4.1 Sagres HF Radar:

4.1.1 Discussion Concerning the Sagres HF Radar System Against Single ODAS Buoys Measurements Results:

From the time-series of SWH, MWP and MWD parameters present in figure 3.01, it is possible to recognise that the highest SWH and MWP mean values recorded were measured by the HF radar system.

Following figure 3.01.c), figure 3.01.a) and figure 3.01.b), it can be observed that when similar values of MWD are measured between the Sines coastal buoy, the Sagres HF radar system and the Faro offshore buoy, similar values of SWH and MWP are retrieved by these measuring systems (i.e. 20th four hours-time interval and 35th). As result, when North-Westwards and Westward sea-states occur, they are measured with a similar MWD value by the Faro coastal and offshore buoys and by the HF radar system, leading to a characterization of SWH, MWP and MWD for the levant sea-states as can be observed by observations intervals from 125th observation to 130th observation in figures 3.01.

By analyses of figure 3.01.c), it is thus recognisable that MWD measurements by the HF radar system have higher variability than the ODAS buoys measurements for this parameter and hence it can be due to HF radar systems having a wider range of measurements than the ODAS buoys systems (i.e. HF radar measurements are retrieved for a given circular crown around the radar site, with an associated range and angular aperture while the ODAS buoys systems are considered to be *in situ*).

MWP values retrieved by the HF radar system can be regarded as overestimated when comparing its values with the ones retrieved by ODAS buoys systems when considering wave-sets with similar MWD and this might be due to the fact that MWP values are retrieved from the second-order moment of the variance density spectrum (as described in section 2.2.2) and hence, the MWP values are more subjected to the perturbations in the energy spectrum due to the fact that, they are multiplied by the square of the variable where the integration of the spectrum is performed. Also, the variance density spectrum can be altered by several atmospheric conditions and environmental noise as described by Holthuijsen (2007) and thus it can act as a bias for the MWP value retrieving justifying in this way the overestimation of this parameter by the HF radar system.

From inspection of MWE directional distribution plotted for all measuring systems presented in figure 3.02, it is possible to recognise the effect of the wider range of measurements for the HF radar system when comparing with the ODAS buoys systems, leading to the possibility of measuring MWD in all directions within the mean-range cell interval whereas ODAS buoys systems can only measure the MWD of waves that affect the buoy directly.

Given that the SWH and MWP values retrieved by the HF radar system are typically higher in magnitude than the values retrieved by the ODAS buoys as previously described and as can be observed in figure 3.01.a), figure 3.01.b) and from table 3.01, the radial contour scales of figures 3.02. are different between the HF radar system and the Faro coastal buoy.

Furthermore, the MWE values in figure 3.02.b) corresponding to MWD interval from 270º to 320º can be associated with the MWE values presented in the MWE distribution for the Sines coastal buoy present in figure 3.02.a), namely for the MWP values in the range of 8 s to 10 s interval.

It is important not to left unnoticed the presence of very energetic wave-sets coming from shore direction with MWP ranging from approximately 6.7 s to 7 s present in the HF radar MWE distribution as can be observed in figure 3.02.b). Since these values of MWP are generally associated with local-wind sea-states and that the distance from shore where these measurements are considered (half of the

radar maximum range), 15 km, is not sufficiently large for the development of SWH up to 7 m, this kind of sea-states should be considered as suspicious.

The similarity shown between the HF radar MWE directional distribution and the MWE directional distribution obtained for each of the buoys measuring system lead to the hypothesis that the measured signal by the HF radar system can be considered as a combination of the signals measured by each ODAS buoys system as present in section 2.6.

From figure 3.03.a) and figure 3.03.b), it can be recognized that the Faro coastal buoy is associated to higher relative error values, respectively for the SWH (up to four points of relative error value) and MWP (up to about two points of relative error values) properties.

Regarding figure 3.03.a), it can be observed that the relative error values associated with the SWH parameter, tend to increase until the 2.8 m value for all the buoys systems and then tend to decrease regarding the full SWH range of measurements. In particular, it can also be concluded from figure 3.30.a) that this decrease in the relative error series is more significant for the Sines and Faro offshore buoys than it is for the Faro coastal buoy. These results can be supported by verifying that the Sagres HF radar tends to over-estimated (more than the complete SWH range) the higher SWH values retrieved by the Faro coastal buoy as can be verified from figure A.03.a) in appendix A, being a more or less under-estimation/ over-estimation uniform distribution of SWH values retrieved by the Sagres HF radar when comparing with the values retrieved by the Sines and Faro offshore buoy across the full range of SWH measurements as can be verified from figures A.01.a) and figure A.02.a) also in appendix A.

As for the relative error values regarding the MWP it can be concluded from figure 3.03.b) that for the Faro coastal and Sines buoys, smaller MWP values represent lower relative error values and that these relative error values tend to increase as the MWP values increase. It is important to note that the MWP time-series retrieved by the Sagres HF radar does no correctly describes the MWP time-series retrieved by the Sines and Faro coastal buoys as can be verified from figure A.01.b), figure A.02.b), table A.01 and table A.02 in appendix A. As for the Faro offshore buoy, it is possible to verify from figure 3.03.b), that its associated MWP relative error series value increases as the MWP increases until the MWP value of 11 seconds. From the 11 s value until the full range of the MWP series, the relative error values tend to decrease. The lower relative error values, concerning the MWP values from 11 seconds to the MWP range are associated to the fact that for the higher MWP values both the Sagres HF radar and the Faro offshore buoy tend to retrieved similar MWP values as can be verified from figure A.02.b) in appendix A.

When concerning with the MWD relative error series, it can be observed from figure 3.03.c) that for the Sines coastal buoy the relative error values tend to increase as the MWD values retrieved by the Sagres HF radar tend to be differ from the mean MWD value (see table 3.01) retrieved by the Sines coastal buoy.

As for the MWD relative error time-series computed between the Faro buoys and the Sagres HF radar it can be verified from figure 3.03.c) that the relative error values tend to decrease when performing MWD measurements around the 75º MWD values (Westward sea-states) and around the MWD values identical to the mean MWD values computed for the Faro buoys time-series (see table 3.01). This result associated with figure A.01.c), figure A.02.c) and figure A.02.c) in appendix A further support the different type of measurements between the buoy and the radar systems behind the buoy measurements well more localized whereas the HF radar system performs sea-surface measurements across a given circular crown as described in section 1.3.

Nonetheless, these relative error results for each of the retrieved parameters should not be considered individually. I.e., each set of parameters should be considered to describe a given wave-set (SWH, MWP, and MWD) in order not to fall into the trap that a good agreement between only one parameter is due to the good measuring of the HF radar system when it can be due to the randomness of the sea-states.

When concerning with the mean range-cell hypothesis results presented in figure 3.04, it can be concluded for the SWH parameter that all grouped range-cell sets have identical median values and that the two-closer range-cells from shore have higher inter-quartile and higher variability than the remaining range-cells sets. From figure 3.04.a) it can be observed that the box-plot representing the SWH values retrieved by the Sines coastal buoy has a similar statistical distribution to the ones computed for the Sagres HF radar range-cell sets and mean range-cell. Nevertheless, this alike statistical SWH distribution does not necessarily represent the same sea-states and does not indicates that the Sines coastal buoy could act as a validation system for the Sagres HF radar measurements. It is also possible to conclude from this figure that the mean-range cell hypothesis can be used for the SWH parameter without loss of information when compared with the measurements retrieved by all the ODAS buoys systems.

When considering with the MWP parameter, it can be concluded from figure 3.04.b) that the all the range-cells sets represent an MWP distribution with higher median value and higher inter-quartile distribution than the ones computed from the ODAS buoys data. From this figure, it is impossible to conclude which buoys location should be used to validate the Sagres HF radar MWP measurements. Furthermore, it can be concluded from the same figure that the mean-range cell hypothesis can also be used without loss of generality when concerning the MWP parameter.

Lastly, for the MWD parameter, it can be concluded from figure 3.04.c) that the distribution of the retrieved MWD parameters indeed varies within the distance from the HF radar thus resulting in a change of MWD values due to wave refraction and diffraction as expected for the Sagres location (Holthuijsen (2007)). Nonetheless, it can be concluded from the same figure that the ODAS buoys MWD measurements have a relatively smaller range of measurements than the MWD measurements performed by the Sagres HF radar and thus, even though there is MWD variability within each range-cell set, the mean range-cell hypothesis can be considered as reasonable because it cannot be decided from the figure 3.04.c) which ODAS buoy system is more suitable for the validation of MWD measurements performed by the Sagres HF radar system.

4.1.2 Discussion Concerning the Sagres HF Radar System Against the Combined Signal Results From the 1st to the 24th of April 2018 Temporal Period:

Taking into consideration the time-series representation for the SWH and MWD parameters presented in figure 3.05.a) and figure 3.05.c), it is possible to verify that both signals appear to have the same behaviour thus describing the same physical wave-sets.

From the SWH time-series shown in figure 3.05.a), it can be verified that the highest SWH values were measured by the HF radar system although a SWH maximum was still measured by the ODAS buoys combined signal for the same measurements point as can be verified from the 20th, the 60th, the 85th and the 110th four-hours time-interval. From table 3.03, it is possible to verify that the composed signal has a lower RMSE value than when comparing the RMSE values computed from every single buoy as in table 3.01. This means that a more accurate comparison is achieved when validating HF radar measurements with the measurements attained by the composed signal instead of using only the measurements retrieved by a single ODAS buoy system.

Regardless, a Pearson linear correlation coefficient of 0.81 was achieved when regarding the SWH time-series retrieved from the Faro coastal buoy against the 0.8 value achieved when considering the combined signal indicating that an identical linear relation between the HF radar system in Sagres and the Faro coastal buoy (see figure A.03) and between the HF radar system in Sagres and the combined signal (see figure 3.06.a) for this parameter. Nonetheless, this linear relation is subjected to a higher slope (m) and bias (b) values as can be seen from table 3.02 and table A.03 which are not desirable.

Taking into consideration the MWE directional distribution for the temporal period ranging from the 1st to the 24th of April 2018 presented in figure 3.07, it can be seen that the MWE distribution

obtained by the combination of several ODAS buoys represents more accurately the Sagres HF radar MWE than when considering the individual ODAS buoys systems configuration (see figure 3.02), in particular by examination of figure 3.07, it can be seen that for the MWD interval from 180º to 300º, both MWE distribution computed for the Sagres HF radar system and for the combined signal (figure 3.07.a) and figure 3.07.b)) show the same MWE distribution, with different MWP values.

Regarding the MWP time-series, it is possible to conclude by examination of figure 3.05.b) and table 3.03, that the MWP time-series represents a more complex behaviour.

When comparing the MWP time-series retrieved by the Sagres HF radar system with the one attained by the combined signal, a RMSE value of 1.68 s and Pearson linear correlation coefficient of 0.43 was obtained. Furthermore, it can be concluded from figure 3.06.b) and from the Pearson linear relation coefficient value presented in table 3.03 that a strong linear relationship exists between these two measuring systems with 69% of the MWP time-series retrieved by the Sagres HF radar system being described by a linear relation with the combined signal.

Also, it can be seen from figure 3.06, that the MWP scatter plot between the two systems does not show a clear linear scattering hence indicating that MWP values retrieved by the HF radar need a deeper understanding and are not well described by the combined signal hypothesis for the Sagres location.

For the MWD time series presented in figure 3.05.c), it is thus possible to verify that despite the fact that the HF radar measurements have higher variability, both retrieved time series show the same tendency regarding the analysed time period thus indicating that the MWD values retrieved by the HF radar can be taken as a linear combination of the signal measured by the Sines and Faro ODAS buoys systems with a RMSE value of 45.67º and a Pearson linear correlation coefficient of 0.7.

These values show that the combined signal represents the Sagres HF radar signal with a higher accuracy and higher linearity (see figure 3.06.c)) than the signal retrieved individually by any of the ODAS buoys systems studied as can be verified from table 3.01 and table 3.03 (from figure A.03 and table A.03 in Appendix A).

Furthermore, it is possible to conclude from table 3.04 that for the SWH parameter, with a confidence level of 99%, the two time-series were generated by the same physical phenomena, meaning that indeed, the Sagres HF radar system retrieves a SWH signal that is the combination of the signal retrieved by the Sines and Faro ODAS buoys due to its wider range of measurements of the sea and range for measurements. Nevertheless, the same conclusions are not true for the MWP and MWD parameter where the K-S test rejected the null hypothesis within the two measuring systems indicating that the MWP and MWD time-series retrieved by both systems were not generated by the same physical phenomena.

It is presented in figure 3.08 a scatter plot representation of the relative error values as a function of the SWH, MWP and MWD parameters retrieved by the Sagres HF radar. It can be seen from figure 3.08.a) that the SWH relative error for the combined signal has a similar behaviour to the one obtained for the SWH relative error achieved for the Sines and Faro offshore buoys measurements (see section 3.1.1, figure 3.03.a)) as it is expected since the SWH combined signal is exclusively composed of measurements performed by these buoys (section 3.1.2, figure 3.09 and table 3.05). It can be concluded from figure 3.08.a) that the SWH relative error values tend to increase until the 3 meters value and tend to decrease and remain constant up to the maximum SWH range (SWH HF radar range from 1.2 m to 7.05 m).

Concerning the with the MWP parameter, its respective relative error tends to increase for MWP values equal or higher than 9 s. This MWP relative error results can be regarded as a combination of the MWP relative error values obtained for the Sines and Faro offshore buoys since the combined signal is

exclusively composed of measurements performed by these buoys as can be verified from figure 3.09 and table 3.05 in section 3.1.2.

As for the MWD relative error series regarding the combined signal method it can be seen from figure 3.08.c) the presence of the four fundamental MWD direction. These principal MWD directions are around the 100º value, representing the Westward sea-states (levant-sea states) and around 220º, 260º and 300º values representing respectively the mean MWD value for the Faro coastal, Faro offshore and Sines coastal buoys time-series (see table 3.01, section 3.1.1) as the MWD combined signal is composed of measurements performed by these buoys (see figure 3.09 in section 3.1.2). These principal MWD direction zones are defined by a lower value of the MWD relative error and further support the wide range of sea-states measurements performed by the HF radar.

It is presented in figure 3.09 which ODAS buoy system was used to create the SWH, MWP and MWD combined signal at a given instant. It is thus possible to conclude from figure 3.09.a) and figure 3.09.b), that for the SWH and MWP parameters, the combined signal was exclusively composed of measurements performed by the Sines coastal and Faro offshore buoys. This may be to the fact that the wave-sets measured by these systems represent more energetic wave-sets as can be regarded from figure 3.01.a) and are associated with a higher signal-to-noise ratio as previously described. The fact that some measurement points for the MWD parameter combined signal were retrieved by the Faro coastal buoy associated with SWH/MWP parameters retrieved from the Sines coastal/Faro offshore buoys might be due to some data incoherence due to the different sampling rates between the measuring systems as described in section 2.4. Nevertheless, the selection of more energetic wave-sets by the HF radar can be verified from the 55th four hours time interval in the temporal time-series derived by each buoy (figure 3.01.c)) and by the contribution of each buoy for the combined signal in figure 3.09.c).

As can be seen from table 3.05 the respective relative occurrence coefficients vary within each measured parameter within the same measuring system. This, although being a peculiar result, may also indicate that the signal-to-noise ratio significantly affects the parameter derived value by the use of the zeroth-order moment for the SWH parameter and the second-order moment for the MWP.

4.1.3 Discussion Concerning the Sagres HF Radar System Against the Combined Signal Results From the 1st of January to the 24th of April 2018 Temporal Period:

Considering the SWH parameter retrieved by both the Sagres HF radar and the combined signal it is possible to verify from figure 3.10.a) and figure 3.11.a) that generally for SWH values lower than 2.5 m the Sagres HF radar and the combined signal tend to retrieve similar SWH values. As for SWH values higher than 2.5 m, the HF radar tends to overshoot these measurements when in comparison with the combined signal. This can be further supported by the mean and standard deviation values retrieved for the SWH time-series obtained by the two systems, presented in table 3.07 where an identical mean value was obtained by the two systems and a higher standard deviation value was attained when considering the HF radar time-series indicating a higher degree of variability.

Regarding a possible linear relation between the two measuring systems for the SWH parameter, table 3.07, indicates a Pearson linear coefficient value of 0.45, indicating that 20% of the behaviour between the two time-series can be justified by a linear relationship between these two measuring systems where the data-dispersion and the linear fit can be seen from figure 3.11 and the fitting parameters can be found in table 3.06 where a slope and bias values of respectively 0.89 m and 0.80 m were achieved with a bias uncertainty of 0.19 m thus in a closer agreement with the linear theory of measurements exposed in appendix A. Nonetheless, an RMSE for the SWH parametervalue lower than the HF radar standard deviation indicates that the disparity between the two measuring systems for the SWH parameter is smaller than the HF radar spread out of data measured by its standard deviation associated with the SWH time-series.

Regarding the MWP parameter, it can be observed in figure 3.10.b) that the Sagres HF radar system overshoots the values when comparing with the values retrieved by the combined signal.

When considering a possible linear relationship between the two systems for the MWP parameter, it can be concluded from figure 3.11.b) and table 3.06, that a linear relation is not very trivial with the MWP data-sets points forming a not very specific straight line of dispersion (see fitting parameters from table 3.06 with a particularly high bias value of 6.67 s) with its Pearson linear coefficient value being of 0.38, indicating that only 14% of the behaviour of the HF radar MWP data-series can be described with a linear relation to the MWP data-series retrieved by the combined signal.

Nevertheless, it can be concluded from table 3.07 that although the two measuring systems have alike standard deviation values, the mean MWP value retrieved for the HF radar system is significantly higher than the mean MWP value obtained for the combined signal time series (about 23% higher) and the RMSE computed for the comparison between the two time-series is 6.5% higher than the HF radar standard deviation value, indicating that the disparity between the two retrieved signals was higher than the HF radar spread of data.

A last note on the MWP time-series retrieved by the Sagres HF radar system is that when comparing it with the MWP time-series retrieved by the combined signal, it can be verified that the Sagres HF radar system has a minimum MWP retrievable value of 6 s. This is important to note because it was only found one reference of the MWP measurements range in the literature (Lipa and Nyden, (2005)) and thus a further effort should be taken to understand this range of MWP integration.

When considering the retrieved time-series for the MWD parameter shown in figure 3.10.c), it is possible to identify that as in resemblance of what happened in section 4.1.2 for the MWD parameter, the Sagres HF radar system data has a higher degree of variability than the data attained by the combined signal. This can be confirmed by the standard deviation values retrieved by both measuring systems presented in table 3.07, being the standard deviation value attained for the HF radar time-series around 2 times higher than the combined signal MWD standard deviation value which can be regarded as an expected result due to the wider range of measurements performed by the HF radar system.

Regardless, the RMSE value associated with the MWD parameter is smaller than the standard deviation value attained for the HF radar MWD data as can be concluded from table 3.07. Thus, when regarding a possible linear relation between the MWD parameter retrieved by both the time-series, a value of 0.77 was obtained for the Pearson linear coefficient for the two time-series meaning that about 59% percent of the relation between the two signals can be described by a linear relationship between the two systems as can be seen from figure 3.11.c) and with linear fit parameters of 0.38 for the slope and 174.22º for the bias of a possible linear relationship between these two systems as can be concluded from table 3.07. The bias value of 174.22º represents a possible “calibration” difference between the Sagres HF radar and the combined signal as presented in appendix A.

When considering the results attained for the MWE directional distribution, it can be examined from figure 3.12 that as expected and as the analysed period increases, the HF radar and combined signal MWE directional distributions tend to become similar. In particular, it can be verified from the same figure that for the 180º to 315º MWD values, both the systems appear to be measuring the same kind of sea-states, MWE and MWP values (noting that both figures have different scales for the energy maps and MWP radial values). Still, the MWE values retrieved for the MWD interval from 345º to 150º, representing wave-sets with MWE values from 2.5 to 7.5 times the mean MWE computed fort the Sagres HF radar system is not represented in the combined signal MWE directional distribution plot for the combined signal thus further supporting the hypothesis that this kind of measurements do not represent real wave sets.

Here, the results for the Kolmogorov-Smirnov test presented in table 3.08 are discussed. Since the K-S test was rejected for all the retrieved parameters, namely SWH, MWP and MWD it is concluded that none of the retrieved data-sets represents the same physical phenomena. Nonetheless, these rejected

test might be as can be concluded from analyses of figure 3.12, to a lack of information in the combined signal to describe precisely the HF radar signal, in particular, considering the MWD interval from 330º to 180º and thus it is left here as a hypothesis that a more precise combined signal could be obtained by the mooring of a coastal buoy near Sagres resulting hence in accepted K-S tests.

When considering the relative error results associated with with the SWH parameter presented in figure 3.13.a), it can be concluded that these relative error values tend to increase as the SWH parameter retrieved by the Sagres HF radar increases. This is in agreedment with the discussion of the results presented for the SWH time-series, where it was concluded that the Sagres HF radar overshoots the SWH values higher than 2.5 meters and thus higher relative error values were achieved from this SWH value.

As for the MWP relative error values, it is possible to verify from figure 3.13.b) that lower MWP retrievals are associated with lower relative error values and that as the MWP values increase, the relative error values also increase.

Relatively to the MWD relative error values presented in figure 3.13.c), it can be verified that the resulting combined signal is able to describe in a more accurate way the MWD time-series retrieved by the Sagres HF radar, where the MWD zones respective to each buoy are now better described by the combined signal method than when considering the individual MWD measurements of each buoys system as presented in section 3.1.1 and described in section 4.1.1.

From figure 3.14, it is possible to verify for a given instant that the buoy used to build the SWH combined signal may not be the same as the one used for the MWP and MWD combined signal (as an example, see the 150th six hours time interval measurements, where it was used a SWH measurement performed by the Faro offshore buoy for the combined signal, a MWP measurement performed by the Sines coastal buoy for the MWP and a MWD measurement performed by the Faro coastal buoy). It appears to me that the only fair way to justify this kind of behaviour as previously described in section 4.1.2, is by the mixing of results due to the different sampling frequency within each measuring system. Regardless, it is important to note that higher SWH values are generally associated with measurements performed by the Sines coastal and the Faro offshore buoys and that less energetic sea-states are more frequently associated with sea-states measured by the Faro coastal buoy.

When considering the MWP parameter, it is important to notice that most of the values used for the combined signal were obtained by the Sines coastal buoy with some lower MWP values being associated with measurements retrieved by the Faro offshore buoy.

As for the MWD parameter, it can be concluded from figure 3.14.c) that the buoy used to retrieve MWD values closer to the HF radar mean MWD value (see table 3.09) was the Faro coastal buoy. Also, it can be regarded from the same figure that MWD values retrieved by the Sagres HF radar system associated with North-Eastward sea-states are consistently associated with measurements performed by either the Sines coastal buoy or the Faro offshore buoy due to the shore morphology.

With respected to the relative occurrence frequency coefficients for the SWH, MWP and MWD, these can be checked from table 3.14 to assess the relative contribution of each buoy for the elaboration of the combined signal.

From figure 3.15, it is possible to identify the measurement range of each of the retrieved parameters corresponding to measurements performed by each of the measuring systems and to examine if a particular sea-state creates a more recurrent measurement within a given ODAS buoys and the HF radar.

Regarding the SWH parameter in figure 3.15.a), it is possible to assess that SWH values lower than 1m are retrieved by the Faro and Sines buoys and that the HF radar system can follow the ODAS buoys measuring systems range from SWH values of 1 m up to 7 m. Furthermore, it is important to note that the HF radar SWH range of measurements is in agreement with the theoretical limit values described

in section 1.2.1 thus increasing the confidence in the retrieved data, respectively for the higher and lower SWH values.

When considering the MWP parameter, it is possible to verify from figure 3.15.b) that the Sagres HF radar system cannot resolve MWP values lower than 6 s whereas all the considered ODAS buoy system can resolve MWP values from 4 s to 6 s. Nonetheless, it is also possible to verify that the Sagres HF radar system detects MWP values in the 6 s to the 12 s range being these retrieved values also measured by the associated ODAS buoys systems. The more frequent MWP values retrieved values are also associated with MWP values attained by the Sines coastal buoy (see table 3.09), although it is important to note that this does not necessarily mean that the same sea-states were simultaneously measured by the two measuring systems.

Regarding the MWD values retrieved by both systems, it is possible to verify from figure 3.15.c), that the Sagres HF radar MWD interval of measurements ranges from 0º to 360º while measurements performed by the ODAS buoys systems are well more focused. Nevertheless, it is possible to identify from figure 3.16 and figure 3.15.c) the two main sea-states present at the Sagres location, namely the Westward sea-states with MWD values ranging from 120º to 180º and Eastward sea-states with MWD values ranging from 180º to 300º.

MWD values in the interval from 330º to 120º are associated with MWD wave-sets from shore. If these wave-sets are associated with low MWP and low SWH values, they can be linked with locally generated wind-seas sea-states (Kinsman (1965)) and thus this kind of measurements can be considered as reliable. By examination of figure 3.12 and figure 3.16.a), it is possible to verify that MWD values in the range of 330º to 120º are also linked with very energetic wave-sets, i.e. with SWH values in the interval from 4.5 m to 6 m and to MWP values in the range from 4 s to 6 s (as can be verified from figure 3.16.b)).

The fact that some of the measurements of the Sagres HF radar indicate waves-sets with SWH in the range of 4.5 m to 6 m from shore turns this kind of measurements as dubious. Since the mean-range cell hypothesis indicates that waves are being measured within an angular sector placed 15 km from shore it results in a maximum fetch of 15 km. In fact, Gröen and Dorrestein (1976) have computed that for a maximum fetch of 15 km, for wind-speeds of about 30 m/s blowing in a steady state for about 1.5 hours, the maximum characteristic[6] wave height attainable is of 3.5 m and hence, the arise of waves with such SWH values seems very unlikely as that this kind of fetch is too small for the generation of this kind of waves.

It can be verified from figure 3.16 and figure 1.07, that the MWD measurements performed by the Sagres HF radar agree with the climatological mean wave directions derived by Costa *et al.* (2001) when regarding that the MWD directional histogram for the Sagres HF radar can be considered as combination of the climatological directional plots attained for the Sines and Faro regions.

Considering the mean range-cell hypothesis and ODAS buoys results presented in figure 3.17 for all the retrieved parameters, it is possible to conclude from figure 3.17.a) that for the HF radar system, the closer to the radar set of range cells retrieved higher SWH values and that the set of range-cells located further from the radar retrieve lower SWH values. Since it was assumed the deep water hypothesis, the fact that the closer to shore range cells set retrieved higher SWH values should not be due to the shoaling of sea-waves as the distance from the shore decreases and thus, due to energy flux conservation principles, the height of a given wave-set has to increase, as described by Holthuijsen (2007). It should instead be due to the fact that closer to shore range-cells sets, result in scattered electromagnetic wave closer to the shore and thus are subjected to less attenuation and thus result in a more energetic sea-spectrum.

[6] The characteristic wave height (observed visually) is biased slightly high than the significant wave height which is assessed from instruments.

In terms of statistical values, the mean-range cell has an identical median and inter-quartile distribution to the Sines coastal buoy and the further range-cell sets, namely the distance sets from 15 km to 20 km, 20 km to 25 km and 25 to 30 km retrieved a data-set with identical statistical properties as the one obtained for the Faro offshore although with a higher degree of variability.

When considering the mean-range cell hypothesis for the MWP, a different kind of behaviour is obtained. For the MWP mean-range cell hypothesis, the Sagres HF radar MWP periods were retrieved in a way that similar results were attained within each range-cell group as would be expected by the linear deep-water theory (Holthuijsen, 2007). Also, it is possible to verify that the values retrieved by the ODAS buyos systems are clearly inferior to the ones retrieve by the Sagres HF radar again further supporting the suspicions that the Sagres HF radar system overestimates MWP values. Nevertheless, the mean-range cell set gives a good description of the MWP values retrieved by all the range-cells sets.

Recalling the mean-range cell hypothesis for the MWD parameter, it is possible to conclude from figure 3.17.c) that MWD values change considerably within each range-cell set as expected according to wave diffraction and refraction phenomena described by Holthuijsen (2007). Waves follow a perpendicular path to the parallel depth contour lines thus allowing a lower propagation speed and changing their direction towards the shore as the water depth decreases. The results in figure 3.17.c) show that range-cell sets further from the shore represent wave-sets with higher MWD values and also that, range-cell sets closer to the shore wave represent waves with lower MWD values. Since none of the ODAS buoys show a similar MWD behaviour as the ones described by each single range-cell set, the mean-range cell hypothesis was considered as valid.

4.2 Alfanzina HF Radar System:

4.2.1 Discussion Concerning the Alfanzina HF Radar System Against Single ODAS Buoys Measurements Results:

In this section, the obtained results concerning the validation and assessment of the Alfanzina HF radar measurements resorting to individual measurements performed by either the Faro offshore or coastal buoy are analysed and discussed.

Regarding the SWH, MWP and MWD time-series retrieved by the Alfanzina HF radar and the ODAS buoys systems presented in figure 3.18, it is possible to identify a similar tendency of the MWD time-series for all the measuring systems which lead to similar SWH and MWP time-series. In particular, it can be observed for the Faro offshore buoy MWD time series (25^{th}, 90^{th} and 105^{th} four hours time intervals) the occurrence of South-Eastward wave-sets which are not detected by the HF radar MWD time-series due to the morphology of the Algarve shore, thus resulting in higher SWH values for the Faro offshore buoy SWH time-series but not in the Alfanzina HF radar or Faro coastal buoys time series.

It is interesting to note that even though these highest SWH values are not presented in the Alfanzina HF radar SWH time-series, similar MWP values were measured simultaneously by the Faro offshore buoy and the Alfanzina HF radar system. This behaviour can be regarded as an incoherence between the retrieved MWD values and their respective MWP retrieved by both systems since it indicates that the measuring systems were measuring different sea-states at the same instant i.e. sea-states with different genesis zones as in agreement with their MWD values but with identical MWP time-series values. As an example of this behaviour, the 110^{th} four hours-time intervals can be considered, indicating South-Eastward sea-states according to the Faro offshore buoy and Westward sea-states according to the Alfanzina HF radar MWD values.

Also, it can be noted from the SWH time-series, that a good agreement between HF radar measurements and Faro coastal buoy measurements is achieved for values of SWH lower than 1.5 m. Regarding the Westward sea-states detected in the MWD time series for the 5^{th} to 10^{th} four hours-time

intervals, it can be concluded that the closer values of SWH and MWP were retrieved by both the Faro offshore buoy and the HF radar system. As for the 100th to 125th four hours-time intervals, it can be observed that the HF radar system was the first measuring system to detect the Levant sea-states. This might be due to the generation of local waves, due to the Easterly wind influence, which were first detected by the HF radar system and then by the ODAS buoys systems and is supported by a decrease in the MWP time-series values as expected.

Regarding the mean and standard deviation values for the SWH parameter retrieved by both the HF radar system and the ODAS buoys systems, it is possible to conclude from table 3.09 that the closest values within the measuring system were achieved when considering the Alfanzina HF radar system and the Faro coastal buoy. This conclusion is also supported by the RMSE and the Pearson linear coefficient values being the first the lowest and the former the highest within the Faro ODAS buoys systems and by the linear fits parameters that can be consulted in Appendix A, (see table A.04 and table A.05).

In respect to the MWP parameter, it is clear from the statistical analyses presented also in table 3.09 and by the MWP time-series represented in figure 3.18.b) that the HF radar system clearly overestimates the MWP values when comparing these results with the ones retrieved by the Faro coastal buoy and a nearly identical time-series was achieved between the HF radar system and the Faro offshore buoy. Even though a similar Pearson linear coefficient value was achieved when considering the MWP series retrieved by both the Faro offshore and Faro coastal buoys, it can be conclude from figure A.04.b), figure A.05.b), table A.04 and from table A.05, that more desirable linear fitting parameters were obtained when considering the MWP time series between the Alfanzina HF radar system and the Faro offshore buoy.

The large standard deviation value computed for the Alfanzina HF radar MWD time-series indicates a greater variability as can be observed from figure 3.18.c) than when considering the MWD time-series retrieved by the Faro offshore buoys. A stronger linear relation and greater accuracy were achieved when comparing the HF radar retrieved values with the values retrieved by the Faro coastal buoy than when considering the results retrieved by the Faro offshore buoy as indicated by the lower RMSE and higher Pearson linear coefficient values.

By observation of the MWE directional distribution plot regarding the 1st to the 24th of April 2018 time period for the HF radar system in figure 3.19.a) and by comparing it with the mean directional energy for the Faro ODAS buoys systems in 3.19.b) and 3.19.c), it is possible to recognise that the HF radar system has a wider angular range of measurements as presented in section 2.1, where its wider angular range can incorporate measurements from both the Faro buoys although noting that the angular interval from 270º to approximately 325º presented in the Faro offshore buoy MWE plot cannot be measured by the HF radar system due to the shore morphology.

Nonetheless, it is possible to observe that the MWE directional distribution for the Alfanzina HF radar system and for the Faro offshore buoy share the same MWP scale in agreement with the MWP time series present in figure 3.18.b) and that the MWE scale is similar between measuring systems as can be deduced by figure 3.19 and figure 3.02.c). Also, similar MWE and MWP retrieved values for the levant sea-states can be observed in figure 3.19 recalling the MWD values within the 100º to 125º interval and for the Southern sea-states concerning MWD values of 180º.

When comparing the Alfanzina HF radar system MWE directional distribution with the one obtained for the Faro coastal buoy, it is possible to observe that the radial scale (MWP) for the coastal buoy MWE directional distribution is smaller than the radial scale in the MWE directional distribution for the HF radar system meaning that the MWP values measured by the HF radar system are significantly higher than the ones retrieved by the Faro coastal buoy. In spite of the scale differences, it is possible to conclude from figure 3.19.a) and figure 3.19.c) that identical MWE values are presented in the MWE directional distribution plots for both systems when regarding the MWD values around 180º and from 225º to 255º.

It is also important to notice the presence of very energetic wave sets in the Alfanzina HF radar MWE directional distribution with MWD values in the interval from 45º to 60º, indicating that this kind of sea-states are propagating from shore as can be verified from figure 3.19 with MWP ranging from approximately 5.7 s to 13 s. Since in this analyses it is considered that the Alfanzina HF radar system measures an angular sector within a distance from the radar equal to half of the radar maximum range it comes as very unlikely the presence of such energetic wave-sets coming from shore, due to the fact that this distance is not sufficiently large for the generation of wave-sets with such SWH values from local winds (Gröen and Dorrestein, 1976) and also that MWP values of 13 s are associated with swell generated sea-states and thus are unlikely to be generated from shore (Kinsman (1965)).

About figure 3.18.a) and figure 3.20.a), it is possible to conclude that when less energetic sea-states were being recorded (SWH values lower than 1.5 m), the Faro coastal buoy retrieved SWH values closer to the ones retrieved by the Alfanzina HF radar and thus, resulting in smaller relative error values than when comparing with measurements performed by the Faro offshore buoy for the same sea-states. When concerning with higher sea-states, the relative error values associated with the SWH parameter tend to increase when dealing with measurements performed by the Faro coastal buoy and tend to decrease when dealing with measurements performed by the Faro offshore buoy. Hence, it is possible to conclude that generally the lower sea-states retrieved by the Alfanzina HF radar are more accurately described by measurements performed by the Faro coastal buoy and that the higher sea-states retrieved by the HF radar are more accurately described by measurements performed by the Faro offshore buoy.

Regarding the MWP relative error parameter in figure 3.20.b), it can be verified that both buoys systems represent an identical relative error distribution throughout the full MWP range of measurements retrieved by the Alfanzina HF radar. The fact that the relative error associated to measurements performed by the Faro offshore buoy tend to be lower than the ones associated with measurements performed by the Faro coastal buoy may be due to the over-estimation of MWP values measured by the Faro coastal buoy by the HF radar (see figure 3.18 and figure A.04.b), figure A.05.b), table A.04 and table A.05 in appendix A) and thus, since the Faro offshore buoy retrieved higher MWP values, they are closer to the ones retrieved by the Alfanzina HF radar, hence leading to lower relative error values.

When concerning with MWD relative error values regarding figure 3.20.c), it can be verified that these relative error values tend to decrease for three MWD zones. The first MWD zone is due to the Westward sea-states, from 90º to the 120º values. The other two zones are linked to the mean MWD values computed for the MWD time-series retrieved by both buoys systems. These values are 221.63º for the Faro coastal buoy and 260.5º for the Faro offshore buoy (see table 3.09). From figure 3.20.c) it is possible to recognized that the Alfanzina HF radar does not correctly describe the mean MWD retrieved by the Faro offshore buoy (where a minimum of the MWD relative error was expected as in resemblance to figure 3.03 in section 3.1.1) and also the wider measurements of sea-states by the HF radar than when comparing with the ODAS buoys systems.

By inspection of figure 3.21.a) it is possible to recognise that there is a slight variation of the SWH parameters throughout the range-cell intervals. Respectively, this parameter shows a tendency to increase as the distance from the HF radar system increases. It can also be concluded from the same figure that the SWH values retrieved from closer range cells sets have statistical properties such as median and 25% to 75% percentile distribution closer to the ones retrieved by the Faro coastal buoy for the same parameter as expected since the Faro coastal buoy is moored at about 6 km from shore. As a comparison with the Faro offshore buoy, neither the grouped range-cells sets nor the mean range-cell group shares the same statistical properties.

As for the MWP parameter it can be concluded from figure 3.21.b) that identical statistical quantities were shared by the grouped range cell sets with a more extended 25% to 75% percentile distribution and lower median value again for the 5-10km group. Also, a more extended 25% to 75% percentile distribution for the 15-20km group was computed. When regarding the MWD properties it is

possible to conclude by inspection of figure 3.21.c), none of the Faro buoys systems share the same statistical properties as the Alfanzina HF radar system. The mean range cell was thus, considered the best hypothesis as a comparison quantity regarding the retrieved SWH, MWP and MWD parameters.

4.2.2 Discussion Concerning the Alfanzina HF Radar System Against the Combined Signal Results From the 1st to the 24th of April 2018 Temporal Period:

Regarding the obtained results in figure 3.22 for all the retrieved parameters, namely, SWH, MWP and MWD it can be verified that these parameters share a similar behaviour throughout the full time-series period and thus should be hypothesized that these retrieved signals represent the same physical phenomena. Thus, recalling figure 3.22.a), it can be verified that the highest deviation between signals arouse for the 25th four hours time intervals and it was due to the lack of data from the Faro coastal buoy for this given period of the time-series and thus a significantly higher value obtained by the Faro offshore was used for the elaboration of the combined signal as can be verified from figure 3.05.a). Nevertheless, it can be verified from table 3.11 that both the retrieved signal for the SWH time-series have identical mean and standard deviation values.

A smaller RMSE value was also achieved when considering the dispersion of the Alfanzina HF radar signal from the combined signal than when considering its deviation from the signal derived by each individual ODAS buoys as can be confirmed from table 3.11 and table 3.01 for the SWH parameter. A Pearson linear coefficient value of 0.83 was obtained when considering a possible linear relation between the HF radar signal and the ODAS buoy combined signal and this linear relation can be verified from the data scattering plot in figure 3.23 and its respective fitting parameters in table 3.10. Although this Pearson linear coefficient value was the same value to the one obtained for the SWH parameter when considering measurements performed between the Alfanzina HF radar system and the Faro coastal buoy, the fitting parameters are more desirable when considering the combined signal than when considering the values retrieved by only the Faro coastal buoy because they represent a slope (m) value closer to one and a bias (b) values closer to zero as can be verified from table 3.10 and table A.05 in Appendix A.

The Kolmogorov-Smirnov test applied to these two SWH data-sets indicates with a 99% confidence interval that the two time-series were indeed due to the same physical phenomena as can be verified from table 3.12.

As for the MWP time series, the problem of the missing data from the Faro coastal buoy is not significant due to the fact that MWP values retrieved by the Alfanzina HF radar system are generally closer to the MWP values retrieved by the Faro offshore buoy excluding punctual occurrences where MWP values get closer to the ones retrieved by the Faro coastal buoy. Regardless, the combined signal from both buoys measurements describes a more realistic representation of the signal retrieved by the Alfanzina HF radar signal as can be verified by comparison of table 3.09 and table 3.11. It is hence verifiable that the combined signal has a smaller RMSE value and higher Pearson linear coefficient than when considering the RMSE and Pearson linear coefficients values achieved by each single buoy measurements. These values result in higher accuracy and stronger linear relation between the HF radar signal and the combined signal than when comparing the Alfanzina HF radar MWP time-series with each single ODAS buoys measurements as can also be verified from the examination of figure 3.22.b) and figure 3.23.b).

Despite these positive results regarding the MWP combined signal, the Kolmogorov-Smirnov test rejects the null hypothesis (see table 3.12) between the two signals thus indicating that the two signals were generated by different wind-driven surface waves.

Recalling the MWD time-series present in figure 3.22.c), it can be verified that both the HF radar and combined signal share the same temporal tendency although the HF radar results show a higher

variability with a higher amplitude as can also be verified by comparison of the standard deviation values present in table 3.11. Once again, the lack of data from the Faro coastal buoys is visible regarding the 25th four hours time intervals measurement, where data from the offshore buoy was used to create the combined signal and thus, generating a higher discrepancy within time-series as can be confirmed from figure 3.18.c) and figure 3.22.c). Also when regarding table 3.11, it is possible to verify that a lower RMSE and higher Pearson linear coefficient were computed for the MWD parameter derived from the combined signal than when testing against each single ODAS buoys measurements, indicating once again a higher accuracy and stronger linear relation between the HF radar signal and combined signal than when comparing the HF radar system with each single buoy measurement.

Still, for the MWD parameter the Kolmogorov-Smirnov test rejects the null hypothesis using a confidence level of 99%, indicating that the two signals were not generated by the same wave-sets as can be verified from table 3.12.

From figure 3.23 and table 3.10 it is possible to verify that the quality of linear fits to the SWH and MWD parameters has increased for combined signal method than when considering the single buoy method (presented in Appendix A, figure A.04, table A.04 and figure A.05, table A.05), in particular by verifying that the slope values obtained were closer to one and the bias values were closer to zero as theoretically predicted. The same is not valid for the MWP time-series where more favourable slope and bias values were attained when considering the single buoy method. Still, the fact that a higher Pearson linear coefficient was attained when considering the combined signal method give more credibility to the linear fits parameters obtained for this method than for the values of the linear fits computed regarding the single buoy method.

When considering the MWE distribution regarding the Alfanzina HF radar system and the combined signal in figure 3.24, it can be verified that for the 100º to 270º MWD interval both the measuring systems show relatively identical MWE values that were even measured for the similar MWP values. The MWE values associated to the MWD values intervals from 270º to 300º obtained by the combined signal are not presented in the MWE directional distribution plot obtained by the HF radar system due to the shore morphology (these kind of MWD measurements were performed by the Faro offshore buoy since Cape St. Vicent acts as a curtain for these wave-sets for the Faro coastal buoy and the Alfanzina HF radar) although wave-sets with MWE values of about 3.5 times the HF radar mean MWE were measured by the HF radar signal for the 270º to 360º MWD interval.

From figure 3.25.a), it is possible to verify that for the lower SWH there are high and low relative error values although lower relative error values are more frequent than the higher ones until the 2.5 m SWH value. From the 2.5 m values up to the maximum SWH range, the relative error values tend to remain almost constant.

Recalling the MWP relative error in figure 3.25.b), it can be observed that for the MWP interval ranging from 8 s to 9.5 s a higher relative error was obtained. Noting that the MWP values from 8 s to 9.5 s are commonly associated with wind-sea sea-states (Kinsman (1965)) and recognizing also from figure 3.25.b) that the higher MWP values are associated with smaller MWP relative error, it can thus be concluded that the higher MWP sea-states (swell-sea states) are more precisely resolved by this HF radar system.

Regarding the relative error concerning the MWD parameter, it can once again be seen the presence of two MWD zones, namely the Westward zones for MWD values around 120º and the mean of the combined signal MWD series for the 250.25º value (see table 3.03). These MWD zones are associated with low values of the relative error parameter and support the capabilities of the HF radar system to describe several sea-states.

The fact that, in general, the magnitude of the relative error for every single parameter tends to be smaller than when considering measurements from each single ODAS buoys results from the method of composition of the composed signal, as described in section 2.4.

Regarding the SWH parameter, it can be concluded from figure 3.26.a) that higher SWH values retrieved by the HF radar are generally associated with measurements performed by the Faro offshore buoy whereas smaller SWH values are typically associated with measurements performed by the Faro coastal buoy.

When considering the MWP time-series, it can be concluded from figure 3.26.b) that the values retrieved by the HF radar system are typically more concordant with the measurements retrieved by the Faro offshore buoy as could be previously predicted by inspection of the MWP time series retrieved individually by the Alfanzina HF radar system and the Faro offshore buoy presented in figure 3.18.b).

As for the MWD parameter, it can be regarded from figure 3.26.c), that generally North-Westward sea-states are associated with measurements retrieved by the Faro coastal buoy, as whereas Westward and North-Eastward sea-states are typically linked with measurements performed by the Faro offshore buoy.

It is also important to note here that Westward sea-states are typically linked with more energetic wave-sets as shown in figure 3.22.a) and figure 3.22.c) for the 60th, and 105th to 120th four hours time-intervals and due to this result, it is left as an hypothesis for the more extend time-series analysis that typically more energetic wave-sets measured by the Alfanzina HF radar system are closer to measurements performed by the Faro offshore buoy whereas less energetic sea-states measured by the Alfanzina HF radar system are typically closer to measurements performed by the Faro coastal buoy, due to the exposition of the Faro offshore buoy to the offshore sea-states

Again, it is possible to verify from table 3.13 that the relative occurrence frequency coefficients vary within the same measuring system for different retrieved parameters as verified for the same temporal period for the Sagres HF radar system as described in section 4.1.3 (see table 3.05).

4.2.3 Discussion Concerning the Alfanzina HF Radar System Against the Combined Signal Results From the 1st of January to the 24th of April 2018 Temporal Period:

Here the results obtained when considering the measurements performed by the Alfanzina HF radar system and the combined signal for the temporal period ranging from the 1st of January to the 24th of April 2018 are interpreted and discussed.

Regarding the SWH parameter in figure 3.27.a), it is possible to conclude that both the retrieved time-series show a similar behaviour throughout the whole studied period. It is also possible to conclude that the highest SWH values recorded were measured by the HF radar system. However, a good response of the HF radar signal to the less energetic waves was also achieved and can be verified by regarding that this system was able to measure SWH values of 0.5 m. Since the minimum theoretical SWH retrievable value for HF radar systems with the same physical characteristics as the Alfanzina HF radar system is set to be 0.5 m (see section 1.2.1) it is important to verify the accuracy of this HF radar system when describing sea-states with such low signal-to-noise ratios. As for the upper SWH retrievable value limit, it was impossible to verify the response of the Alfanzina HF radar system to such sea-states due to the fact that such energetic wave-sets were recorded by neither of the measuring systems considered.

Recalling table 3.15, it is possible to verify that both the measuring systems have similar SWH mean values, respectively 1.53 m for the HF radar system and 1.56 m for the combined signal although a higher standard deviation value of 1.16 m was achieved for the HF radar system measurements whereas a value of 0.82 m was achieved for the combined signal time-series.

When concerning with the RMSE, a value of 1.12 m was computed and since this value is smaller than the standard deviation value achieved for the HF radar time-series, it means that the natural

spread of the HF radar retrieved data is higher than the spread of data within each measuring system indicating a good accuracy between the retrieved values by the two system.

From figure 3.28.a) it is possible to verify that the lower SWH values retrieved follow a more desirable linear relation within the two systems than when considering higher SWH values. For the higher SWH values, it can also be seen from figure 3.28.a) that the Alfanzina HF radar system tends to overestimates most of the measurements retrieved by the combined signal method although it is also possible to verify that there were some high SWH values that were also under-estimated by the HF radar. Regarding table 3.15, a value of 0.4 is presented for the Pearson linear coefficient indicating that about 16% percent of the Alfanzina HF radar signal can be reconstructed by a linear relation from the SWH values retrieved by the combined signal.

Hence, when inspecting the results for the Kolmogorov-Smirnov test presented in table 3.16, it can be verified that the null hypothesis between the two time-series was rejected with a p-value of virtually zero, thus indicating within a 99% confidence interval that our SWH time-series were generated by the different physical phenomena hence showing that the two measuring systems where not measuring the same SWH sea-states throughout the whole time series.

When recalling the MWP parameter time-series, it is possible to verify from figure 3.27.b) and figure 3.28.b) that the Alfanzina HF radar signal is not well described by retrievals attained from the combined signal. In particular, it can be confirmed by these figures that the Alfanzina HF radar system tends to overestimate the MWP values retrieved by the combined signal specifically when considering values higher than 8 s and also, again considering figure 3.28.b), it is possible to recognise that the scatter plot created from the time-series retrieved by the combined signal and the HF radar does not show a clear linear relationship between the scattered data.

Form table 3.15 it is possible to identify that the HF radar MWP time-series has a higher mean value than the one attained for the combined signal time-series. A RMSE value lower than the HF radar standard deviation was obtained thus indicating that the spread-out of data within the two measuring systems is lower than the natural spread of data retrieved by the HF radar system. Also, when analysing the obtained Pearson linear coefficient value obtained for the linear relation between the two time-series, a value of 0.37 was achieved indicating that only 3% of the HF radar retrieved signal can be described with a linear relation from the combined signal.

Furthermore, it is important to refer the result of the Kolmogorov-Smirnov test shown in table 3.16 where it is shown that the null hypothesis proposed for the two data-sets was rejected with its associated p-value being of technically zero thus indicating that the two data-sets are not representative of the same physical phenomena and hence a deeper understanding of HF radar MWP measurements should be considered.

About the MWD parameter, it can be concluded from figure 3.27.c) and figure 3.28.c) that a linear relationship between the two systems is also not trivial. It can be concluded from figure 3.27.c) that the HF radar MWD time-series has relatively higher variability than the MWD time-series obtained by the combined signal. These results are further supported by the mean and standard deviation values computed for both MWD series in table 3.15. Hence, the HF radar MWD mean value is significantly different from the mean value obtained for the combined signal and that the standard deviation value associated with HF radar measurements is relatively higher than the standard deviation value computed for the combined signal. Regardless, it is possible to verify that the RMSE value computed between the two time-series is inferior to the HF radar standard deviation value, thus indicating that the data spread within measuring systems is inferior to the natural data spread of HF radar system MWD measurements.

Furthermore, it is possible to conclude from the Pearson linear coefficient value presented in table 3.15 and by the MWD scatter plot data in figure 3.28.c), where the respective linear fits parameters can be observed from table 3.15 that for the MWD parameter, a linear relationship between the two

signals is not clear with only about 4% of the behaviour of the Alfanzina HF radar MWD time-series being described by this hypothetical linear relation with the combined signal.

From inspection of table 3.16, it can be concluded that the null hypothesis set by the Kolmogorov-Smirnov test was also rejected with it associated p-value being virtually zero as in resemblance with the SWH and MWP parameters time-series and thus the conclusion that the obtained time-series described the same physical phenomena does not apply.

From figure 3.29, it can be concluded that even though the combined signal MWE does not represent the full MWE directional distribution attained for the Alfanzina HF radar system, both MWE directional distributions show a great amount of energy respectively with 6 to 13 times the mean MWE value for the Alfanzina HF radar system and with 4 to 6 times the mean MWE value for the combined signal regarding the MWD interval from 90º to 120º.

As for the MWE directional distributions in the MWD ranges from 210º to 240º it is important to notice that even though the MWE and MWP scales differ within each measuring system, both systems identify more energetic wave-sets in this MWD interval.

It is also possible to verify from figure 3.29.a), (a larger version of this figure for the MWP class ranging from 9 s to 12 s is presented in the appendix A) that for the MWD interval from 30º to 90º the HF radar retrieved very energetic sea-states, respectively with MWE energies from 6 to 13 times the mean MWE for the Alfanzina HF radar system. Once again and as already described in section 4.2.2**,** this kind of sea-states are dubious since a 15 km fetch distance is not a sufficiently large distance for such MWE (SWH) values to be developed from local wind-sea states. From figure 3.33.b) it is possible to verify that these kinds of sea-states are typically linked to MWP values in the range from 9 s to 12 s. According to Kinsman (1965), this values of MWP values are normally associated with swell sea-states and since it is impossible to have swell-seas originating from shore for such a fetch distance, these HF radar measurements turn as unlikely.

As for the SWH relative error results presented in figure 3.30.a), it can be verified that these values tend to increase as the SWH value increases. These results were not expected since the more energetic wave-sets (higher SWH values) are associated with higher signal-to-noise ratios and thus SWH relative error values computed for more energetic wave-sets were expected to be lower than the ones computed for less energetic wave-sets.

When regarding the MWP relative error distribution in figure 3.30.b), it can be concluded that higher MWP relative error values are also associated with higher MWP values and that the computed MWP relative error values tend to increase as the MWP values increase.

Lastly, when concerning the MWD parameter relative error, it can be seen from figure 3.30.c) that these relative error values tend to decrease until the mean MWD value computed for the combined signal (238.1º, see table 3.15) thus showing the HF radar capability to measure several sea-states.

Recalling the results from figure 3.31, it is thus possible to assess which of the Faro buoys was used for the elaboration of the combined signal at a given point of measurements. Regarding the SWH parameter, one can conclude by analyses of figure 3.31.a) that the lower SWH values retrieved were typically associated with measurements performed by the Faro coastal buoy system and that for more energetic sea-states, the HF radar system generally retrieved sea-states described by both buoys, in particular, although more frequently higher SWH values were associated with measurements performed by the Faro offshore buoy, the most energetic sea-states recorded by the Alfanzina HF radar system were associated with measurements performed by the Faro coastal buoy (see the point measurements interval for the 225th six hours time period to the 245th six hours time period in figure 3.31.a)) for the temporal period considered. Furthermore, it is possible to conclude from table 3.17 that the buoy which contributed more frequently to the SWH combined signal was the Faro coastal buoy.

Taking into the consideration the buoys measurements used for the elaboration of the MWP combined signal, it can be verified from figure 3.31.b) that most frequently the MWP values retrieved by the Alfanzina HF radar system were associated with MWP values retrieved by Faro offshore buoy and that only the lower MWP retrieved values were associated with measurements performed by the Faro coastal buoy. Regarding the MWP values time-series presented in section 3.1.1 for the individual comparison of the HF radar time-series with the time-series retrieved by each of the Faro ODAS buoys, it was thus possible to verify that the MWP values retrieved by the Alfanzina HF radar system were more suitable for comparison with MWP values retrieved by the Faro offshore buoy and thus it was reasonable to expect that the most used buoy for the elaboration of MWP combined signal was the Faro offshore buoy as can be confirmed by the relative occurrence frequency coefficients presented in table 3.17.

As for the elaboration of the MWD combined signal, it can be verified from figure 3.31.c) and from table 3.17 that the MWD combined signal was essentially composed of measurements performed by the Faro coastal buoy.

Regarding the SWH, MWP and MWD histograms presented in figure 3.32 concerning measurements performed by both the Alfanzina HF radar and the Faro offshore and coastal buoys, it can be verified from figure 3.32.a) that the HF radar system was capable of performing SWH in all the SWH range also measured by both the buoys systems, in particular regarding SWH values from 0.5 m to 6.5 m, thus in agreement with the theoretical SWH limits defined in section 1.2.1.

With respect to the MWP parameter, it is possible to verify from figure 3.32.b) that the Alfanzina HF radar system does not identify the wave-sets with lower MWP values, in particular, the ones around the 4 s values. Regardless, the Alfanzina HF radar system could measure the highest MWP values also recorded from the ODAS buoys systems. It is also possible to conclude from the same figure that the MWP time-series retrieved by the HF radar system has a different distribution than the ones retrieved by the ODAS buoys systems, thus further underlining the need to study retrieving of MWP values by HF radar systems.

When concerning with the MWD histogram in figure 3.32.c), it is possible to verify that the HF radar system has a wider range of MWD measurements, and it is thus capable of measuring the North-Westwards, North-Eastwards and Eastwards sea-states present at the Alfanzina location. The most frequent MWD values measured by the Faro offshore buoy were not detected by the Alfanzina HF radar system because of the morphology of the Algarve shore. When concerning with the MWD measurements retrieved by the HF radar system within the range from 30º to 90º degrees, it can be verified from figure 3.29.a) and from figure 3.33.a) that as in resemblance of what was described in section 4.2.2, some very energetic wave-sets propagating from shore associated with MWP values from 9s to 12s were retrieved as can be concluded from figure 3.33.b). According to Kinsman (1965) these MWP values are associated with swell-sea sea-states thus indicating that the HF radar measured swell-sea sea-states with MWD pointing from the shore which is unlikely as already described.

As a final statement, it can be verified from figure 3.33 the similarity between the *waverose* histograms plotted for the Alfanzina HF radar system and the mean wave direction climatological histogram created by Costa *et al.* (2001) shown in figure 1.07.b) and hence indicating that, overall the Alfanzina HF radar measurements represent the actual sea-states within the HF radar measurements range.

As for the mean-range cell hypothesis present in figure 3.34 and starting with the SWH parameter in figure 3.34.a), it can be concluded that all the range-cell sets wave a similar median and 25% to 75% percentile distribution and thus the mean-range cell hypothesis can be used without significant loss of information. Furthermore, the SWH measurements retrieved by the Faro coastal buoy have a similar median value as the one computed when considering the HF radar mean-range cell hypothesis thought with a smaller 25% to 75% percentile distribution.

When concerning with the MWP grouped range-cell values, it can be seen from figure 3.34.b) that all the grouped range cells wave a similar median value and 25% to 75% percentile distribution with the closer to shore range-cell sets retrieving higher MWP values than the ones further from the shore. It is also possible to conclude that both buoys retrieved MWP values lower than the ones retrieved by the HF radar system and thus figure 3.34.b) can also be used to support the suspicions that the HF radar system tends to over-estimate the MWP values measured.

As for the MWD mean range-cell hypothesis, it can be concluded from figure 3.34.c) that a similar median value was achieved within all the range-cell groups with a wider 25% to 75% percentile distribution being obtained by the 15-20 km and 20-25 km range cells. It can also be verified that the uniformness of MWD values within each range-cell sets might be due to the absence of wave refraction and wave diffraction phenomena due to the morphology of the shore and as in contrast to what happened for the Sagres HF radar system described in section 4.1.3.

As a conclusion, it is to be mention that the different MWD distribution attained by the Faro buoys presented in figure 3.34.c) when comparing with the MWD distribution values achieved for the mean range-cell hypothesis is due to the fact the measurements performed by the ODAS buoys systems are well more localized than the HF radar measurements.

5 Summary and Conclusion:

In this section of the current dissertation, a summary of the discussion of the results, as well as the main achieved conclusions and further research suggestions, are presented.

Since the principal focus of this study was to validate and to assess the quality of HF radar SWH, MWP and MWD measurements resorting to ODAS buoys as validation systems, the first conclusion that one can get from section 3.1.1 and section 3.2.1 is that the HF radar systems perform wave-characterization measurements in discretized circular crowns of the sea-surface and thus, their measurements should not be assessed using a single ODAS buoy system in particular for regions where more than one sea-states are frequent. This wider range of measurements could explain the conclusions achieved by Aghabahazadeh (1994) where, if a combined signal composed from several measuring systems in different locations were to be used to validate the HF radar measurements, it results could have been more appealing in particular for the MWD conclusions.

The second main conclusion of this work was that HF radar range-cells transmit information about a variety of sea-states at different distances from the shore till the maximum radar range and thus a box plot (as an example) could be used to retrieve information about a particular sea-region and to assess the sea-states spatial variation as the distances from shore varies. Nonetheless, it is also possible to conclude from this study that, the mean range-cell hypothesis can be used as an *a priori* tool for the validation of HF radar measurements although the legitimacy of this hypothesis should always be checked with (again as an example) a box plot.

When considering the shallow-water limit of HF radar measurements, it was verified with this study that, the minimum necessary depth for HF radar wave-characterization measurements are clearly ensured for the minimum range-cell distance from shore for the Algarve HF radar network and thus no problem arises when considering the interpretation of the results due to the water depth.

Regarding the theoretical limits for the measurements of SWH values related to the signal-to-noise ratio as described in section 1.2.1, respectively for the minimum and maximum allowed values, it was concluded for the Sagres region (see figure 3.10.a) and figure 3.15.a)) that the minimum values of SWH recorded by the Sagres HF radar system were values of 1 m. Even though that in the combined signal SWH time-series the minimum SWH value presented is of 1 m, it can be seen from figure 3.15.a) that the Sines and Faro buoys were able to retrieve SWH values of 0.5 m in their respective time-series. The fact that the 0.5 m value is not presented in the combined signal time-series is due to the method used for the composition of this signal (see section 2.6) and thus it should be further investigated if the Sagres HF radar can actually retrieve sea-states with SWH values of 0.5 m or if its lower retrievable SWH value is of 1 m. According to Saviano *et al.* (2019), it was expected for the Sagres HF radar to record SWH values until 0.5 m and hence, if its lower SWH limit is to be of 1 m, it indicates that a higher signal-to-noise ratio is necessary for this HF radar to recorded lower SWH values. As for the upper limit of SWH retrievable values, even though the more energetic sea-states tend to be over-estimated by the HF radar system (see figure 3.10.a)), its highest recorded values, as well as the ones recorded by the combined signal, were inferior to the maximum theoretical SWH value allowed thus nothing can be concluded for the upper SWH limit for the Sagres HF radar system.

As for the Alfanzina location (see figure 3.27.a)), since the upper limit for the SWH parameter was not exceed for either the measurements performed by the HF radar (even considering that the HF radar over-estimates the higher SWH values) or by the combined signal nothing can be concluded for this upper limit. When considering the lower SWH limit for the Alfanzina HF radar, it was possible to verify from the same figure that SWH values equal to the lower limit, 0.5 m, were simultaneously recorded by the HF radar system and by the combined signal and hence it was concluded that the this HF radar system can accurately describe the less energetic sea-states.

As for the MWP parameter, it was found for the Sagres radar time series (figure 3.10.b), that the lowest values recorded by this radar were of 6 s whereas its respective validation combined signal was able to record considerably lower MWP values. Since a theoretical limit for the MWP parameter was not clearly found in the literature (only a brief reference from Lipa and Nyden (2005) '…The upper (lower) period limit on derived wave spectra was set at 17 s (4 s), respectively…'), a further effort to understand if these limiting values are due to the HF radar site or due to MWP retrieving method should be performed. Nevertheless, due to the fact that the Sagres HF radar system over-estimates the MWP values in the interval from 7.5 s to 9 s and that the Alfanzina HF radar system over-estimates the MWP values in the interval from 6 s to 8 s (see figures 3.11.b) and figure 3.28.b)), the method for the retrieving of MWP should be further studied and discussed.

When interpreting MWD values retrieved by a HF radar system it is important to keep in mind that these systems perform sea-surface measurements within a given circular-crown and thus this values are associated to a given distance from the shore and a respective direction as in opposition from an ODAS buoys system where measurements are considered to be representative of a given sea-state at the buoy mooring site. Hence, it is important to remember that HF radar measurements should always be considered attending first to the MWD value and then to the MWP and SWH to gain knowledge about the direction of the wave-sets at a given location.

Regarding the comparison of the time-series considerer for this study, in particular when validating the HF radar time series with the signal composed from several ODAS buoys measurements, it was possible to verify that generally, more precise results were attained when considering a smaller time-series than when considering a larger time-series and this might be, in part, due to the difference in the sampling frequencies within measuring systems, thus contributing with data mismatch.

Nevertheless, when considering the Pearson linear coefficient values for the SWH parameter it is possible to conclude from table 3.03 and table 3.07 that the *"strength"* of the linear relation between the data-series retrieved by the Sagres HF radar system concerning the more extended temporal period and its respective combined signal decreased about 58% (from 0.8 to 0.46). The same behaviour was also found for the validation of the Alfanzina HF radar system using its respective combined signal, where the Pearson linear coefficient associated to the SWH parameter decreased about 48% when considering the longer time-series (from 0.83 to 0.4 as can be seen from table 3.11 and 3.15). Due to these results, the retrieving of SWH values by the HF radar systems are taken as accurate but as already described, they should be paired with a MWD value also retrieved by the HF radar system to identify the sea region from where this sea-states were originated.

Also, it is possible to verify that for the validation of the Sagres HF radar system the Pearson linear coefficient associated with MWP value were practically constant within the two studied time-series (i.e. 0.43 for the first temporal-period and 0.38 for the second time-series see table 3.03 and table 3.07) and also, a similar Pearson linear coefficient value was computed for the second temporal period regarding the MWP time-series retrieved by the Alfanzina HF radar system and the signal composed from the Faro buoys (Pearson linear coefficient of 0.36, see table 3.15) thus indicating that about of 13% of the MWP time-series retrieved by a given HF radar system can be described by a linear relation with a combined signal composed of measurements performed by several ODAS buoys subject to the same sea-states and thus strengthening the precision of HF radar MWP measurements. This low accuracy of the HF radar system when retrieving the MWP parameter might be due to the retrieving method using the second-order momenta of the variance density spectrum as described in section 2.2 and hence be more susceptible to the presence of noise in HF radar measurements.

Concerning with the MWD parameter, it was observed that the computed Pearson linear coefficients for the two radar sites decreased from the first temporal period to the second temporal period (as can be once again verified from table 3.03 and table 3.07 for the Sagres HF radar and table 3.11 to table 3.15 for the Alfanzina radar site). Regardless, Pearson linear coefficient values of 0.90 and 0.69 were initially computed for the validation of the Sagres and Alfanzina HF radar systems respectively and were subsequently reduced to 0.59 and 0.03. These differences in the Pearson linear coefficient

values concerning the two studied radar location might be due to the fact that the signal composed from the Faro buoys is not sufficient embracing to describe the MWD time-series retrieved by the Alfanzina HF radar system and thus a wider range of MWD measurements can be seen in the Alfanzina HF radar time-series than in the time-series retrieved by the combined signal as can be concluded from figure 3.24.c) and 3.29.c).

Regardless, it is important to mention the high Pearson linear coefficient associated with the MWD parameter retrieved by the Sagres HF radar system, showing that 80% for the first temporal period and 59% for the second temporal period of the MWD time-series can be justified from a linear relation with the MWD time-series retrieved by the combined signal composed. The fact that the Sagres region is a location of sea-bimodality turns these results even more exciting and thus validates the Sagres HF radar MWD measurements hence bearing in mind that these retrieved values are valid for a given circular crown around the radar site.

As for the MWD time-series obtained by the Alfanzina HF radar system, a further effort should be taken to understand if a more accurate comparison between the MWD values retrieved by this HF radar and the combined signal could be obtained if another ODAS buoy system was incorporated in the combined signal, in particular to describe the North-Eastward sea-states detected by the HF radar system and not by the combined signal as can be verified from figure 3.29. (MWD values from 90º to 150º) or if the MWD values are associated with deviations of HF radar measured antenna pattern from the ideal antenna pattern thus correctable by a software upgrade as already described. Nonetheless, it is important to note that the North-Eastward sea-states presented in the Alfanzina HF radar MWE directional plot (figure 3.29) can also be observed in the climatological directional histograms elaborated by Costa *et al.* (2001) for the Faro region as can be observed from figure 1.08.b) with a relative occurrence coefficients of 23.2% thus emphasizing the need of another ODAS buoy in the Faro combined signal in order to correctly validate and assess the Alfanzina HF radar measurements.

Furthermore, the presence of very energetic sea-states with MWD values from shore represents an unlikely phenomenon since a fetch distance of 15 km (according to the mean-range cell hypothesis in section 2.3 is not sufficiently large for the generation of such energetic wave-sets from local-winds and should be further investigate in particular by taking wind-speed and wind-direction data retrieved from a local meteorological station into consideration. Similar results of energetic sea-states with MWD values from shore can also be seen from Liu *et al.* (2011) in figure 7.d although without a further explanation.

When concerning with the SWH *waveroses* retrieved by both the Sagres and Alfanzina HF radar systems in figures 3.16.a) and figure 3.33.a) respectively, from where it can be seen that these directional histograms are in agreement with the climatological directional histograms studied by Costa *et al.* (2001) and presented in figure 1.08 for the Sines and Faro region hence further supporting the validity of the Sagres and Alfanzina HF radar measurements.

Finally, the most important conclusion to take from this work is that HF radar have a different way of retrieving the sea-states information than the buoys systems due to the fact that their measurements range is wider than the buoys range and thus when possible and in particular for region where sea bi-modality is expected, HF radar measurements should not be directly tested against measurements performed by a single ODAS buoy system.

6 References:

Aghababazadeh, F. (1994); “Comparison of Sea Wave Measurements Using HF Radar and Numerical Model (HISWA) Hindcast”; MSc. Thesis; Tu Delft; June 1994.

Barrick, Donal E. (1971); “First-Order Theory and Analysis of MF/HF/VHF Scatter from the Sea”; IEEE Transaction on Antennas and Propagation; January 1972; Pages 2-10.

Barrick, Donal E. and Lipa, Belinda J. (1986); “Correcting for Distorted Antenna Patterns in CODAR Ocean-Surface Measurements”; IEEE Journal of Oceanic Engineering; Vol.11; Nº2; April 1986; Pages 304-309.

Barrick, Donald E. (1976); “Extraction of Wave Parameters from Measured HF Radar Sea-Echo Doppler Spectra”; Radio Science; Vol.12; Nº3; May-June 1977; Pages 415-424.

Barrick, Donald E. (1977); “HF Radio Oceanography – A Review”; Boundary-Layer Meteorology; Vol.13; (1978); Pages 23-43.

Calisal, S.M.; (1983); “A Note On The Derivation Of Potential Energy For Two-Dimensional Water Waves”; Ocean Engineering; Vol.10; Nº2; 1983; Pages 133-138.

Chen, Zhao; Zezong, Chen; Yammi, Jiang; Kingang, Fan and Gengfei, Zeng (2013); “Exploration and Validation of wave-Height Measurements Using Multifrequency HF Radar”; Journal of Atmospheric and Oceanic Technology; Vol.30; Nº1; September 2013; Pages 2189-2202.

Cheng, David K.; “Field and Wave Electromagnetics”; Pearson; 2nd Edition; 1989

CODAR Ocean Sensors (2016); “CODAR Ocean Seansors SeaSonde Remote Unite System Specifications”.

Costa, Mariana; Silva, Raquel; and Vitorino, João; (2001); “Contribuição Para o Estado da Agitação Marítima na Costa Portuguesa”; Comunicação Instituto Hidrográfico.

Göen, P. and Dorrestein; (1976); “Zeegolven. KNMI Opstellen op Oceanografisch en Maritiem Meteorologisch Gebied”; Vol.11, Page 124.

Graber, Hans C. and Heron, Malcolm L. (1997); “Wave Height Measurements from HF Radar”; Oceanography; Vol.10; Nº2; Pages 90-92.

Gurgel, K.-W; Essen, H.-H and Kingsley, S. P. (1999); “HF Radars: Physical Limitations and Recent Developments”; Coastal Engineering; Vol.37; Nº3-4; Pages 201-218.

Gurgel, Kauls-Werner and Schlick, Thomas (2006); “An Empirical Method to Derive Ocean Waves from Second-Order Bragg Scattering: Prospects and Limitations”; IEEE Journal of Oceanic Engineering; Vol.31; Nº4; October 2006; Pages 804-811.

Holthuijsen, Leo H.; “Waves in Oceanic and Coastal Water”; Cambridge; 2007

Huang, Weinin and Gill, Eric W. (2019); “HF Surface Wave Radar”; Wiley Encyclopaedia of Electrical and Electronics Engineering; February 2019; Pages 1-11.

Hussein, Rosul and Alkareem, Farah Abd (2018); “Gage Repeatability and Reproducibility Study”: Association of Arab Universities Journal of Engineering Sciences; Vol.25; Nº1; 2018; Pages 213-225.

Kohut, Josh T and Glenn, Scott M. (2002); “Improving HF Radar Surface Current Measurements with Measured Antenna Beam Patterns”; Journal of Atmospheric and Oceanic technology, Vol.20; September 2003; Pages 1303-1316.

Kuik, A. J. (1988); “A method for the Routine Analysis of Pitch-And-Roll Buoy Wave Data”; Journal of Physical Oceanography; Vol.18; July 1988; Pages 1020-1034.

Laws, Kenmeth; Paduan, Jeffrey D.; Verecky, John (2009); “Estimation and Assessment of Errors Related to Antenna Pattern Distortion in CODAR SeaSonde High-Frequency Ocean Current Measurements”; Journal of Atmospheric and Oceanic Technology; Vol.27; June 2010; Pages 1029-1043.

Lipa, Belinda (1976); “Derivation of Directional Ocean-Wave Spectra by Integral Inversion of Second-Order Radar Echoes”; Radio Science; Vol.12; Nº3; May-June 1977; Pages 425-434.

Lipa, Belinda and Barrick, Donald (1980); “Methods for the Extraction of Long-period Ocean Wave Parameters from Narrow Beam HF Radar Sea Echo”; Radio Science; Vol.15; Nº4; July-August 1980; Pages 843-853.

Lipa, Belinda and Nyden, Bruce (2005); “Directional Wave Information from the SeaSonde”; IEEE Journal of Oceanic Engineering; Vol. 30; Nº1; January 2005; Pages 221-231.

Lipa, Belinda J.; Barrick, Donald E. (1983); “Least-Squares Methods for the extraction of Surface Currents from CODAR Crossed-Loop Data: Applications at ARSLOE”; IEEE Journal of Oceanic Engineering; Vol.8; Nº4; October 1984; Pages 226-253.

Liu, Yonggang; Weiserberg, Robert H. and Merz, Clifford R. (2010); “HF Radar Performance in a Low-Energy Environment: CODAR SeaSonde Experience on the West Florida Shelf”; Journal of Atmospheric and Oceanic Technology; Vol.27; October 2010; Pages 1689-1710.

Long, Regan M.; Barrick, Don; Largier, John L. and Garfield, Newell (2011); “Wave Observations from Central California: SeaSonde Systems and In Situ Wave Buoys”; Journal of Sensors; 2011; 18 pages.

Lopes, Raul H. C.; Reid, Ivan and Hobron, Peter R; (2007); “The two-dimensional Kolmogorov-Smirnov Test”; Proceeding of Science; XI International Workshop on Advanced Computing and Analysis Techniques in Physics Research; April 23-27 2007; Amsterdam, the Netherlands.

Lorent, P.; Piedracoba, S.; and Fanjul, E. Alvarez (2014); “Validation of High-Frequency Radar Ocean Surface Current Observations in the NW of the Iberian Peninsula”; Continental Shelf Research; Vol.92; 2015; Pages 1-15.

Maat, N.; Kraan, C. and Oos, W. A. (1990); “The Roughness of Wind Waves”; Boundary-Layer Meteorology; Vol.2; 1991; Pages 89-103;

Manton, M. J (1971); “On the Generation of Sea Waves by a Turbulent Wind”; Boundary-Layer Meteorology; Vol.2; 1972; Pages 248-364.

Mao, Yadan; Heron, Malcolm L. (2007); “The Influence of Fetch on the Response of Surface Currents to Wind Studied by HF Ocean Surface Radar”; Journal of Physical Oceanography; Vol.38; May 2008; Pages 1107-1121.

Martens, Pim; McEvoy, Danyn and Chang Chieng (2009); “The Climate Change Challenge: Linking Vulnerability, Adaptation and Mitigation”; Current Opinion in Environment, Adaptation and Mitigation; Vol.1; August 2009; Pages 14-18.

Massey, Frank J. Jr (1951); “The Kolmogorov-Smirnov Test for Goodness of Fit”; Journal of the American Statistical Association; Vol.46; Nº253; March 1951; Pages 68-78.

McGranahan, Gordon; Balk, Deborah and Anderson, Bridget (2007); “The Rising Tide: Assessing the Risk of Climate Change and Human Settlements in Low Elevation Coastal Zone”; Environment & Urbanization; Vol.19; Nº1; April 2007; Pages 17-37.

Meindl, A. (1996); “Guide to Moored Buoys and Other Ocean Data Acquisition Systems”; World Meteorological Organization; Pages 17-18.

Paduan, Jeffrey D. and Graber, Hans C. (1997); “Introduction to High-Frequency Radar: reality and Myth”; Oceanography; Vol.10; Nº2; Pages 36-39.

Paduan, Jeffrey D.; Kim, Kyung Cheal; Cook, Michael S. and Chavez, Francisco P. (2005); “Calibration and Validation of Direction-Finding High-Frequency Radar Ocean Surface Current Observations”; IEEE of Oceanic Engineering; Vol.31; Nº4; October 2006; Pages 862-875.

Peixoto, José P. and Oort, Abraham H.; “Physics of Climate”; AIP-Press; 1992

Raven, J. A. and Falkowski, P.G. (1999); “Oceanic Sinks for Atmospheric CO2”; Plant, Cell and Environment; Vol.22; 1999; Pages 741-755.

Saviano, Simona; Kalampokis, Alkiviadis; Zambianchi, Enrico and Uttieri, Marco (2019); “A Year-Long Assessment of Wave Measurements Retrieved from an HF Radar Network in the Gulf of Naples (Tyrrhenian Sea, Western Mediterranean Sea)”; Journal of Operational Oceanography; Vol.12; Nº1; 2019; Pages 1-15.

Small, Christopher and Nicholls, Robert J. (2003); “A Global Analysis of Human Settlement in Coastal Zone”; Journal of Coastal Research; Vol.19; Nº3; Summer 2003; Pages 584-599.

Spirlet, Maxime; Geuzaine, Christophe and Beavais, Véronique (2017); “Experimental Correction of Radiation Patterns Between Electromagnetic Environments”; IEEE Transaction on Antenna and Propagation; Vol.65; Nº3; March 2017; Pages 1330-1338.

Teng, Chung-Chu; Bauchad, R. and Taft, B. (2004); “Determination of Pitch and Roll Angles from Data Buoys”; Oceans '04 MTS/IEEE Techno-Ocean '04; 9-12 November 2004.

Tian, Yingwei; Wen, Biyang; Li, Ziyan; Yin, Yukun; Huang, Weimin (2019); “Analysis and Validation of an Improved Method for Measuring HF Surface Wave Radar Antenna Pattern”; IEEE Antenna and Wireless Propagation Letters; Vol.18; Nº4; April 2019; Pages: 659-663.

Trenberth, Kelvin E.; Solomon, Amy (1993); “The Global Heat Balance: Heat Transports in the Atmosphere and Ocean”; Climate Dynamics; Vol.10; 1999; Pages 107-134.

Watermann, Jügen; Magunin, Arnfried; Gambetta, Marco and Bozzo, Emanuele (1998); “The Ocean Wave Dynamo: A Source of Magnetic Field Fluctuations”; Annali di Geofisisca; Vol.41; Nº3; August 1998; Pages 299-306.

Wyatt, Lucy R. (2018); “Wave and Tidal Power Measurements Using HF Radar”; International Marine Energy Journal, Vol.1; Nº2: November 2018; Pages 123-127.

Wyatt, Lucy R.; Green, J. Jim and Middleditch, A. (2010); “HF Radar Data Quality Requirements for Wave Measurements”; Coastal Engineering; Vol.58; 2011; Pages 327-336.

Appendix A:

Introduction:

In this section of the current work, it is presented the scatter plots of the parameters retrieved by the HF radar systems and the ODAS buoys systems as well as its respective linear fits for the results representing either the comparison of HF radar measurements with each single ODAS buoys measurements (section 3.1.1 and section 3.1.2).

When considering the retrieved parameters between the two measuring systems, a linear relationship between the two systems was expected.

Ideally, a relation of the following form would be expected to obtain:

$$HF_{radar} = Buoy \quad (A.01);$$

When considering practical results, a relation of the following form is obtained considering the hypothesis of a linear relationship between the two measuring systems:

$$HF_{radar} = m * Buoy + b \quad (A.02);$$

Where m is the slope of the linear relation between the two systems meaning that the HF radar measurements overestimate the buoys measurements if $m > 1$ or that HF radar measurements underestimate the buoys measurements if $m < 1$.

Considering the b parameter, it represents the intercept at the origin, indicating the bias between the two systems probably due to calibration set-ups.

Scatter Plots and Linear Fits Considering the Comparison of the Sagres HF Radar System Measurements Against Single ODAS Buoys:

The following results were attained when considering the comparison of the retrieved parameters by the Sagres HF radar system with the ones retrieved by the Sines coastal buoy.

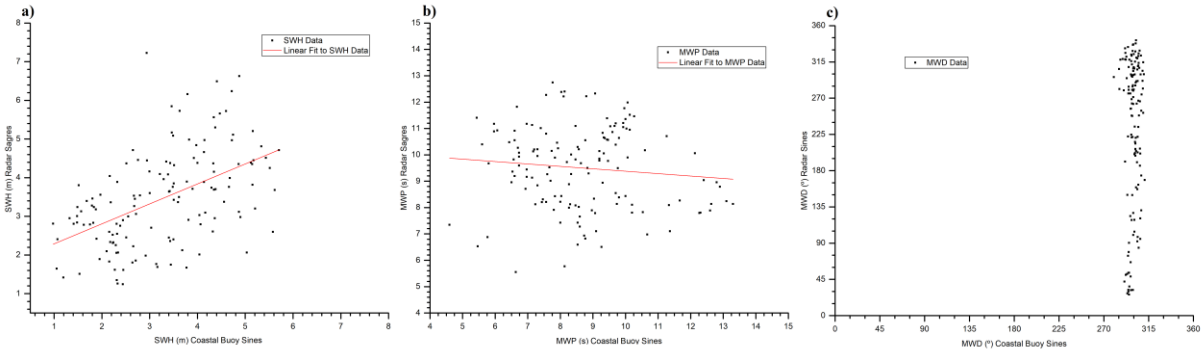

Figure A.01: Scatter plot representation and respective linear fits to for the a) SWH, b) MWP data retrieved by the Sines coastal buoy versus the data retrieved by the Sagres HF radar system recalling the first temporal period. A linear fit was not applied to the MWD data.

Table A.01: Linear fit parameters for the data retrieved by the Sines coastal buoy versus the data retrieved by the Sagres HF radar system for the first temporal period. A linear fit was not performed to the MWD data.

	SWH	MWP	MWD
m	0.52	-0.09	--

Δm	0.08	0.07	--
b	1.77 (m)	10.30 (s)	--
Δb	0.27 (m)	0.66 (s)	--
r^2	0.24	0.004	--

Below are the results concerning the comparison of the measurements performed by the Sagres HF radar systems with the ones performed by the Faro offshore buoy.

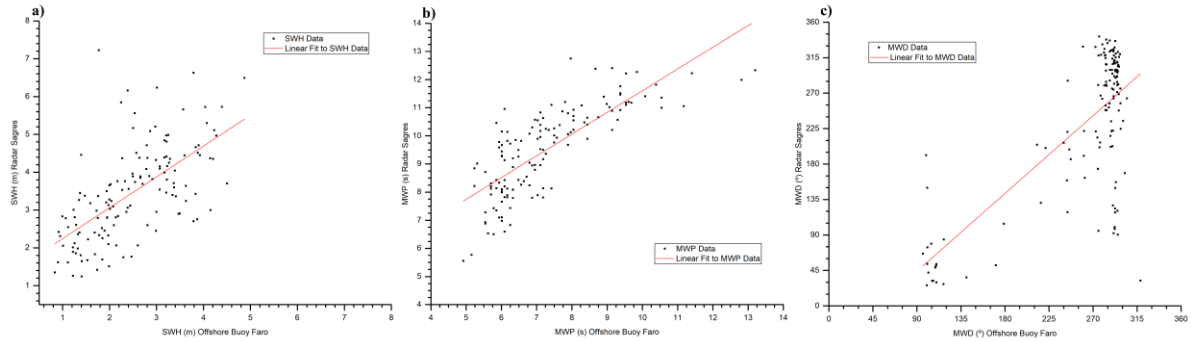

Figure A.02: Scatter plot representation and respective linear fits to the a) SWH, b) MWP and c) MWD data retrieved by the Faro offshore buoy versus the data retrieved by the Sagres HF radar system recalling the first temporal period.

Table A.02: Linear fit parameters for the data retrieved by the Faro offshore buoy versus the data retrieved by the Sagres HF radar system for the first temporal period.

	SWH	MWP	MWD
m	0.82	0.77	1.10
Δm	0.09	0.05	0.09
b	1.43 (m)	3.88 (s)	-54.87 (º)
Δb	0.23 (m)	0.4 (s)	24.73 (º)
r^2	0.39	0.60	0.50

Finally, the results concerning the comparison of the measurements performed by the Sagres HF radar systems with the ones performed by the Faro coastal buoy are presented below.

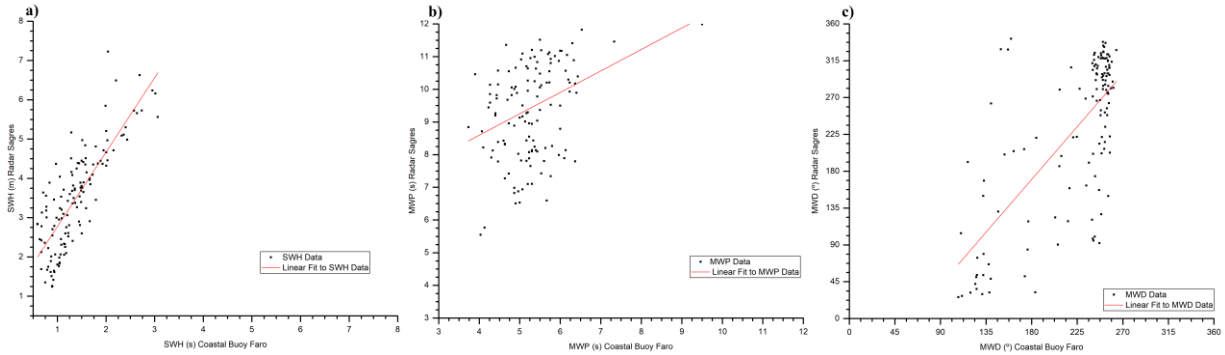

Figure A.03: Scatter plot representation and respective linear fits to the a) SWH, b) MWP and c) MWD data retrieved by the Faro coastal buoy versus the data retrieved by the Sagres HF radar system recalling the first temporal period.

Table A.03: Linear fit parameters for the data retrieved by the Faro coastal buoy versus the data retrieved by the Sagres HF radar system for the first temporal period.

	SWH	MWP	MWD
m	1.89	0.66	1.43
Δm	0.12	0.15	0.13
b	0.88 (m)	5.97 (s)	-87.84 (º)
Δb	0.18 (m)	0.83 (s)	29.09 (º)
r^2	0.66	0.12	0.48

Scatter Plots and Linear Fits Considering the Comparison of the Alfanzina HF Radar System Measurements Against Single ODAS Buoys

The following figures represent the scatter plots and linear fits results for the data comparison between the Alfanzina HF radar system and the Faro offshore buoy for the first temporal period.

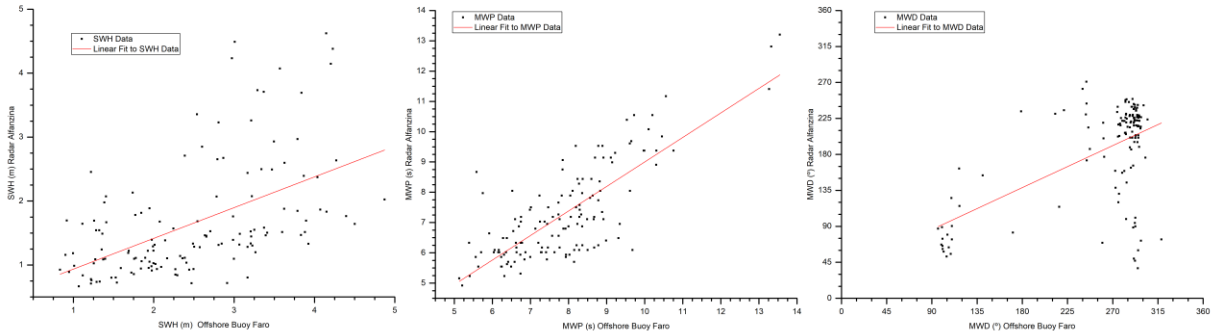

Figure A.04: Scatter plot representation and respective linear fits to the a) SWH, b) MWP and c) MWD data retrieved by the Faro offshore buoy versus the data retrieved by the Alfanzina HF radar system recalling the first temporal period.

Table A.04: Linear fit parameters for the data retrieved by the Faro offshore buoy versus the data retrieved by the Alfanzina HF radar system for the first temporal period.

	SWH	MWP	MWD
m	0.48	0.81	0.58
Δm	0.07	0.05	0.07
b	0.46 (m)	0.91 (s)	33.40 (º)
Δb	0.18 (m)	0.44 (s)	18.99(º)
r^2	0.27	0.61	0.33

Lastly, the results obtained for the data comparison between the Alfanzina HF radar system and the Faro coastal buoy for the first temporal period are shown in the figure below.

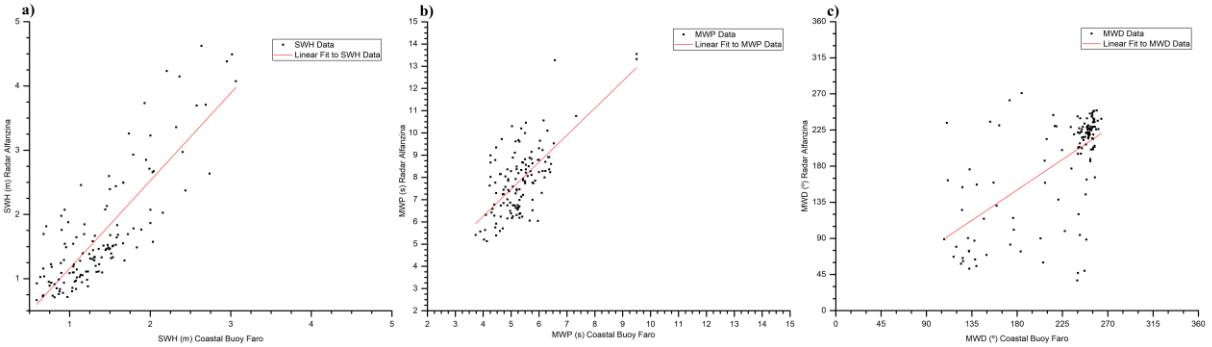

Figure A.05: Scatter plot representation and respective linear fits to the a) SWH, b) MWP and c) MWD data retrieved by the Faro coastal buoy versus the data retrieved by the Alfanzina HF radar system recalling the first temporal period.

Table A.05: Linear fit parameters for the data retrieved by the Faro coastal buoy versus the data retrieved by the Alfanzina HF radar system for the first temporal period.

	SWH	MWP	MWD
m	1.36	1.22	0.84
Δm	0.08	0.12	0.09
b	-0.21 (m)	1.39 (s)	-1.32 (º)
Δb	0.12 (m)	0.64 (s)	20.43 (º)
r^2	0.69	0.43	0.40

Directional Histogram for the MWP Parameter Retrieved by the Alfanzina HF Radar from the 1st of January to the 24th of April 2018:

Image is an enlarged image of figure 3.30.b) for the propose of identification of the MWP values associated with swell-sea states with MWD values from shore.

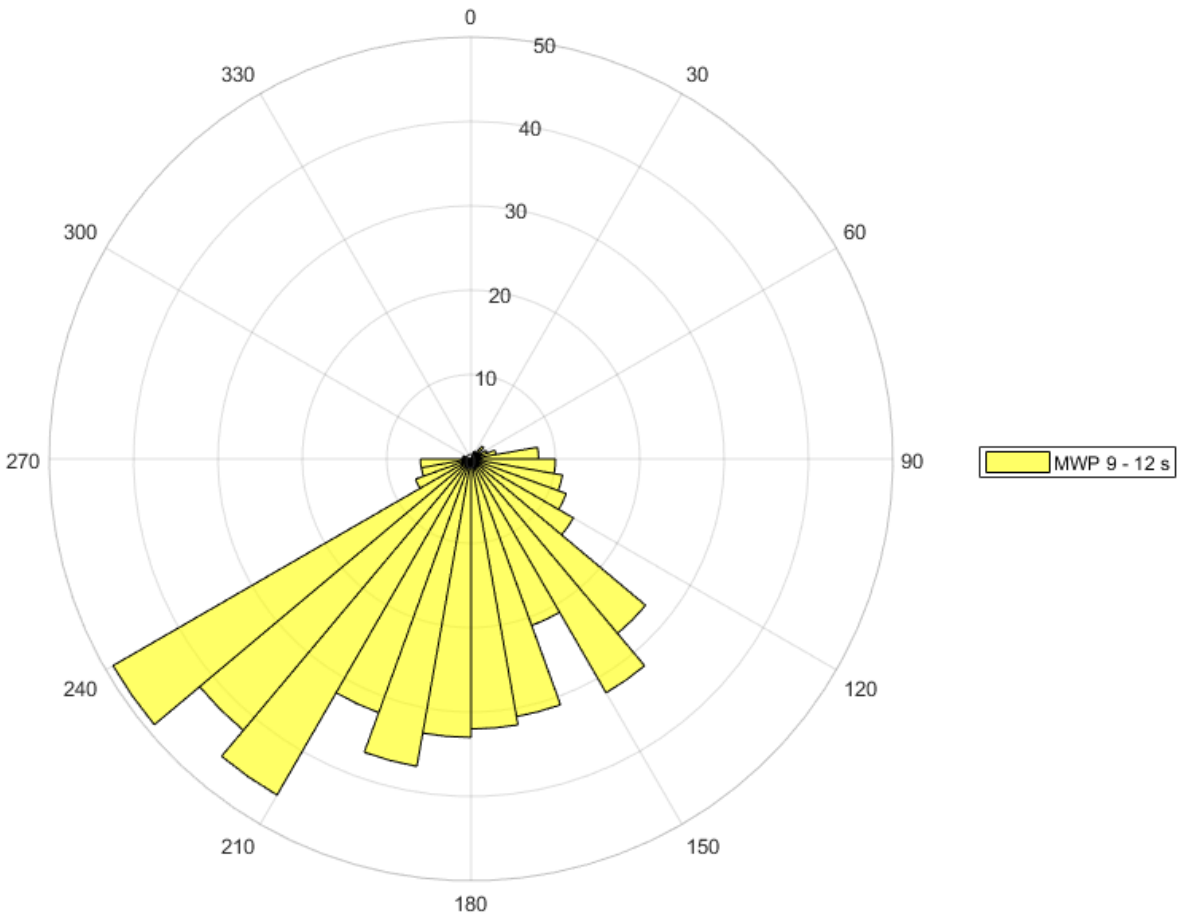

Figure A.06: Directional histogram for the MWP parameter interval ranging from 9 s to 12 s retrieved by the Alfanzina HF radar for the temporal period ranging from the 1st of January to the 24th of April 2018.

Appendix B:

Some work was also done trying to relate the MWD relative error values with the deviation of the HF radar antenna pattern from an ideal antenna pattern following Lipa and Barrick (1986), Tian *et al.* (2019) and Cheng (1989). Unfortunately, significant conclusions were not reached.

Nevertheless, the next two figures represent, just for the sake of work coherence, the electromagnetic far-field pattern generated by the Sagres and the Alfanzina HF radar antennas.

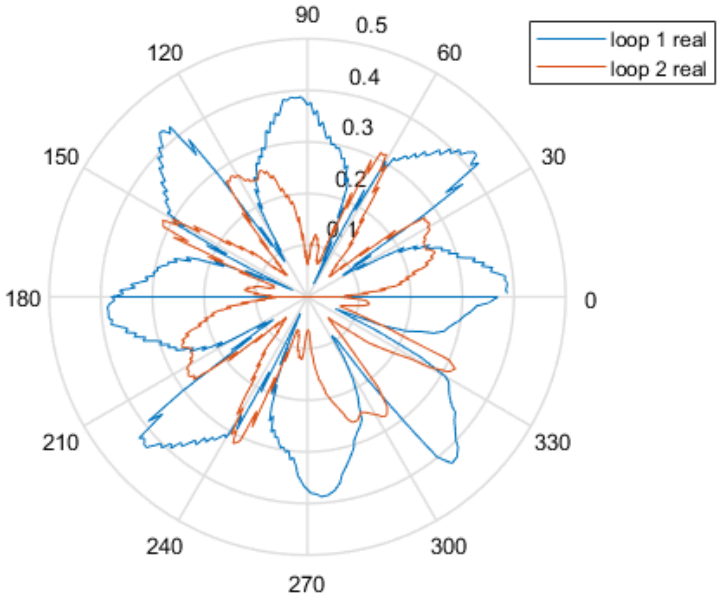

Figure B.01: Sagres HF radar antenna electromagnetic far-field pattern (normalized by the mean value of the electric field for each loop) measured in 23/10/2015.

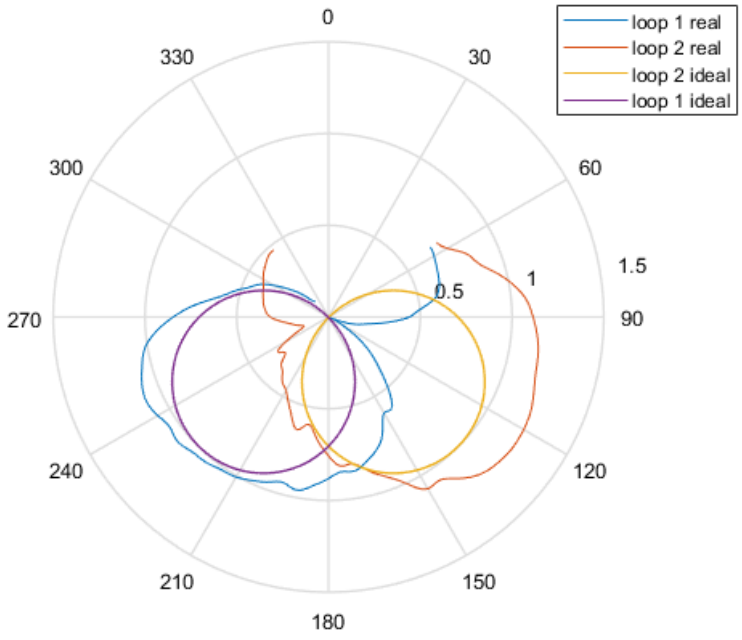

Figure B.02: Alfanzina HF radar antenna electromagnetic far-field pattern (blue and red) and the ideal electromagnetic far-field pattern (purple and yellow), (real loops normalized by the mean value of ideal electromagnetic field) measured in 17/06/2015.

Appendix C:

In this appendix, the parameters used for the validation and assessment of HF radar wave measurements are defined.

Relative error:

The relative error series (RE) were used in this work as a measure of precision and were defined using the following relation:

$$RE = \frac{|HF - Buoy|}{Buoy} \quad (9.01);$$

Where the buoys measurements were considered to be the exact values and the HF radar measurements were considered to be the approximated values.

Mean Value:

The mean value of a given retrieved parameter, $\langle x \rangle$ was computed according to the next formula:

$$\langle x \rangle = \frac{1}{N} \sum_{i=1}^{N} x_i \quad (9.02);$$

Where N is the length of the parameter series and x_i is the i^{th} parameter in the series.

Standard Deviation:

The standard deviation parameter (σ) was used to quantify the dispersion of a given data series. It was computed according to the relation presented below:

$$\sigma = \sqrt{\frac{1}{N-1} \sum_{i=1}^{N} (x_i - \langle x \rangle)^2} \quad (9.03);$$

Where once again N is the length of the parameter series, x_i is the i^{th} parameter in the series and $\langle x \rangle$ is the mean values of the respective parameter.

Root Mean Square Error:

The root-mean-square-error (RMSE), is a measure of the accuracy of a given data-series and was used to quantify the differences between the values measured by the HF radar and the ODAS buoys. It was computed according to the next relation:

$$RMSE = \sqrt{\frac{1}{N} \sum_{i=1}^{N} ((HF_i - \langle HF \rangle) - (Buoy_i - \langle Buoy \rangle)^2} \quad (9.04);$$

Where HF_i and $Buoy_i$ are respectively the i^{th} HF radar and ODAS buoys measurements concerning a given wave parameter and $\langle HF \rangle$ and $\langle Buoy \rangle$ are the mean values of the series retrieved respectively by the HF radar and the ODAS buoys for the parameter.

Pearson Linear Correlation Coefficient:

The Pearson linear correlation coefficient can be used to quantify a linear relation between a given parameter retrieved by the two systems. It was computed following the next relation:

$$r = \frac{cov(Buoy, HF)}{\sigma_{buoys} \cdot \sigma_{HF}} \quad (9.05);$$

Where $cov(Buoy, HF)$ represents the covariance between the data-series retrieved by the two systems and σ_{buoys} and σ_{HF} represents respectively the ODAS buoys and the HF radar standard deviation concerning a given parameter.

Mean Wave Energy:

It is presented in the work of Calisal (1983) the linear energies densities and total linear energy density expressions for finite depth water waves. According to this author, the kinetic energy (KE) and the potential energy (PE) per linaer density can be computed from the following formulas:

$$KE = \frac{g * A^2}{4} \quad (9.05);$$

And;

$$PE = \frac{g * A^2}{4} \quad (9.06);$$

Where g is the gravity acceleration (taken as $9.8\ m/s$) and A is respectively the amplitude of the given wave.

Thus, the total energy per linear density of a given wave (in this work called the mean wave energy[7] (MWE)) can be computed from the next relation:

$$MWE = KE + PE \quad (9.07);$$

And hence;

$$MWE = \frac{g * A^2}{2} \quad (9.08);$$

Posteriorly, the MWE polar plots were created using the OriginLab software, where for a given measurement the significant height value of each measurement was used as the A parameter. the MWE value (z-axis) was associated with its respectively retrieved MWP value (r-axis) as well as with its associated MWD value (θ-axis). All the MWE polar plots are respectively normalized by the mean MWE computed for the respective HF radar system for each of the temporal periods considered.

The mean MWE energy retrieved for each of the considered measuring systems regarding each studied temporal series were computed from the mean significant wave height values. I.e., for a given

[7] Since the value of A used to compute the MWE as the significant wave height (SWH), the MWE should more accurately be called the Significant Wave Energy.

measuring system the mean MWE value was computed using the mean significant wave height value of a given temporal period.

Kolmogorov-Smirnov Test:

The Kolmogorov-Smirnov test is a non-parametric test (i.e. independent of the sample distribution), that quantifies the distance between the empirical distribution functions of the two samples. It relies on the null hypothesis (that states that there is no significant difference between two empirical distribution functions and thus that the two samples are due to the same physical phenomena), as stated by the following relation (Lopes *et al.*, 2007):

$$D = sup|\psi_1 - \psi_2| \quad (9.09);$$

Where sup represents the $supreme$ of the given set and ψ_1, ψ_2 are respectively the empirical distribution functions of the two samples.

Thus, the null hypothesis assumption is rejected if D is superior to a given threshold level previously tabulated.

This test was applied with a significance level (the probability of rejecting the null when it is true) $\alpha = 0.01$, and thus a 1% probability of rejecting the null hypothesis when it is actually true.

Relative Occurrence Coefficients:

The relative occurrence coefficients represent the number of times a given ODAS buoy system (i.e., the Sines coastal buoy or the Faro buoys) was used for the creation of the combined signal. It is expected since the HF radar system measures within a given circular crown (see figure 2.01), that these relative occurrence coefficients translate into the relative frequency of occurrence of a given sea-state at the radar site. In particular, it is expected that the relative occurrence coefficients related to the Sines buoy represent the South-Eastward sea-states, the relative occurrence coefficients related to Faro offshore buoy represent North-Eastward/Westward sea-states and the relative occurrence coefficients related to the Faro coastal buoy represent the Westward sea-states.

Hence, the relative occurrence coefficients were defined according to the following formula:

$$Relative\ Occurence\ Coefficients = \frac{number\ of\ measurents\ given\ buoy}{total\ number\ of\ measurements} \quad (9.10);$$

Appendix D:

It is here presented the bathymetric contour lines for Continental Portugal computed from the GEBCO 2014 data.

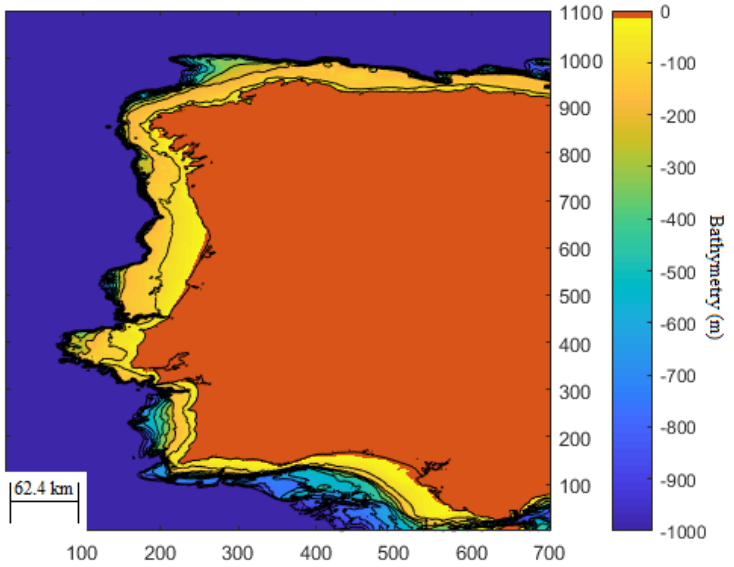

Figure D.01: Bathymetry contours for Continental Portugal using the General Bathymetric Chart of the Oceans (GEBCO) 2014 data.

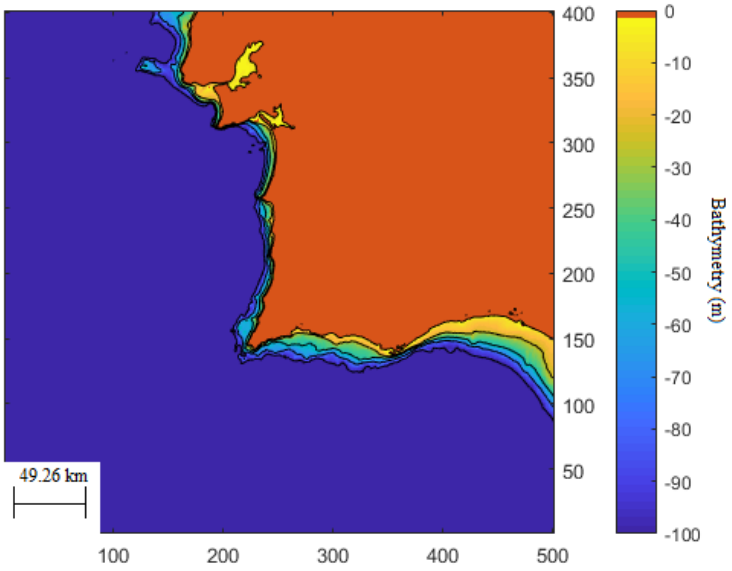

Figure D.02: Bathymetry contours for the South of Portugal using the General Bathymetric Chart of the Oceans (GEBCO) 2014 data.